RADIATIVE HEAT TRANSFER IN GALLIUM ARSENIDE LEC CRYSTAL PULLERS

By

Muna Bakeer

B. Sc. (Civil Engineering)

B. Sc. (Mechanical Engineering)

M. Sc. (Mechanical Engineering)

Washington University, St. Louis, Missouri

A THESIS SUBMITTED IN PARTIAL FULFILLMENT OF

THE REQUIREMENTS FOR THE DEGREE OF

MASTER OF APPLIED SCIENCE

in

THE FACULTY OF GRADUATE STUDIES

MECHANICAL ENGINEERING

We accept this thesis as conforming

to the required standard

THE UNIVERSITY OF BRITISH COLUMBIA

November 1990

In presenting this thesis in partial fulfilment of the requirements for an advanced degree at the University of British Columbia, I agree that the Library shall make it freely available for reference and study. I further agree that permission for extensive copying of this thesis for scholarly purposes may be granted by the head of my department or by his or her representatives. It is understood that copying or publication of this thesis for financial gain shall not be allowed without my written permission.

Department of Mechanical Engineering

The University of British Columbia
Vancouver, Canada

Date Dec. 20th, 1990

Abstract

A numerical analysis of radiative heat transfer in a liquid encapsulant Czochralski gallium arsenide crystal puller is developed. The heat transfer and equivilent ambient temperature of each surface element are calculated using the Gebhart radiative model. The effective ambient temperature, to which each surface element is radiating, is found to vary indicating that assuming a constant ambient temperature for all surfaces (simplified radiative model) is incorrect.

The importance of including the middle and top cylinders of the growth chamber in numerical analysis of radiative heat transfer in the system is evaluated in the study. The upper section could be replaced by one isothermal surface without significant change of the effective ambient temperature distribution.

Fluid flow and heat transfer in the $GaAs$ melt, crystal and encapsulant are calculated using a three dimensional axisymmetric finite difference code which includes the detailed radiative model. The mathematical modelling of the fluid and heat flow describes steady state transport phenomena in a three dimensional solution domain with latent heat release at the liquid/solid interface.

The predicted flow and temperature fields using the detailed radiative model differ considerably from the predicted fields using the simplified model. The simplified model shows high axial and low radial temperature gradients in the crystal near the encapsulant region; the axial gradient decreases and the radial gradient increases with increasing distance from the encapsulant top. The detailed model shows a high radial temperature gradient in the crystal near the crystal-encapsulant-ambient junction and nearly flat isotherms in the top half of the crystal.

Nomenclature

A	area, m^2 ; optical absorbance
C_i	convective flux from boundary i
C_p	specific heat, J/gmK
D_i	diffussive flux from boundary i
F_{ij}	configuration factor from surface i to surface j
f_i'	energy fraction emitted at T_i below $\lambda = 2\mu m$
f_i	length ratio
G_{ij}	Gebhart factor for surface i
h'	height, m
$h_{convection}$	convective heat transfer coefficient, W/cm^2K
k	thermal conductivity, $W/cm.K$
m_i	mass flow rate in face i of the control volume
p	pressure, N/m^2
Pe	Peclet number
r	radius, m
R_ϕ	residual of ϕ
S	source term
T	temperature, K
u, v, w	$x-$, $r-$, $\theta-$direction velocity component, respectively, m/s
u_p	crystal pulling velocity, m/s
V	volume, m^3
α	underrelaxation factor; absorption coefficient cm^{-1}
β	thermal expansion coefficient, K^{-1}

δx, δr, $\delta\theta$	$x-$, $r-$, $\theta-$ direction distance between two adjacent grid points
Δx, Δr, $\Delta\theta$	$x-$, $r-$, $\theta-$ direction width of the control volume
ϵ	emissivity
Γ	general diffusion coefficient, $kg/(ms)$
γ	approximation coefficient
λ	wavelength, μm
μ	dynamic viscosity, Ns/m^2
ρ'	density, kg/m^3
ρ	reflectivity
ϕ	general dependent variable
σ	Planck's constant, $5.729 * 10^{-8} W/m^2K^4$

Subscripts

amb	ambient
c	crucible
co	outer wall of crucible
E	neighbour in the positive x–direction, i.e., on the east side
e	control–volume face between P and E; encapsulant
enc	enclosure
m	melt
mc	middle cylinder wall
mcla	middle cylinder lower annulus
mcta	middle cylinder top annulus
N	neighbour in the positive r–direction, i.e., on the north side
n	control–volume face between P and N
P	central grid point under consideration

S	neighbour in the negative r–direction, i.e., on the south side
s	control–volume face between P and S; crystal
st	crystal top
tcw	top cylinder wall
tct	top cylinder top
W	neighbour in the negative x–direction, i.e., on the west side
w	control–volume face between P and W

Superscripts

$*$	previous–iteration value of a variable

Table of Contents

Acknowledgement

I wish to thank Dr. M. Salcudean for giving me the opportunity to work on a very interesting project, and for her financial and moral support during my stay at UBC. I also wish to thank Dr. M. Iqbal for his financial support, Dr. I. Gartshore for his continuous support and encouragement and Dr. P. Sabhapathy for his valuable comments.

My thanks go to Mr. A. Steeves who was very helpful in offering assistance with using VAX/VMS system at the Department of Mechanical Engineering.

I would like to thank all my friends especially C. Backhouse, V. LeMay and P. Pottier whose continuous support made my path easier to travel.

Chapter 1

INTRODUCTION

1.1 General

Gallium arsenide is an electronic material that is emerging, not as a substitute for silicon, but as an important complement to it. Gallium arsenide has many properties that are useful in electronic equipment. Some of those properties include the following:

- Speed/power capability that is significantly superior to that of silicon.
- Higher radiation resistance of its devices when compared with silicon devices.
- Operation at higher temperatures than silicon.
- Higher efficiency for solar cells in space applications.
- Combining the processing of both light and electronic data on a single chip.
- The possibility of being alloyed with other III-V compounds, such as AlAs, InAs, InP and GaP for a broad spectrum of useful properties.

Gallium arsenide does however have one major disadvantage – COST. The gallium in a *GaAs* wafer costs more than ten times as much as the polysilicon in silicon wafers. Therefore, it is imperative to produce crystals with low dislocation densities and point defects in order to improve production yield. *GaAs* is composed of the low melting point metal gallium and the volatile metal arsenic. Consequently, it shows a very high arsenic

dissociation pressure (about 0.1 MPa) at the melting point ($1238°C$). This fact makes it hard to grow stable crystals [1].

1.2 The Liquid Encapsulant Czochralski Crystal Growth Process

1.2.1 Process History

Metz, Miller and Mazelsky [2] first introduced the liquid encapsulant Czochralski (LEC) method in the early sixties. They pulled PbTe and PbSe crystals using molten boron trioxide (B_2O_3) as the liquid encapsulant. They chose molten B_2O_3 because it is less dense than the materials pulled and thus it floats on top of the semiconductor melt. In addition, it has a low vapour pressure which means that it will not evaporate under atmospheric or higher pressures. Also, the liquid metals they used were not soluble in and did not react with the molten boron trioxide. One of the other beneficial properties of boron trioxide is that it is transparent in the visible region which permits direct observation of the melt surface. It is rather viscous and tends to cling to the pulled crystal covering a large fraction of its surface, thus preventing arsenic evaporation from the crystal. However, it is soluble in hot water and may easily be removed from the finished crystals. B_2O_3 is also used as an encapsulant in the LEC crystal growth of $GaAs$.

1.2.2 Process Description

The LEC growth process is a major means of producing $GaAs$ crystals. The LEC growth chamber is shown in figure 1.1. It consists of a cylindrical crucible that holds the melt and encapsulant. The crucible is heated from the side. The encapsulant covers the melt; its thickness varies depending on (a) the crystal length and diameter, and (b) whether high or low pressure is used (1 versus 4 MPa). A typical thickness is 2-cm. The optimum thickness has not been determined yet, even though full encapsulation seems to allow

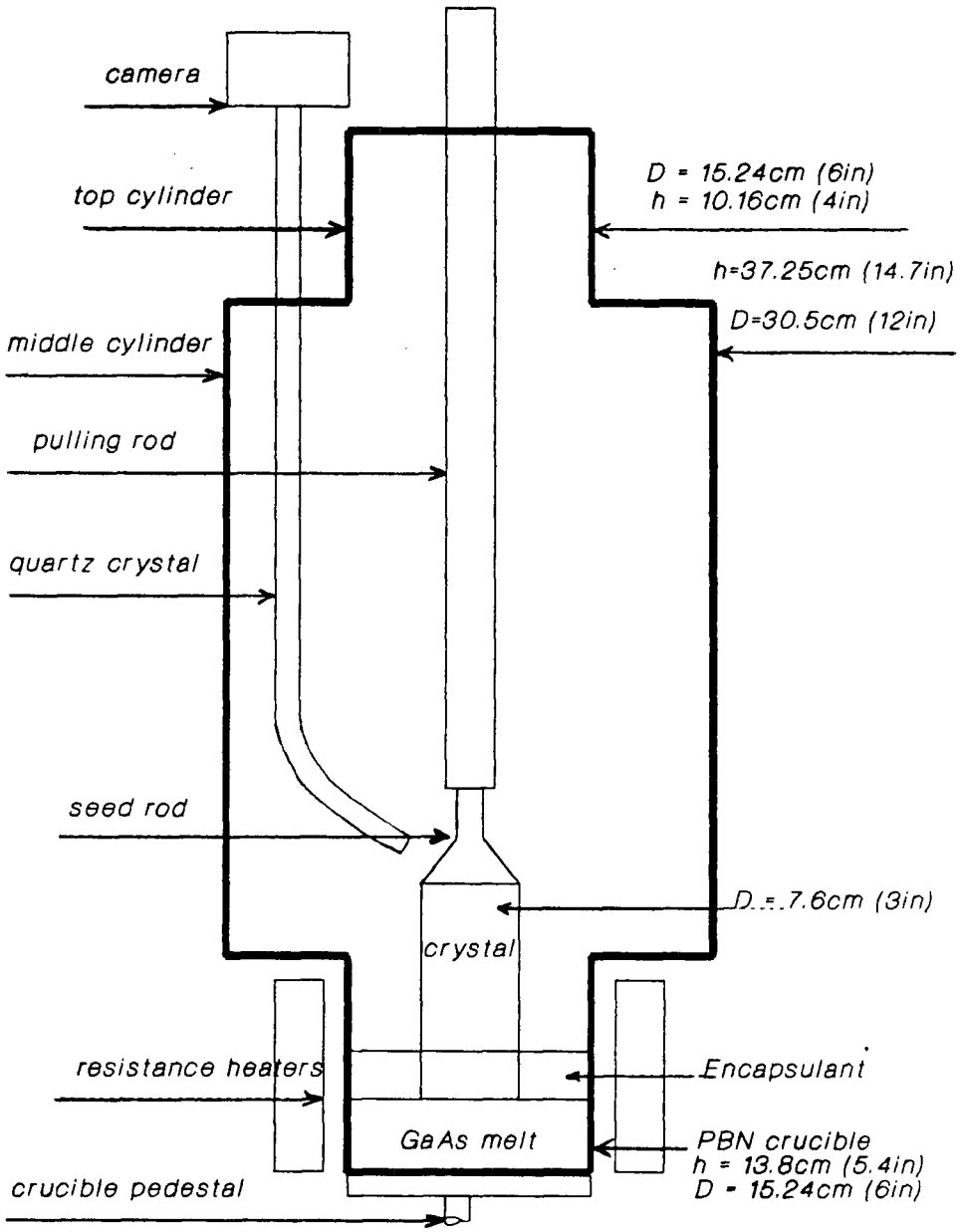

Figure 1.1: Schematic showing *GaAs* liquid encapsulant Czochralski crsytal puller.

the growth of least stressed crystals. Full encapsulation implies that the whole crystal is covered with the encapsulant material as it grows. A seed that is attached to the pulling rod is inserted from the top so that it touches the melt surface. The gas surrounding the crystal - nitrogen or argon - is pressurized up to 4-MPa in order to reduce arsenic evaporation from the crystal and melt. The crucible and crystal are rotated either in the same direction (isorotation) or in opposite directions (counterrotation), at the same or at different speeds. The crucible is rotated to minimize the thermal asymmetry of the system. The crystal is rotated to create a uniform boundary layer at the solid/liquid interface through which heat and mass transfer take place. This boundary layer isolates the growth interface from the velocity fluctuations in the bulk of the melt. Crystal rotation also helps in shaping a cylindrical crystal. The crucible is raised by movement of the pedestal so that the solidification front remains in a specified region of the heater as the melt level drops. The growth process is viewed through a quartz crystal that is positioned as shown in figure 1.1.

Maintaining the same heat transfer conditions throughout the growth of the crystal is complicated by imperfections in the heat transfer environment and by instabilities thought to be inherent in the Czochralski growth configuration. The process is also complicated by the batchwise nature caused by the decreasing depth of the melt in the crucible and the changing heat exchange characteristics between the melt, crucible and ambient gas.

The use of B_2O_3 as an encapsulant introduces the following difficulties:

1. Crystal diameter control becomes difficult because B_2O_3 which has a large heat capacity, induces a time lag in the temperature control and thereby in the diameter control.

2. The large temperature gradient of B_2O_3, which has a small thermal conductivity, causes a high temperature gradient in the crystal which induces high thermal stresses leading to an increase in dislocation density. The dislocations in turn alter the electrical properties of the $GaAs$ wafers thus degrading device performance. (Dislocations are also caused by propagation and multiplication from an imperfect seed.)

3. Reaction between B_2O_3 and impurities in the gallium arsenide melt affects impurity concentration in the grown crystal, although B_2O_3 rarely reacts with the melt itself.

Thus, it is important to study the fluid flow and heat transfer in the melt, encapsulant and surrounding gas to understand how they affect the growing crystal and to determine the best conditions for growing $GaAs$ crystals. Also, the information provides data needed for the design of the crystal pullers.

Chapter 2

LITERATURE SURVEY

2.1 Introduction

The areas of research in the crystal growth field that are of interest here include :

- Fluid flow analysis of the melt, encapsulant and gas.
- Thermal flow (heat transfer) in the melt, encapsulant, crystal and furnace environment.

The literature survey includes both experimental and analytical work. It is found that most studies concentrated on fluid or heat transfer analysis in the melt and did not include the encapsulant as a part of the system, i.e., the analysis was done on a Czochralski – not a liquid encapsulant Czochralski – crystal growth system. However, some recent studies did include the encapsulant region.

2.2 Experimental Studies

In 1968 Mullin et al [3] used the liquid encapsulation method to pull GaP and InP crystals. They designed a high pressure chamber which could have been obtained as a standard attachment to commercial versions of the crystal puller available then. Their study was aimed at confirming the viability of the technique and assessing the chemical purity of crystals grown in silica and vitrious carbon crucibles.

They concluded that silica crucibles did contaminate GaP and InP melts. However, the vitrious carbon crucibles did not contaminate the melt. They found that the starting material was the most likely potential source of carbon.

Lamprecht et al [4] did experiments to investigate the flow and temperature distributions in a Czochralski configuration. The experiments were designed to study the importance of buoyacy, thermocapillary and forced convection on the crystal growth. They used $NaNO_3$ melt in an iridium crucible. They reported qualitative agreement between their experimental results and numerical results obtained by Langlois in [5, 6, 7]. The agreement showed the importance of thermocapillary forces when considering the problem of fluid flow transition leading to interface transitions. They also emphasized the importance of buoyancy and thermocapillary forces for heat dissipation from the melt surface as well as mass transport through the melt surface.

Terashima and Fukuda [8] designed a new magnetic field LEC pulling apparatus. They concluded from their experiments that the higher the magnetic field applied, the lower the temperature fluctuation in the melt and encapsulant. Also, higher pressure in the chamber which caused a large temperature gradient in the melt and encapsulant and increased thermal convection, required a higher magnetic field to suppress the melt and encapsulant temperature fluctuation.

Osaka et al [9] grew GaAs crystals using the LEC method in a growth apparatus designed for the study which used a two-heater configuration and controled the main heater power by a computer. They monitored the crystal diameter using a load cell that measured crystal weight during growth. In order to reduce the temperature gradient in the encapsulant, they used a thick layer of boron trioxide. They reported a gradient of $100°C/cm$ for a 2-cm thick layer and $35°C/cm$ for an 8-cm thick layer. They concluded from their experiments that the yield of single $< 100 >$ oriented crystal reached nearly 100% when the solid/liquid interface profile was controlled such that it was convex

towards the melt.

Kohda et al [10] grew dislocation-free and striation-free GaAs crystals using fully encapsulated Czochralski method. The crystal diameter was 50-mm. They used a 50-mm B_2O_3 layer which allowed full encapsulation of the pulled crystal. This method reduced stress induced dislocations because arsenic evaporation, which caused surface irregularities, was effectively suppressed from the crystal surface. By using two heaters that were controlled individually, a temperature gradient of $30-50°C/cm$ was maintained along the growth direction in the encapsulant layer.

Ozawa and Fukuda [11] observed the solid-liquid interface of GaAs grown by the LEC method. They reported that the region of stable crystal growth was indicated by a meniscus angle β in the range of 18° to 45°where β is defined as shown in figure 2.2.

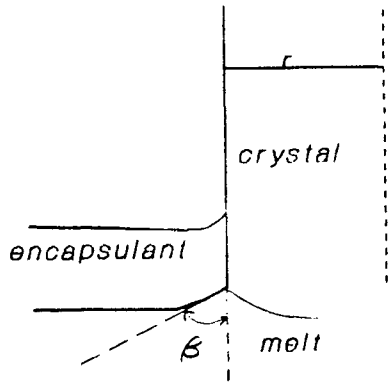

Figure 2.2: Meniscus angle β which must be between 18° and 45° for stable crystal growth.

Kakimoto et al [12] observed directly the convection in boron trioxide during GaAs crystal growth using x-ray radiography. They studied natural convection in B_2O_3 with and without crystal in order to seperate the effect of forced convection attributed to

crystal and crucible rotation. For that case, they estimated the flow velocity to be about 0.3mm/sec which was two orders of magnitude less than that in the semiconductor melt. In the presence of a crystal, the flow velocity was about 0.03-0.05 mm/sec which was one order of magnitude smaller than that without a crystal. This reduction in flow velocity was attributed to shear viscous flow near the crystal wall. The results of the numerical simulation of the flow in B_2O_3 agreed very well with the experimental results (0.1-0.5 mm/sec). Their exercise showed that the flow in the encapsulant was steady and axisymmetric. Also, since the flow velocity was two orders of magnitude less than that in the semiconductor melt, conduction may be considered to dominate convection in the encapsulant B_2O_3.

2.3 Theoretical Studies

Ramachandran and Duduhovic [13] used a detailed radiative heat transfer model (Gebhart model) when simulating the temperature distribution in crystals grown by the Czochralski method. They also used a simplified model (Stefan's model) for the purpose of comparison. However, they assumed the melt, exposed crucible wall and the enclosing walls to be at uniform temperatures, i.e., they did not divide those surfaces to elements in order to take into account each surface's temperature gradient. By doing that they reduced the computing time required, however they also lost a more accurate representation of the real system.

Atherton et al [14] studied the effect of diffuse-gray radiation on the parametric sensitivity and stability of the Czochralski process for growing silicon. They used a detailed radiative model which used the Gebhart method for computing radiative fluxes in diffuse-gray enclosures. For calculating the view factors, they used the programme FACET which was developed at Lawrence Livermore Laboratory to calculate view factors in an arbitrary

axisymmetric geometry. They calculated view factors for only four surfaces — crystal, crucible, melt and an enclosure that represented the ambient surface which they divided to 20 subsurfaces. They concluded that the importance of including detailed radiation modelling of the entire growth process was emphasized by the simulations which took into account the decreasing melt volume.

Work by Srivastava et al [15] gave similar results as those given in [11] regarding the importance of the meniscus angle. Srivastava et al studied the liquid/solid interface based on a conductive model (conduction being the main mode of heat transfer in the melt and crystal). They used the Gebhart method for calculating radiative heat transfer in the puller. They divided the crystal top, crystal surface and melt surface to N_i elements, and assumed one surface for the crucible wall and one for the enclosing wall. They also assumed the crystal top to lose heat only to the enclosure wall by radiation. They studied the effects of several factors on the interface shape and pulling rate. They found that the effect of the meniscus shape on the interface shape was significant; its incorporation in the solution resulted in an increased concavity of the interface (concavity on the crystal side). The concavity was caused by the reduction in the axial heat transfer from the melt to the interface.

Motakef and Witt [16] studied the effect of liquid encapsulation on the thermal stresses induced in the crystal. They found that stresses are strongly effected by the thermal transparency of the encapsulant.

Derby and Brown [17] used a conduction dominated heat transfer model to form a simulation of the LEC crystal growth. They considered the extreme cases where the encapsulant was treated as either opaque or transparent. However, neither side of that treatment represented the actual case, since B_2O_3 was neither opaque nor fully transparent to the energy transferred from the melt. They found that in the case of a transparent

encapsulant the direction of heat transfer in the encapsulant was horizontal (radially inward) from the wall to the crystal, while in the opaque case it was vertical – from the melt to the ambient (vertical isotherms versus horizontal isotherms). The melt/solid interface shape changed from concave into the crystal for a transparent layer to fully convex from the crystal for an opaque layer. The results of their work indicated that the optical properties of boron trioxide are of great importance in determining the amount of energy that was transmitted from its surface. However, these optical properties were not determind in the temperature range of interest until recently and only by one source. It is worth mentioning here that even though B_2O_3 is transparent to radiation in the visible region, in the temperature range of interest here, only 1 % of the energy emitted lies within the visible region — assuming blackbody radiation at the GaAs melting temperature.

Hicks [18] studied the fluid motion in the encapsulant assuming a temperature dependent viscosity and constant thermal conductivity. He introduced the Steffan-Boltzman radiation condition at the encapsulant/ambient interface and assumed a temperature distribution on the crystal-encapsulant, crucible-encapsulant and melt-encapsulant interface. He concluded from his results that the flow was predominantly in the azimuthal direction — caused by crystal and crucible rotation — while the flow in the meridional direction was negligible. He also concluded that heat flow was upward and conduction predominated convection in the encapsulant and thus the convective effects could be negelected. The latter result contradicted what Jordan [19] suggested that heat transfer between the crystal and encapsulant was strongly influenced by convective heat transfer within the encapsulant.

Thomas et al [20] extended their thermal capillary model to include a low-pressure LEC system for growth of GaAs in an axial magnetic field that was strong enough that convective heat transport became unimportant. They assumed the encapsulant layer to be semitransparent using the data obtained from Ostrogorsky et al [21] to determine

that condition. (Semitransparent means that the layer is transparent to radiation below a certain wavelength and opaque to radiation above that wavelength.) They also assumed the crystal, crucible, melt and surrounding surfaces to be diffuse gray surfaces for radiative heat transfer calculations. They considered the surrounding surfaces to be at a constant temperature — one surface only. They used Gebhart's method for diffuse gray surfaces to calculate the radiative heat exchange between the surfaces. They found that the crystal shape predicted by assuming a semitransparent encapsulant, different emissivities for the melt, crystal and encapsulated crystal, and an enhanced encapsulant conductivity was the closest to that produced experimentally.

Schvezov et al [22] calculated the temperature distribution in the crystal using a finite element model of the heat flow in the LEC growth system. They compared their results with an analytical solution of a simplified similar problem [23] and also with experimental results obtained from [24]. They found good agreement between their numerical and experimental results with the numerical results underpredicting the temperature distribution. They also compared the crystal axial temperature gradient and found the measured gradients to be significantly lower than those calculated near the interface, and above the calculated values away from the interface.

Sabhapathy and Salcudean [25] studied numerically the effects of melt height and crystal radius on the melt natural convection in LEC growth of GaAs. They also analysed the effect of top and bottom crucible heating on the isotherms. They accounted for top heating by increasing the ambient temperature to which the system is exposed. They used a simplified radiation model in which all surfaces radiate to the same ambient temperature. They investigated the effect of melt height and crystal radius on the critical crucible temperature T_c(above which the crystal starts melting and below which the melt starts freezing at the melt-encapsulant interface). They concluded that by a proper combination of top and bottom heating, the crucible wall temperature could be lowered

and nearly flat isotherms at the crystal-melt interface could be obtained.

Salcudean et al [26] studied free and forced convection in GaAs melt during the LEC crystal growth. They studied free convection due to melt heating at the crucible wall and forced convection due to crystal and crucible rotation. They found the isotherms in the forced convection case to be nearly equally spaced concluding that conduction dominates forced convection (maximum melt velocity in the vertical plane was $0.004m/sec$). However for the free convection case, the isotherms were concentrated near the wall and near the crystal where convective effects were the strongest. For the case of combined forced and free convection, they found the flow to be significantly different from that of the free or forced alone. They concluded that the flow was multicellular with some cells rotating faster than the crucible, and that the flow and temperature fields in the melt beneath the crystal were oscillatory.

Sabhapathy and Salcudean [27] studied numerically fluid flow and heat transfer in the melt and encapsulant of GaAs LEC crystal puller. They assumed the encapsulant to be semitransparent to radiation. They also assumed the melt, crystal and encapsulant to be radiating to the same ambient temperature. Thus they used a simplified radiation model. They concluded for the crystal and crucible dimensions they used that the flow in the melt (when natural and forced convection were included) was often multicellular and effects the temperature field significantly. The melt and the encapsulant were much cooler than in the pure conduction case for the same heat input. They also reported that the isotherms in the melt close to the crystal-melt interface were nearly flat when the crystal rotated faster than the crucible. They stated that the flow in the encapsulant was similar to a couette flow between two rotating concentric cylinders, and that the crystal axial temperature gradient increased strongly with a decrease in the ambient temperature.

2.4 Scope and Objectives of the Present Work

It is clear from the literature survey that the radiative exchange during *GaAs* crystal pulling is an important factor that must be included when modelling the process. However, the assumptions and simplifications used by the authors influenced their results. The treatment of the encapsulant layer is one area that introduces errors. Another is the assumption that all surfaces radiate to an ambient at a constant temperature.

The main objectives of the present work can be listed as follows:

- To calculate the radiative exchange including all surfaces.
- To obtain the best representative values of the material thermophysical properties.
- To evaluate the importance of including radiative exchange of all surfaces versus replacing some of the surfaces by one isothermal surface.
- To include the radiative model in the programme that calculates convection and conduction in the various elements of the crystal puller.
- To evaluate the difference between the simplified and detailed radiative models in the crystal pulling modelling.

In order to achieve those objectives, the radiative view factors which are needed for calculating the Gebhart factors first and heat transfer second, must be calculated. The Gebhart method for calculating heat transfer is a detailed one which includes the effect of multiple reflections in the calculation of heat transfer. A computer code is developed by the author to calculate all the required variables.

The programme that models fluid flow and heat transfer in the melt and encapsulant and heat transfer in the crystal has been developed by Salcudean and Sabhapathy [25, 26, 27]. The programme solves the mass, momentum and energy equations using a

finite-difference control-volume method. The method is described fully in the text. The author's code is included with Salcudean and Sabhapathy's programme and a comparison between the velocity and temperature fields obtained using the simplified radiative model and the detailed Gebhart model is presented.

Chapter 3

Radiative Heat Exchange in LEC GaAs Crystal Pullers

3.1 Introduction

The position and the shape of the crystal/melt interface during the crystal pulling process and the temperature distribution in the crystal are important factors determining the crystal quality. Also, adverse thermal gradients in the melt may result in solid/liquid interface instabilities or in excessive thermal stresses leading to a poor quality crystal. Therefore, the melt temperature profile, which is coupled with the flow field due to the interaction of natural and forced convection and thermocapillary flow, is an important element in the crystal growth. The convection in the melt is also affected by radiation from its surface.

The main objective of this part of the thesis is to determine qualitatively and quantitatively the radiative heat transfer in the crystal puller. Thus, system geometry and radiative properties are of great importance.

3.2 Crystal Puller Geometry Assumptions

The real system will be simplified for the purpose of the present study. However, the simplifications made will be such that the results can still be representative of the original system. The following assumptions are made:

1. The seed rod and the quartz crystal are not included as part of the system since their surface areas are small compared to the middle cylinder area to which they

will mostly radiate. The seed rod – and quartz crystal – middle cylinder radii ratios are 1:12 and 1:6, respectively.

2. All surfaces are assumed to be diffuse gray (emissivity is equal to the absorptivity, $\epsilon = \alpha$, and the reflectivity $\rho = 1.0 - \alpha = 1.0 - \epsilon$). A diffuse gray surface absorbs a fixed fraction of incident radiation from any direction and at any wave length. It emits radiation that is a fixed fraction of blackbody radiation for all directions and wavelengths.

3. The melt, encapsulant and crystal surfaces are assumed to be flat. This assumption is acceptable when calculating radiative view factors and radiative heat transfer.

4. The crucible and crystal are assumed to be cylindrical in shape of radii R_c and R_s, respectively.

3.3 Mathematical Modelling

3.3.1 Configuration Factor Calculation

The configuration factor is defined as the fraction of the radiation leaving one surface that reaches another surface. The calculations of radiative heat transfer in any system require evaluating the configuration factors of all the system surfaces. In the case of a *GaAs* crystal puller, the system is composed of the following surfaces:

1. Melt (m).

2. Encapsulant (e).

3. Crucible wall (c).

4. Crystal wall (s).

5. Middle cylinder wall (mcw).
6. Middle cylinder lower annulus (mcla).
7. Crucible outer wall (co).
8. Crystal top (st).
9. Middle cylinder top annulus (mcta).
10. Top cylinder wall (tcw).
11. Top cylinder top (tct).

Surfaces 1-8 will have to be divided into elements each at a uniform temperature for the purpose of configuration factor and later heat transfer calculations. The reason for that is the requirement that configuration factors be calculated between surfaces of uniform temperatures. Since it is desirable to simplify the system as much as possible without losing the heat transfer characteristics of the actual crystal puller, a comparison will be made between the heat transfer calculations obtained before and after simplifying the enclosure of the growth chamber (surfaces 5, 6, 9, 10 and 11) down to one surface.

The equations used for calculating the configuration factors between all surfaces are given in appendix A. The reciprocity relationship is used for surfaces that are not related by direct equations.

3.3.2 Description of the Analysed Cases

The following section describes the cases that are considered in the full chamber and simplified chamber configurations :

- System consisting of the melt, encapsulant and upper chamber. Configuration factors and heat transfer from the melt surface first and from the encapsulant

surface second are calculated . The reason for anlysing this case is to determine the radiative heat transfer that is taking place in the system during the seeding process which is a very crucial step of the crystal growth process. If too much heat is applied then the seed will melt, while not enough heat will cause the melt to freeze on the seed at a fast rate without allowing for good diameter control. Figure 3.3 shows a schematic of the full chamber including the elemental division of the surfaces, while figure 3.4 (a) shows the simplified chamber system.

- System consisting of the crystal growing at the rate of 1cm/hr past the encapsulant top taking into account the dropping melt level but without allowing the crucible to protrude into the upper chamber. All other surfaces included are as in the previous case. For this case, the crystal is growing at the indicated rate and thus the configuration factors are calculated for crystal height of 3cm, 4cm, 5cm... until the crystal height reaches the crucible edge. Since this growth process is a batch process, the melt height decreases thus exposing more of the crucible wall. The number of surfaces for this case is increased from the previous case by an amount equal to the number of elements on the crystal wall and crystal top. Figure 3.5 shows a schematic of the system and figure 3.4 (b) shows the simplified system.

- System consisting of melt, encapsulant, crystal and upper chamber with crystal extending above the crucible edge and the crucible protruding through the upper chamber. The number of surfaces here is increased from the previous case by the number of the elements on the outer surface of the crucible wall. The crucible protrudes through the upper chamber so that the centre of the heating goes through the centre of the melt. Figure 3.6 shows a schematic of the surfaces and figure 3.4 (c) shows the simplified chamber.

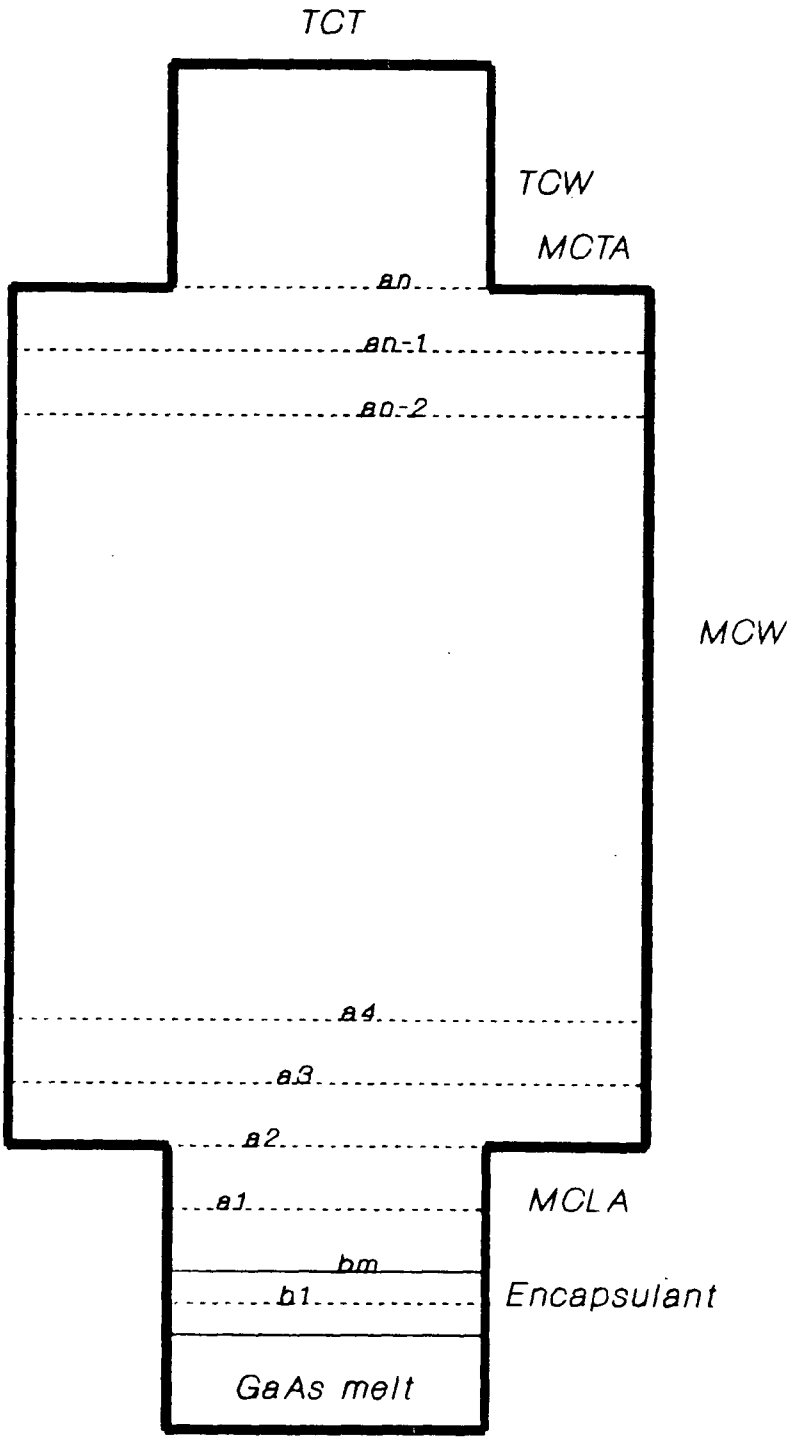

Figure 3.3: Schematic showing the system when there is no crystal (case–I).

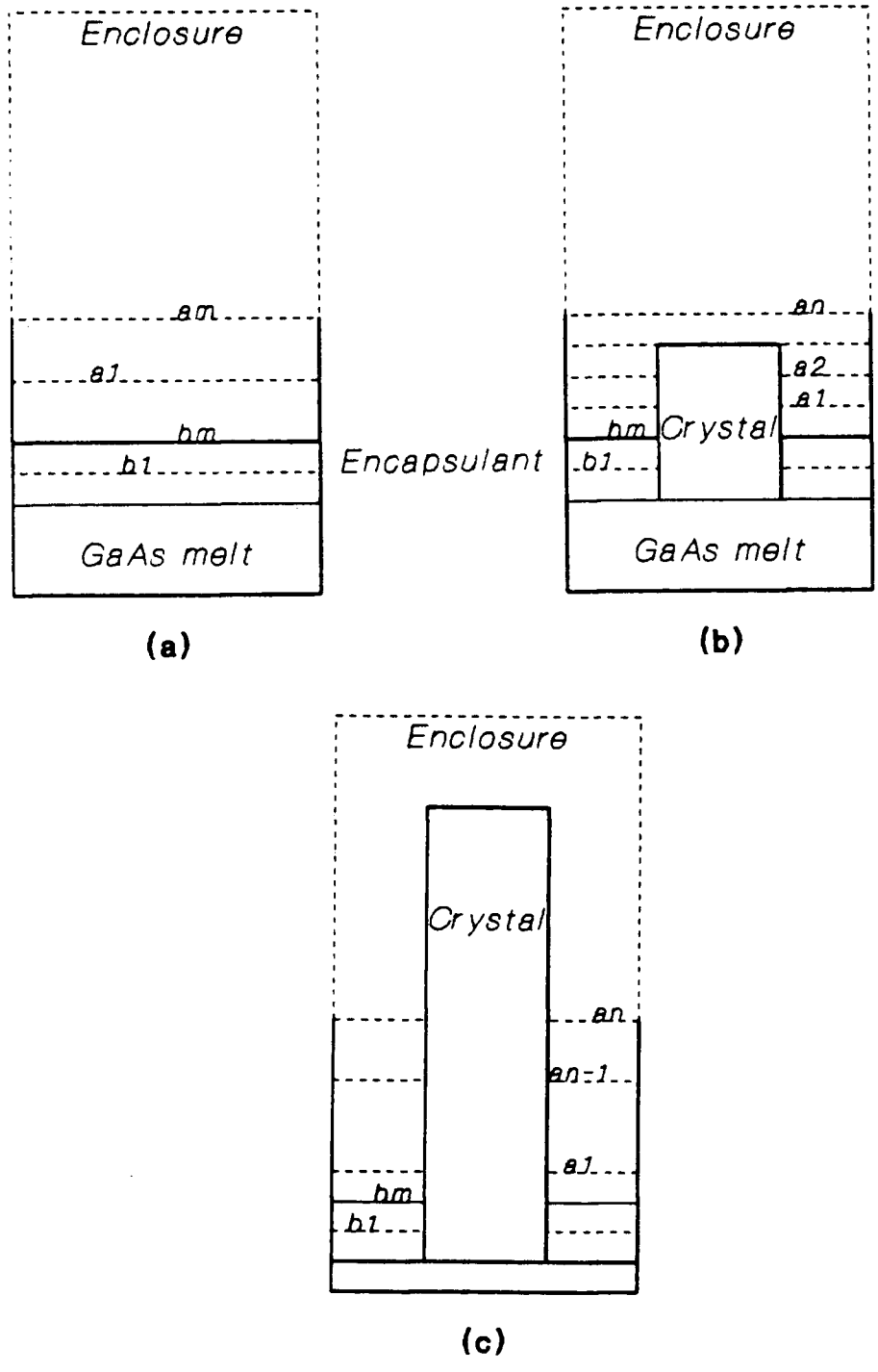

Figure 3.4: Schematic showing the simplified chamber system: (a)case–I, (b)case–II and (c)case–III.

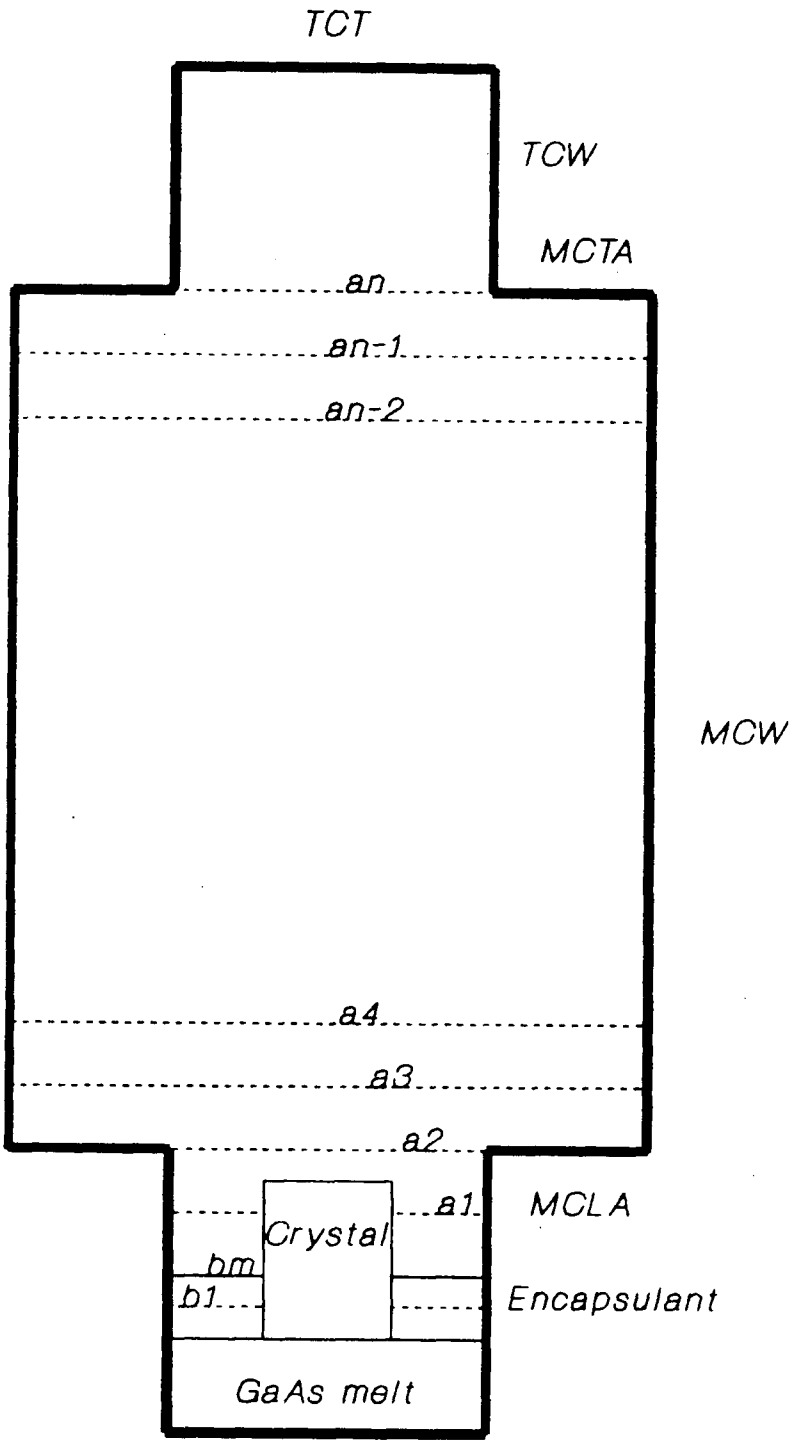

Figure 3.5: Schematic showing the surfaces under consideration for crystal height anywhere between the encapsulant top and the crucible edge (case–II).

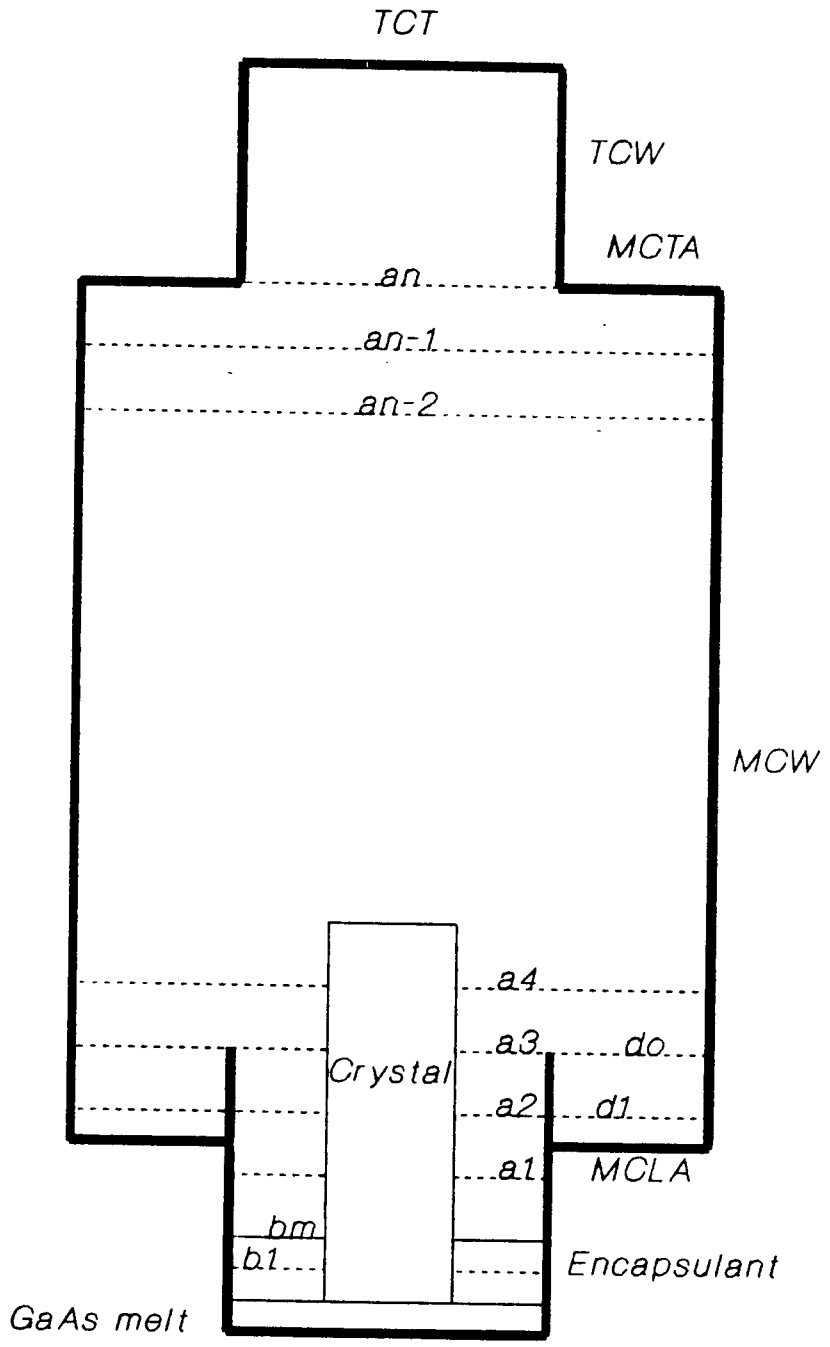

Figure 3.6: Schematic showing the surfaces for the crystal growing past the crucible edge (case–III).

The fictitious surfaces 'a', 'b' and 'd' shown in figures 3.3 to 3.6 are useful in evaluating the configuration factors from some surfaces to others. A description of configuration factor calculations for some surfaces is given in appendix A. The summation of the configuration factors from each surface to all other surfaces must be equal to one. Any deviation from one represents an error. Appendix D gives the results of configuration factor calculations for the simplified system described above.

3.4 Heat Transfer Model

The Gebhart method of determining radiative exchange between surfaces of an enlosure is used here. The method can be used whether heat fluxes or temperature distributions are specified. The general form of the heat equation from [43] obtained by a heat balance on surface k is :

$$Q_k = A_k \epsilon_k \sigma T_j^4 - \sum_{j=1}^{N} A_j \epsilon_j \sigma T_j^4 G_{jk} \tag{3.1}$$

where G_{jk} is the Gebhart factor which is defined as the fraction of the emission from surface A_j that reaches A_k and is absorbed. This includes all the paths for reaching A_k, that is, the direct path, paths by means of one reflection, and paths by means of multiple reflections. In equation form, G_{jk} is given by:

$$\begin{aligned} G_{jk} &= F_{j-k}\epsilon_k + F_{j-1}\rho_1 G_{1-k} + F_{j-2}\rho_2 G_{2-k} \\ &\quad + \ldots\ldots + F_{j-k}\rho_k G_{k-k} + \ldots\ldots + F_{j-N}\rho_N G_{N-k} \end{aligned} \tag{3.2}$$

Appendix B gives the derivation of the Gebhart factor equations for the system surfaces. It also gives the system of equations in matrix form and the method of solution of the

matrices forming the problem. The flow chart of the programme developed to solve the matrices and calculate the radiative heat transfer is given in appendix C.

The net radiation method which was devised by Hottel [40] and later developed by Poljak [41, 42] and the Gebhart method are all equivalent and give the same results. Gebhart's method was chosen in this thesis. The configuration factor calculations were verified by ascertaining that the summation of those factors for each elemental surface is equal to 1.

3.4.1 Diffuse–Gray Surfaces

This study will assume all surfaces to be diffuse–gray. According to [43], diffuse signifies that the emissivity and absorptivity do not depend on direction, and gray signifies that the spectral emissivity and spectral absorptivity do not depend on wave length. Thus, a diffuse–gray surface is one which absorbs a fixed fraction of the incident radiation from any direction and at any wavelength, and it emits a fixed fraction of blackbody radiation for all directions and wavelengths. This assumption is in–line with the data available for the emissivity of the surfaces, and until more data is available it will have to be used. As will be found in the section on material thermophysical properties, the data given is of the total normal emissivity of the surfaces as a function of surface temperature.

3.4.2 Encapsulant Layer Semitransparency

The absorption of the B_2O_3 encapsulant layer is very important for the determination of radiative heat transfer in the system. Only one source of experimental data is available (Ostrogorsky et al [21].) Tables 3.1 and 3.2 give the absorbance and absorption coefficient of B_2O_3 for three layer thicknesses : 1.0cm, 0.4cm and 0.2cm. The absorbance in table 3.1 is obtained from figure 10 of [21] — shown here in figure 3.7. While the absorption coefficient given in table 3.2 is calculated using equation 3.3. Ostrogorsky et al state

that the indicated layer thicknesses are approximate because they were computed from the removal of weighed quantities of B_2O_3. They also state that the non-planarity of the melt surfaces represents another uncertainty. Also, the loss of radiation intensity due to scattering of the radiation at the concave melt surface is increased by the long optical path between the sample and detector. Therefore, the uncertainty in this data should be taken into account when choosing a cutoff wavelength for the encapsulant (above which the encapsulant is opaque and below which it is transparent).

The absorption coefficient α is calculated by substituting the values of L and A in equation-4 of the same reference (repeated here for convenience),

$$A_{B_2O_3} = 0.434\alpha L \tag{3.3}$$

where A is the absorbance, α is the absorption coefficient and L is the layer thickness. Also, the optical transmittance τ is given by :

$$\tau = \frac{I(x)}{I(0)} = exp(-\alpha x) \tag{3.4}$$

where α is as defined earlier and x is a position along the path that the radiation is travelling.

An average thickness of the encapsulant layer during the growth of $GaAs$ crystals is about 2-cm. However, the data that is given is for a layer that is 1cm thick or less. Therefore, extrapolation from the available data is required (another factor of uncertainty). The transmittance at $\lambda = 2.0$ and $2.5\mu m$ is calculated using equation 3.4. The results are given in table 3.3. It is clear that as the layer thickness increases, τ decreases. Also, the values of τ are lower for $\lambda = 2.5\mu m$ than they are for $\lambda = 2.0\mu m$. Thus indicating that for layers thicker than 1cm, and for λ greater than 2.5 μm, the encapsulant is essentially opaque.

Ostrogorsky et al concluded from their data the following:

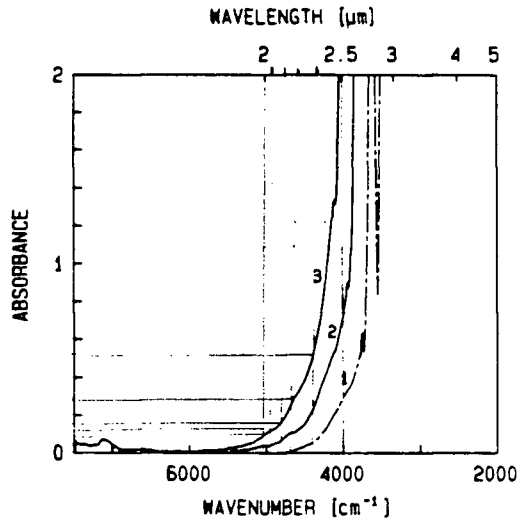

Figure 3.7: Absorbance spectra of B_2O_3 at $1250°C$ for L=0.2cm (1), L=0.4cm (2), and L=1.0cm (3). From Ostrogorsky et al.

Table 3.1: B_2O_3 absorbance for three layer thicknesses obtained from figure-3.7.

Wave Length $\lambda(\mu m)$	Absorbance 'A'		
	L = 1.0cm	L = 0.4cm	L = 0.2cm
2.0	0.081	0.032	0.00
2.1	0.10	0.036	0.00
2.2	0.14	0.064	0.00
2.3	0.23	0.097	0.00
2.4	0.48	0.19	0.032
2.5	2.00	0.71	0.29

Table 3.2: The absorption coefficient of B_2O_3 for three different layer thicknesses.

Wave Length $\lambda(\mu m)$	Absorption Coefficient ' α '		
	L = 1.0cm	L = 0.4cm	L = 0.2cm
2.0	0.19	0.19	0.00
2.1	0.24	0.20	0.00
2.2	0.34	0.37	0.00
2.3	0.52	0.56	0.00
2.4	1.12	1.12	0.37
2.5	4.61	4.09	3.34

- B_2O_3 is transparent for $\lambda < 2\mu m$.
- B_2O_3 is either transparent or opaque depending on the layer thickness for $1.9\mu m < \lambda < 2.8\mu m$.
- B_2O_3 is opaque for $\lambda > 2.8\mu m$.

Since only one source of data is available, and the source describes many areas of uncertainty, it seems impractical and unnecessary to divide the wave-spectrum to more than two regions, thus the decision to have one cutoff wavelength. For this work, the cutoff wavelength will be chosen as 2.0 μm. However, calculations using a cutoff wave length of 2.5 μm will be done for comparison.

The wavelength spectrum is then divided into two regions in order to consider the absorption property of the encapsulant. The first region is below $2\mu m$ where radiative exchange with the melt surface is considered. The second region is above $2\mu m$ where radiative exchange with the encapsulant surface is considered. Under that assumption, the radiative heat flux for any surface segment k will be given by:

$$Q_k = A_k\epsilon_k f_k'\sigma T_j^4 - \sum_{j=1}^{N} A_j\epsilon_j f_j'\sigma T_j^4 G_{jk}^{transparent} \quad for\ \lambda \leq 2 \tag{3.5}$$

$$Q_k = A_k\epsilon_k(1-f_k')\sigma T_j^4 - \sum_{j=1}^{N} A_j\epsilon_j(1-f_j')\sigma T_j^4 G_{jk}^{opaque} \quad for\ \lambda > 2 \tag{3.6}$$

where A_k is the surface area, ϵ_k is the emissivity of the surface, G_{jk} is the Gebhart factor and f'_k is the fraction of energy emitted at T_k below $2\mu m$.

The heat transfer from each surface is summed up and an effective ambient temperature can be calculated as follows :

$$T_{k,a} = (\frac{1}{A_k \epsilon_k}(\sum_{j=1}^{N} A_j \epsilon_j f'_j T_j^4 G_{jk}^{transparent} + \sum_{j=1}^{N} A_j \epsilon_j (1 - f'_j) T_j^4 G_{jk}^{opaque}))^{1/4} \qquad (3.7)$$

This effective temperature can be compared to a constant ambient temperature that the system would be radiating to if a simplified radiative model is used (Stefan's model). It is also used to produce the correct radiative heat flux from the surface when applying the radiative boundary condition during a complete analysis of heat transfer in the system (including conduction in the encapsulant and crystal, and convection in the melt and surrounding gas).

3.4.3 Materials' Thermophysical Properties

The thermophysical properties of the semiconductor $GaAs$, the encapsulant B_2O_3, the surrounding gas Ar, and the other chamber surfaces that form the crystal puller are important factors when calculating the fluid flow and heat tranfer in the puller during the crystal growth process. Jordan [19, 23, 32] presents detailed studies of the properties of $GaAs$ and B_2O_3. He also gives the convective heat transfer coefficient between the encapsulant and crystal, and between the high pressure gas, Ar, and the encapsulant and crystal. The radiative heat transfer coefficient from the $GaAs$ surface is also included. All equations that describe properties that are available from Jordan are included here for the sake of completeness. The equations that describe the heat transfer coefficients are also included.

The temperature dependent equations of $GaAs$ density (ρ'), specific heat (C_p), conductivity (k) and thermal expansion coefficient (β) are listed in table 3.4. The radiative

heat transfer coefficient from the melt and crystal surfaces is also given in the table. While the temperature dependent density and viscosity of the encapsulant B_2O_3 which are available from [30] and temperature dependent conductivity which is obtained from [31] are tabulated in 3.5. The convective heat transfer coefficient between the encapsulant and the crystal is also given in the table.

Table 3.6 gives the properties of high pressure *Ar*. The data is obtained from [33]. M is the molecular weight of argon, and R is the universal gas constant. p represents the gas pressure in atmospheres; it is introduced in the convective heat transfer equation as a correction factor to take into account the high gas pressure during the Czochralski crystal growth.

Properties Used by Different Modellers

Table 3.8 presents the physical properties of *GaAs* (melt and solid), the encapsulant and the chamber surfaces as used by various authors. Some of the references chose to use constant properties while others chose temperature dependent properties. Many references – all not listed in the table, but mentioned in the literature survey – used the values given by Jordan in [19, 23]. It is clear from the table that there is a wide range of values used for the emissivity of *GaAs* liquid and solid (0.3, 0.5, 0.55, 0.7 and 0.75). The values used for the emissivity of the encapsulant layer also varied from one source to another (0, 0.65, 0.75 and 1).

Surface Emissivities

Other sources [33, 34, 35] were researched for material properties especially for the emissivity of the surfaces. The emissivity is very important when calculating radiative heat transfer. Therefore, it is important to use the best representative values. The

Table 3.3: Transmittance for wave lengths of 2 and 2.5 μm for each layer thickness L = 0.2, 0.4 and 1.0cm.

$\lambda(\mu m)$	Transmittance 'τ'		
	L=0.2cm	L=0.4cm	L=1.0cm
2.0	1.00	0.93	0.83
2.5	0.51	0.20	0.01

Table 3.4: Temperature dependent properties of *GaAs*.

PROPERTY	*EQUATION*
Density $\rho'(gm/cm^3)$	$5.32 - 9.91 * 10^{-5}T$
Specific Heat $C_p(J/gm.K)$	$0.302 + 8.1 * 10^{-5}T$
Conductivity $k(W/m.K)$	$20800T^{-1.09}$
Therm. Exp. Coef $\beta(K^{-1})$	$4.68 * 10^{-6} + 3.82 * 10^{-9}T$
$h_{radiation}$ (cm^{-1})	$\frac{2.27*10^{-11}}{k}\epsilon_t T^3_{GaAs}$

Table 3.5: Temperature dependent properties of the encapsulant B_2O_3.

PROPERTY	*EQUATION*
Density $\rho'(gm/cm^3)$	$2.705 - 2.814 * 10^{-3}T + 2.677 * 10^{-6}T^2$ $-1.204 * 10^{-9}T^3 + 2.102 * 10^{-13}T^4$
Them. Exp. Coef. $\beta(K^{-1})$	$-\frac{1}{\rho'}\frac{\partial \rho'}{\partial T}$
Dyn. Viscosity $\mu(poise)$	$log_{10}\mu = -4.343 + 17040T^{-1} - 1.696 * 10^7T^{-2}$ $+7.081 * 10^9T^{-3}$
Conductivity $k(W/cm.K)$	$2.37 * 10^{-3} + 1.1 * 10^{-5}T$
Specific Heat $C_p(J/gm.K)$	1.83
$h_{convection}$ (cm^{-1})	$(\frac{T-T_{B_2O_3}}{l})^{1/4}0.548\frac{k_{B_2O_3}}{k}(g(-\rho'\frac{\partial \rho'}{\partial T}\frac{C_p}{k\mu})_{B_2O_3})^{1/4}$

Table 3.6: Thermophysical properties of high pressure argon as obtained from Touloukian.

PROPERTY	*EQUATION*
Density $\rho'(gm/cm^3)$	$P_{Ar}/(RT_{Ar})$
Therm. Exp. coef. $\beta(K^{-1})$	$1/T_{Ar}$
Dyn. Viscosity $\mu(poise)$	see table 3.7
Conductivity $k(W/cm.K)$	see table 3.7
Specific Heat $C_p(J/gm.K)$	0.5204
$h_{convection}$ (cm^{-1})	$(\frac{T-T_{Ar}}{l})^{1/4} * 0.548\frac{k_{Ar}}{k}(p)^{1/2}(\frac{M^2 g}{R^2 T_{Ar}^3}(\frac{C_p}{k\mu})_{Ar})^{1/4}$

Table 3.7: Viscosity and conductivity of Ar ignoring pressure dependence (from Touloukian).

Temp (K)	μ $(N.sec/m^2)$	k $(W/cm.K)$	*Temp* (K)	μ $(N.sec/m^2)$	k $(W/cm.K)$
600	38.2	$0.301 * 10^{-3}$	760	44.9	$0.356 * 10^{-3}$
620	39.1	0.308	780	45.7	0.362
640	40.0	0.315	800	46.4	0.369
660	40.9	0.322	820	47.2	0.375
680	41.7	0.329	840	47.9	0.381
700	42.5	0.336	860	48.6	0.387
720	43.3	0.343	880	49.4	0.393
740	44.1	0.349	900	50.1	0.398

Table 3.8: Materials' properties as reported in the references cited.

AUTHOR	SURFACE	PROPERTY				
		ρ' (gm/cm^3)	β (K^{-1})	k $(W/m.K)$	C_p $(J/g.k)$	ϵ
Kakimoto	B_2O_3	1.51	$3 * 10^{-5}$	2.0	1.836	N/A
Hicks [a]	B_2O_3	1.52	N/A	1.8	1.830	0.75
Motakef	B_2O_3	N/A	N/A	see [b]	N/A	N/A
& Witt [c]	$GaAs$	N/A	see [d]	see [e]	N/A	0.5
Derby	$GaAs_{melt}$	5.71	N/A	14	0.42	0.55
&	$GaAs_{solid}$	5.17	—	7	0.42	0.55
Brown	B_2O_3	1.51	N/A	2	N/A	0 & 1
	Graphite	1.6	—	0.6	2.1	0.8
	SiO_2liner	2.2	—	0.06	1.3	0.35
Crochet	$GaAs_{melt}$	5.63	$1.89 * 10^{-4}$	15.15	0.507	N/A
et al	$GaAs_{solid}$	5.71	—	15.15	0.507	N/A
Meduoye et al [f]	$GaAs$	N/A	$1 * 10^{-5}$	7.74	N/A	N/A
Thomas	$GaAs_{melt}$	5.71	N/A	14	0.42	0.3
et al	$GaAs_{solid}$	5.17	—	7	0.42	0.55 & 0.7
	B_2O_3	1.51	N/A	2 & 8	N/A	N/A, $\lambda \leq 2$ 0.65, $\lambda > 2$
Dupret	*Steel*	N/A	—	33	N/A	0.6
et al	*Graphite*	N/A	—	41.9	N/A	0.81
	Gr. Felt	N/A	—	2.5	N/A	N/A
Sabhapathy	$GaAs_{melt}$	5.71	$1.87 * 10^{-4}$	17.8	0.434	0.75
&	$GaAs_{solid}$	5.2	—	7	0.42	0.75
Salcudean	B_2O_3	1.5	$5 * 10^{-5}$	1.85	1.83	0.75

[a] $T_{crucible} = 1530K, T_{amb} = 1200K$
[b] $2.37 * 10^{-1} + 1.1 * 10^{-3}T$
[c] $T_{Ar} = 700K, T_{wall} = 400K, (Rad\#)_s = 0.5, (Rad\#)_{B_2O_3} = 1.0$
[d] $4.88 * 10^{-6} + 3.82 * 10^{-9}T$
[e] $208 * T^{-1.09}$
[f] used temperature dependent $h_{convection}$ that is available from Jordan.

emissivity of the melt (*liquid GaAs*), the crystal (*solid GaAs*), the crucible wall (*PBN pyrolytic boron nitride*), and the chamber walls (*stainless steel*) are all required.

Only one source [32] gives data for the emittance of n-type *GaAs* as a function of temperature and the product $C_d t$, where C_d is the doping level or impurity concentration in cm^{-3} and t is the crystal diameter in *cm.* (see figure 3.8). The data given in figure 3.8 was obtained by numerical integration of the spectral emittance between the limits 0.5 and 25 μm in 0.1 μm intervals. It is clear from the figure that the total emittance increases as the product $C_d t$ increases. For the temperature range of interest during crystal growth (1000–1500) K, and for a crystal diameter of 8cm and doping level of $1*10^{16} cm^{-3}$, the total emittance ϵ_t ranges from (0.61–0.66). As the impurity concentration increases for the same temperature range, the total emittance varies from (0.65–0.69). With these results for the crystal diameter and doping level chosen, it is not necessary to use temperature dependent emissivity for $GaAs_{solid}$. Thus, the calculations presented in this work use $\epsilon_t = 0.65$ for $GaAs_{solid}$.

Lemons and Bösch [38] state in their work that the emissivity of molten silicon is substantially lower when compared to that of solid silicon. The emissivity of the *GaAs* melt has not been evaluated experimentally but is expected to be different than that of the *GaAs* solid – in line with silicon. Thomas et al [20] used a value of 0.3 for the emissivity of molten *GaAs*. With lack of better information, the same value will be used here.

For p-type *GaAs*, Braunstein and Kane [39] determined the absorption coefficient between 2 and 25 μm. The result of their work states that the absorption coefficient increases with wavelength and temperature. Because of the high absorption coefficient, the total emittance is related only to the reflectivity. Therefore, the curve for $C_d t > 5 * 10^{17}$ serves as a reasonable estimate of ϵ_t for p-type *GaAs*.

Reference [33] gives data for the normal spectral reflectance and transmittance of

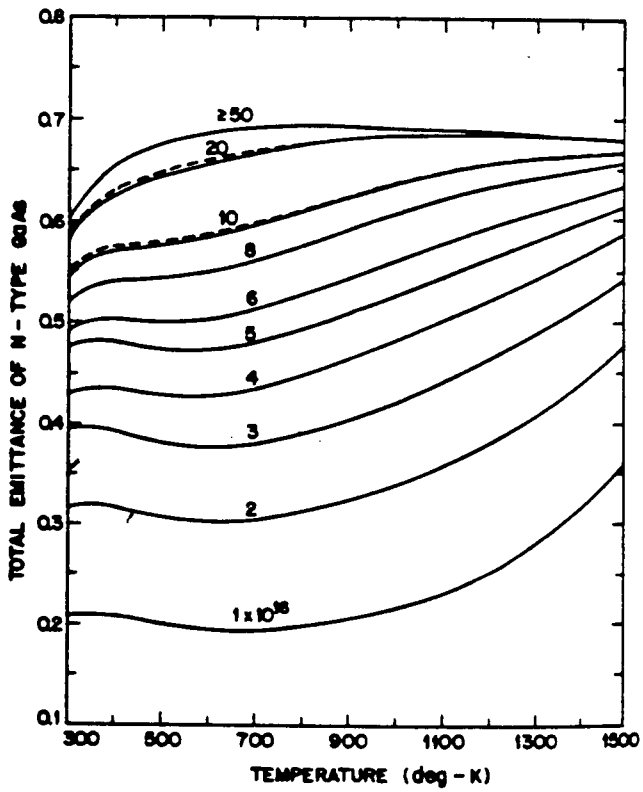

Figure 3.8: The emissivity of *GaAs* as function of temperature and doping density (from Jordan).

GaAs. However, the data is for room temperature only, which means that it is of no use for calculations of the crystal growth process. All other books on the thermophysical properties of materials surveyed [34, 35] do not provide any information on the emissivity of *GaAs*.

The emissivity of the encapsulant B_2O_3 is not available in any of the references researched. Since B_2O_3 is basically glass, the emissivity of glass at high temperatures is obtained from the Handbook of Chemistry and Physics and from [33]. Both references give a value of 0.7 for the emissivity of high temperature glass. Therefore, this study will use 0.7 as a representative value of the emissivity of the encapsulant.

The emittance of stainless steel is available from many sources. Touloukian et al [33] present an excellent collection of data for oxidized, polished and cleaned stainless steels for a wide range of temperature (320 – 1300)K. The graphs and data are available in appendix E. For the crystal puller chamber, cleaned stainless steel is assumed in the temperature range (450 – 800)K for which the normal total emittance range is (0.2 – 0.42).

3.5 Temperature Distribution of the Surfaces

The temperature distributions that are used to calcualte the heat transfer from each surface are based on results obtained from numerical and experimental results [12, 22, 26, 27, 25]. The values obtained are analysed to produce a temperature gradient across the surface which is used to evaluate the temperature of each element that the surface is divided to. The temperature equations used are given in table 3.9. The table gives also the temperature gradient across each surface. The gradient is the slope of the temperature equation.

Table 3.9: Temperature distribution of the surfaces obtained from numerical solutions for cases I, II and III.

SURFACE	TEMPERATURE DISTRIBUTION (K) (radii and heights in m)	TEMPERATURE GRADIENT (K/cm)
Melt (I)	$T_m(i) = 1511 + 656 * (r_m(i) + r_m(i-1))/2$	7
Melt (II & III)	$T_m(i) = 1511 + \frac{T_c(m)-T_s(m)}{r_c-r_s} * (r_m(i) + r_m(i-1))/2$	—
Encapsulant (I)	$T_e(i) = 1320 + 2625 * (r_e(i) + r_e(i-1))/2$	26
Encapsulant (II and III)	$T_e(i) = T_c(e) + \frac{T_c(e)-T_s(e)}{r_c-r_s} * (r_e(i) + r_e(i-1))/2$	—
Crucible (I & II)	$T_c(i) = 1565 - 1312 * (h'_c(i) + h'_c(i-1))/2$	13
Crucible (III)	$T_c(i) = 1530 - 2500 * (h'_c(i) + h'_c(i-1))/2$	25
Mid Cylinder Wall (MCW)	$T_{mc}(i) = 665 - 671 * (h'_{mc}(i) + h'_{mc}(i-1))/2$	7
MCLA	$T_{la}(i) = 1465 - 5249 * (r_{la}(i) + r_{la}(i-1))/2$	52
Crystal	$T_s(i) = 1511 - 3445 * (h'_s(i) + h'_s(i-1))/2$	34
Curcible Outer Wall	$T_{co}(i) = 1565 - 2500 * ((h'_{co}(i) + h'_{co}(i-1))/2 + (H'_c - H'_{co}))$	25
Crystal top	$T_{st} = T_s(ns) - 787 * (r_{st}(i) + r_{st}(i-1))/2$	8
MCTA	$T_{mcta} = 415$	0
TCW	$T_{tcw} = 315$	0
TCT	$T_{tct} = 315$	0

3.6 Analysis of Results

3.6.1 Five Surfaces Enclosure

The results that are given here are obtained using crystal puller dimensions and melt and surface properties that are given in table 3.10. These results are dependent on the temperature distributions which are the best possible estimates. However, some general conclusions can be made regarding the assumptions that are used when analysing global heat transfer in the system. The results of the heat transfer calculations are given in tables 3.11 through 3.15. The calculated effective ambient temperatures for each surface element are plotted versus element number in figures 3.9 to 3.11. The analysis of these results is given next for each case.

3.6.2 Analysis of the results for case–I

Table 3.11 gives the heat transfer from each surface to other surfaces in the enclosure. It also gives the total heat absorbed and emitted and the net heat transferred from each surface. The net exchanged in the system is 4.2kW. The melt, crucible, encapsulant and the middle cylinder lower annulus lose heat, while the middle cylinder wall and the other three surfaces absorb the heat lost from the other surfaces.

The following notes describe the exchange of each surface:

- The melt loses heat mainly to the crucible wall and the middle cylinder wall. It absorbs heat from the crucible.
- The crucible exchanges heat mainly with the encapsulant. It loses six times as much heat to the middle cylinder wall as it does to the melt.
- The middle cylinder wall absorbs heat from the melt, encapsulant, lower annulus and its surface at the same order of magnitude. However, it absorbs heat from the

Table 3.10: Dimensions and surface properties of the crystal puller.

DIMENSION or PROPERTY	SURFACE						
	Melt	Encap	Crucible	Crystal	MCW	MCLA,-TA	Top Cyl
Diameter						(D_i, D_o)	
(mm)	—	—	152.4	76.2	304.8		152.4
(inch)	—	—	6.0	3.0	12.0	(D_c, D_{mc})	6.0
Height							
(mm)	48	20	90–130	0–203	372.5	—	101.6
(inch)	1.9	0.79	3.5–5.1	0–8.0	14.67	—	4.0
ϵ	0.3	0.70	0.5	0.64	0.3	0.3	0.3
Mass							
(Kg)	5.0	—	—	—	—	—	—
Density							
(Kg/m^3)	5720	—	—	5200	—	—	—

Table 3.11: Heat transferred (in Watts) from surface i to surface j for case–I.

SURFACE j	SURFACE i							
	Melt	Crucible	MCW	MCLA	Encap	MCTA	TCW	TCT
Melt	13	262	0	2	—	0	0	0
Crucible	294	2232	17	33	1043	1	0	0
MCW	144	1652	335	928	800	19	3	1
MCLA	19	176	70	118	111	2	0	0
Encapsulant	—	1064	26	41	146	1	0	0
MCTA	25	199	48	115	125	3	0	0
TCW	12	99	26	74	61	1	3	1
TCT	7	43	11	33	35	0	1	0
Emitted (2)	514	5727	533	1344	2321	27	7	2
Absorbed (1)	277	3620	3882	496	1278	515	277	130
Net (2)-(1)	237	2107	-3349	848	1043	-488	-270	-127

crucible that is one order of magnitude higher than the other surfaces.

- The lower annulus exchanges heat mainly with the middle cylinder wall. It also absorbs, through multiple reflections, heat generating from its surface.
- The encapsulant radiates mainly to the crucible and the middle cylinder wall. It absorbs heat from the crucible and, through multiple reflections, from its surface.
- The heat exchanged with the middle cylinder top annulus, top cylinder wall and top is one to three orders of magnitude less than that exchanged between the other surfaces.

Figure 3.9 shows the effective ambient temperature of the surface elements versus the element number. The plot shows clearly that assuming one constant ambient temperature for all surfaces – or all elements of a surface – is a poor assumption. The jump in the crucible curve at node–4 is due to the exposure at that node to the encapsulant surface where a higher radiative exchange between the surfaces takes place. The jump in the middle cylinder wall curve is due to the higher exposure of node–2 to the melt and encapsulant than node–1. Eventhough the melt surface temperature is higher than the encapsulant surface temperature, its effective ambient temperature is lower since only the percentage of the heat radiated below $2\mu m$ reaches the melt from the crystal, crucible and other surfaces. The effective ambient temperature range for this case is (750–1350) K.

3.6.3 Analysis of the results for case–II

The results obtained for this case are calculated for a crystal height of 61–mm (2.4–in). The numerical values of the heat transfer between the surfaces are given in tables 3.12 and 3.13. The net exchange for this case is 2.7kW. The melt, encapsulant, crucible,

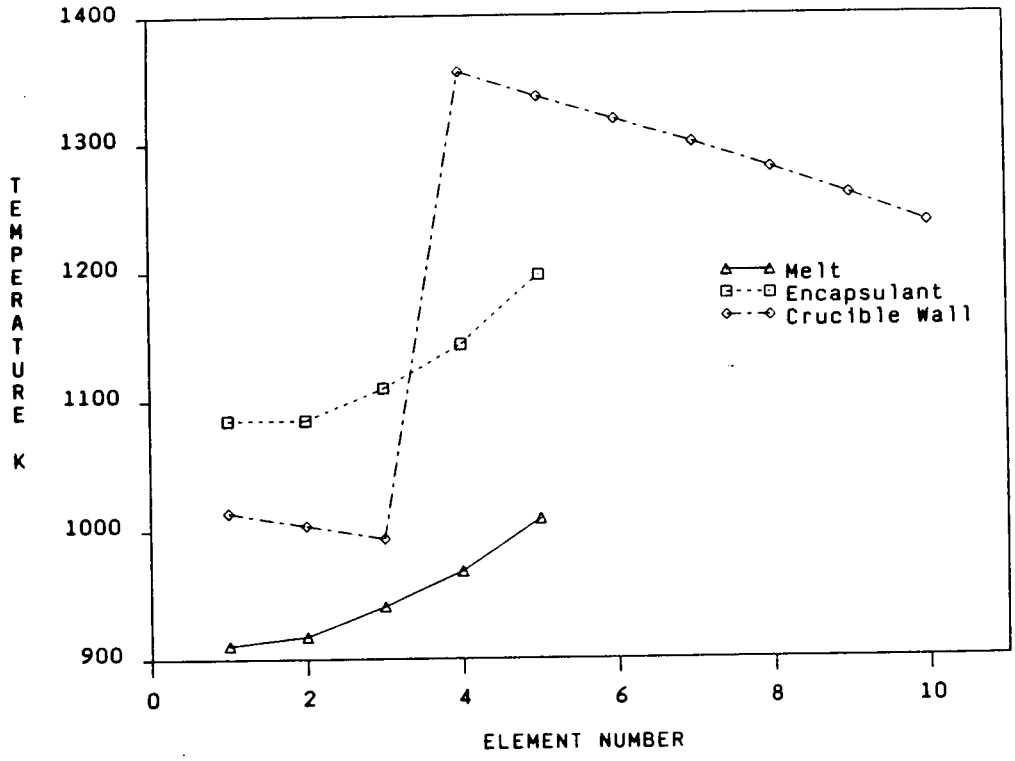

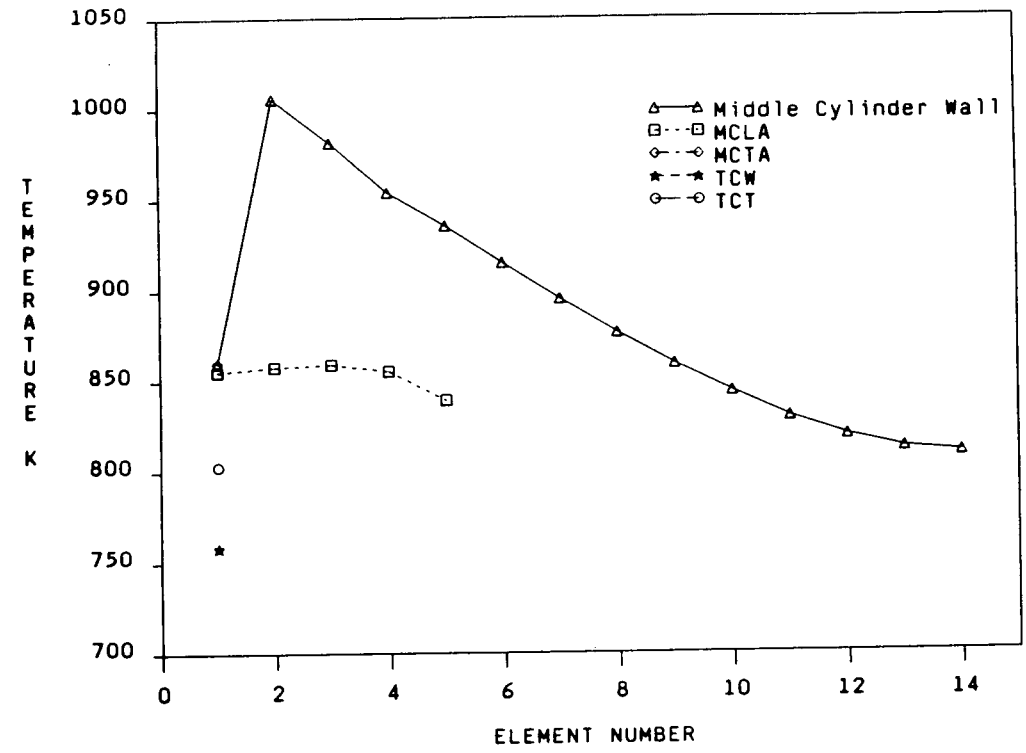

Figure 3.9: Effective ambient temperature versus element number for case–I.

crystal and the middle cylinder lower annulus lose heat, while the middle cylinder wall and the other three surfaces absorb heat. The following notes describe the exchange of each surface. (The numbers between brackets represent the percentage of heat lost or gained by the surface.)

- The melt exchanges heat mainly with the crucible and crystal walls (about 72% of total heat lost and 92% of total heat gained.)

- The crucible wall exchanges heat with (loses to and absorbs from) the encapsulant, crystal, middle cylinder wall and itself. It loses heat to the middle cylinder wall. All quantities lost or absorbed are of the same order of magnitude, however, that exchanged with the melt and crystal top are 2 to 10 times lower.

- The middle cylinder wall absorbs heat from the lower annulus (35%), crucible (22%), encapsulant (12%), crystal (6%), and from its surface(13%).

- The middle cylinder lower annulus loses heat to the middle cylinder wall and top annulus. It absorbs heat from the middle cylinder wall and itself (through multiple reflections). The quantity that is lost to the middle cylinder wall is nine times higher than that lost or absorbed from the other surfaces.

- The encapsulant exchanges heat with the crucible, crystal and it loses heat to the middle cylinder wall . The quantity of heat that is absorbed from the crucible is 4–10 times higher than that absorbed or lost to the other surfaces.

- The crystal loses heat to the crucible wall, the encapsulant, the middle cylinder wall. It absorbs heat from the crucible and the encapsulant. The amount of heat that is exchanged with the crucible wall is 4–6 times higher than that exchanged with the other surfaces.

Table 3.12: Heat transferred (in Watts) from surface i to surface j for case–II / i represents major surfaces.

SURFACE j	SURFACE i					
	Melt	Crucible	MCW	MCLA	Encapsulant	Crystal
Melt	17	157	0	0	—	58
Crucible	159	1204	12	23	527	710
MCW	58	583	334	926	328	153
MCLA	9	86	70	118	51	23
Encapsulant	—	960	13	18	127	266
Crystal	82	952	4	8	252	154
Crystal Top	1	40	8	14	8	6
MCTA	4	39	47	115	23	10
TCW	2	22	26	74	13	6
TCT	1	10	11	33	6	3
Emitted (2)	333	4054	525	1330	1333	1389
Absorbed (1)	233	2662	2624	390	1391	1457
Net (2)-(1)	100	1392	-2099	940	-59	-68

Table 3.13: Heat transferred (in Watts) from surface i to surface j for case–II / i represents minor surfaces.

SURFACE j	SURFACE i			
	Crystal Top	MCTA	TCW	TCT
Melt	1	0	0	0
Crucible	26	0	0	0
MCW	219	19	3	1
MCLA	32	2	1	0
Encapsulant	7	0	0	0
Crystal	5	0	0	0
Crystal top	6	0	0	0
MCTA	32	3	0	0
TCW	16	1	3	1
TCT	9	0	1	0
Emitted (2)	353	25	8	2
Absorbed (1)	83	273	164	74
Net (2)-(1)	270	-248	-156	-72

- The crystal top loses heat mainly to the middle cylinder wall (62% of total heat lost).
- The quantities exchanged between the top cylinder wall and top and all other surfaces are 1–5 orders of magnitude less than those exchanged between the other surfaces.

Figure 3.10 shows the effective ambient temperature versus the element number for the system surfaces. The jump in the crucible wall and crystal curves show the effect of higher heat gain due to location above the encapsulant layer. Element 4 on the crystal and crucible surfaces is the first one above the encapsulant top. The general shape of the melt and encapsulant curves is the same – as expected. However, the encapsulant curve is higher than the melt curve – also as expected. Figure 3.10 also shows a jump at element 2 on the middle cylinder wall curve which is due to exposure of that element to the crucible, crystal and encapsulant more than element 1. The range of the equivilent ambient temperature in this case is (650–1400) K.

3.6.4 Analysis of the results for case–III

Tables 3.14 and 3.15 give the heat transferred between all the surfaces. They also give the total heat absorbed and emitted and the net transferred from each surface. The net heat exchanged in this case is 3.9kW. The crucible, melt, crystal wall and top and middle cylinder lower annulus lose heat. While the encapsulant, middle cylinder wall and top annulus, the top cylinder wall and top absorb the heat lost by the other surfaces. The crystal height in this case is 20.3-cm (8.0-in). The following notes describe the exchange of each surface with the other surfaces. (The percentages in brackets represent percent of total heat that is lost or gained by the surface.)

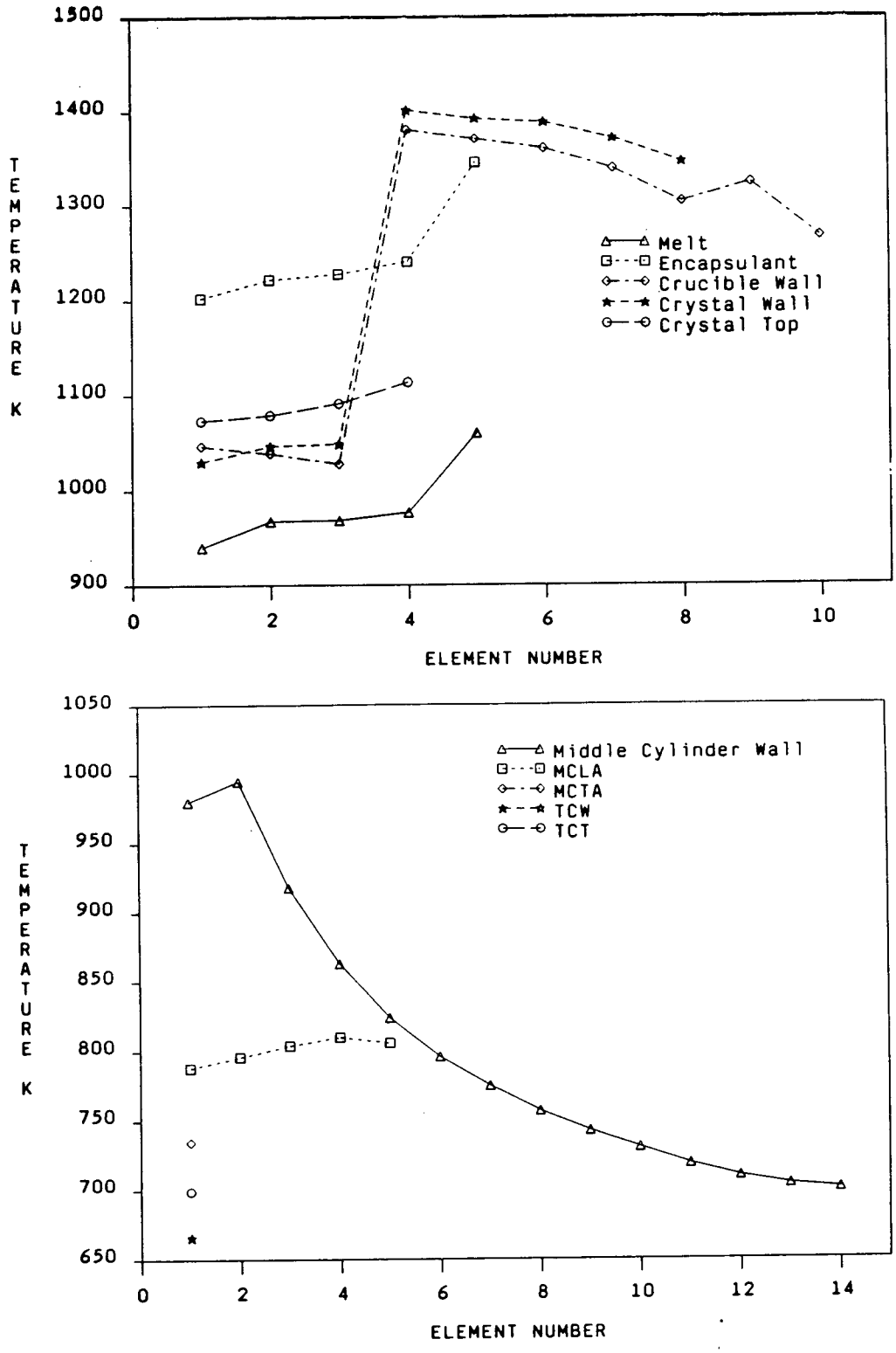

Figure 3.10: Effective ambient temperature versus element number for case–II.

Table 3.14: Heat transferred (in Watts) from surface i to surface j for case–III / i represents major surfaces.

SURFACE j	SURFACE i						
	Melt	Crucible	MCW	MCLA	Encap	Crystal	Crucible OW
Melt	15	136	2	0	—	65	0
Crucible	184	1970	3	4	728	1827	10
MCW	7	262	290	593	50	685	1460
MCLA	1	42	58	82	6	87	486
Encapsulant	—	1078	1	1	133	395	2
Crystal	94	2441	44	65	446	665	140
Crucible OW	1	39	63	276	5	78	346
Crystal Top	0	3	7	7	1	10	13
MCTA	0	18	32	37	5	56	60
TCW	0	19	18	50	3	28	51
TCT	0	7	9	24	1	12	25
Emitted (2)	304	6016	525	1140	1377	3908	2591
Absorbed (1)	217	4718	3465	771	1610	3902	814
Net (2)-(1)	87	1298	-2940	369	-233	6	1777

Table 3.15: Heat transferred (in Watts) from surface i to surface j for case–III / i represents minor surfaces.

SURFACE j	SURFACE i			
	Crystal Top	MCTA	TCW	TCT
Melt	0	0	0	0
Crucible	1	0	0	0
MCW	99	16	2	1
MCLA	6	2	0	0
Encapsulant	0	0	0	0
Crystal	6	1	0	0
Crucible OW	5	1	0	0
Crystal top	2	1	0	0
MCTA	20	2	0	0
TCW	10	1	3	1
TCT	6	0	1	0
Emitted (2)	155	24	6	2
Absorbed (1)	44	230	184	87
Net (2)-(1)	111	-206	-178	-85

- The melt loses heat mainly to the crucible wall (61%) and the crystal (31%). It absorbs heat from the crucible wall (63%).

- The crucible loses heat to the encapsulant, the crystal and itself by an amount that is one order of magnitude higher than that to the melt or the middle cylinder wall. It absorbs heat from the crystal, the encapsulant and melt. The heat absorbed from the crystal is one order of magnitude higher than that absorbed from the melt.

- The middle cylinder wall radiates heat mainly to itself through multiple reflections (55%). It absorbes heat from the crucible (50%), the lower annulus and the crystal.

- The middle cylinder lower annulus radiates mainly to the middle cylinder wall (52%) and the crucible outer wall (24%). It absorbs heat from the crucible outer wall (63%).

- The encapsulant exchanges heat mainly with the crucible and the crystal (about 85% of heat lost and 82% of heat gained).

- The crystal radiates to the crucible (46%), encapsulant, middle cylinder wall and itself – through multiple reflections (44% of total heat lost). It absorbs heat from the crucible mainly (63%) and also from the encapsulant.

- The outer wall of the crucible radiates heat mainly to the middle cylinder wall and the lower annulus (75% of total heat lost). It absorbs heat from the lower annulus (34%) and itself (43%) through multiple reflections.

- The heat exchanged with the crystal top, middle cylinder top annulus, top cylinder wall and top is one to three orders of magnitude less than that exchanged between the other surfaces.

Figure 3.11 shows the effective ambient temperature versus the element number for case–III. The jumps in the crystal curve at nodes 4 and 18 are due to the increased heat exchange with the crucible wall at node–4 and with the middle cylinder wall at node–18. The general shape of the crucible, melt and encapsulant curves is the same as in the previous cases. The temperature range for these surfaces is (650–1400)K in this case.

3.6.5 One Surface Enclosure

The middle cylinder wall, lower and top annuli, and the top cylinder wall and top are replaced by one surface that is referred to as the enclosure. Radiative heat transfer calculations are then performed for the three cases discussed earlier in order to compare the results of the full chamber and the simplified chamber. The numerical values of the heat transferred are given in tables 3.16 to 3.18. The plots of the effective ambient temperature versus the element number are given in figures 3.12 to 3.14. The following is a detailed analysis of each case.

3.6.6 Analysis of Case–I

Table 3.16 gives the heat transfer results for case–I. The net heat exchanged in the system is 2.6kW. The crucible, melt and encapsulant lose heat to the enclosure which is at 600K. The following notes describe the exchange of each surface:

- The melt loses heat to the crucible wall and the enclosure at the same order of magnitude. It absorbs heat from the crucible wall while not absorbing anything from the enclosure.
- The encapsulant exchanges heat with the crucible. It loses heat to the enclosure and absorbs heat originating from its surface through multiple reflections.
- The crucible exchanges comprable quantities with all surfaces (including itself).

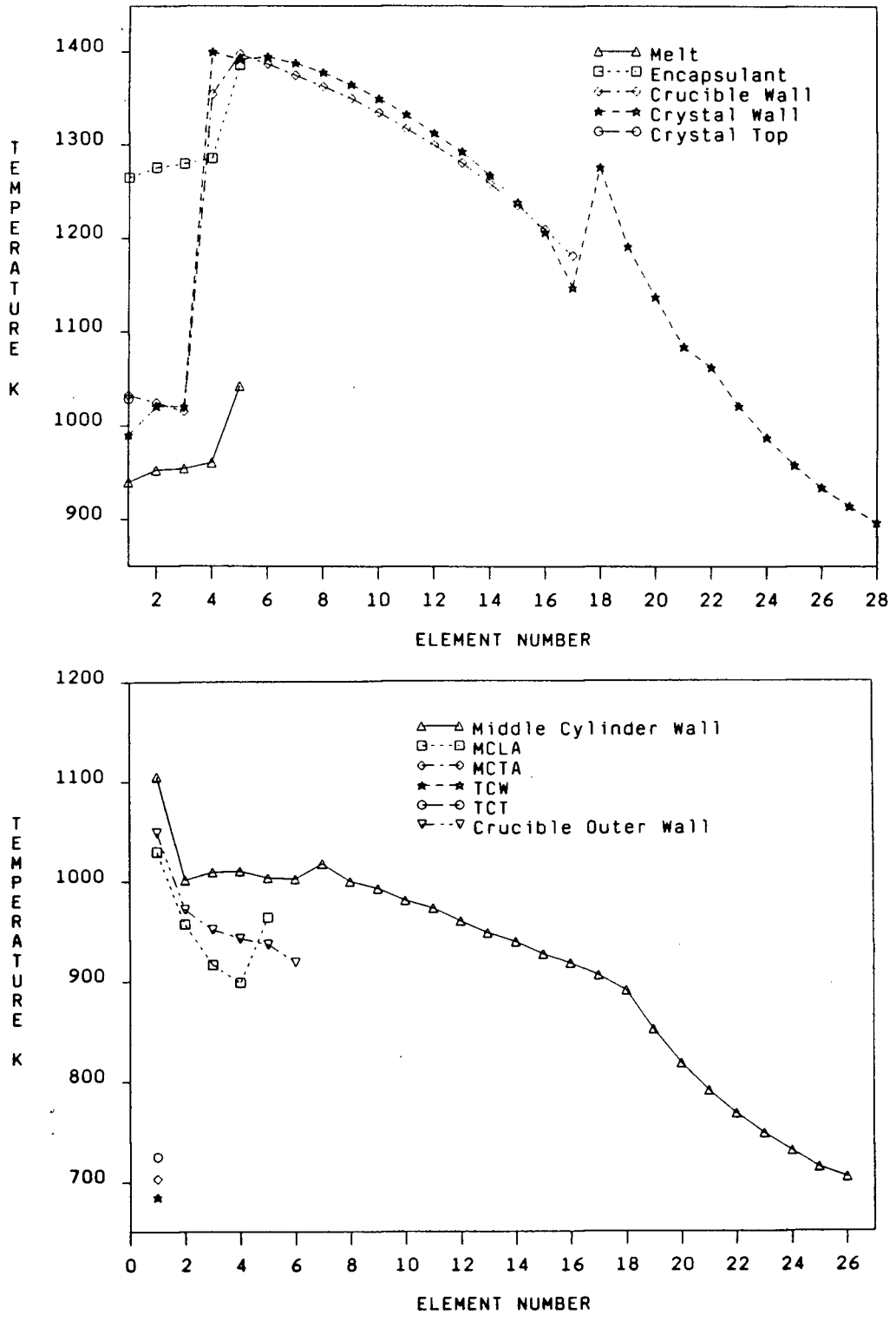

Figure 3.11: Effective ambient temperature versus element number for case–III.

- The enclosure being at a lower temperature absorbs heat from all other surfaces.

Figure 3.12 shows the effective ambient temperature versus element number for this case. It is clear that the general shape of the graph is the same as that for the full chamber case. However, the numerical values are (3–8) % higher for the simplified case.

3.6.7 Analysis of Case–II

Table 3.17 gives the results of the radiative heat transfer calculations for a crystal height that is less than the crucible wall height (2.6-in). The net heat exchanged in this case is 2.1kW. The crucible, melt, crystal and encapsulant lose heat to the enclosure which is at 600K. The following notes can also be obtained by further examination of the table :

- The melt exchanges heat mainly with the crucible and crystal (about 67% of total heat lost and 90% of total heat gained).

- The crucible wall loses heat to the encapsulant, enclosure and crystal wall, and absorbs heat from the encapsulant, crystal wall and itself. All those exchanges are of the same order of magnitude.

- The encapsulant loses heat to the crucible (36%), enclosure (30%) and crystal wall (16%). It absorbs heat from the crucible wall (65%), the crystal (16%) and itself (14% - through multiple reflections). The exchange between the encapsulant and the other surfaces is one to two orders of magnitude lower.

- The crystal wall exchanges heat with the crucible (48% of total heat lost and 64% of total heat gained), encapsulant (18% lost and 17% gained) and enclosure (18% lost and 11% gained). The exchange with the melt is 4–10 times lower than that with the crucible and encapsulant.

Table 3.16: Heat transferred (in Watts) from surface i to surface j for case–I with one surface enclosure.

SURFACE j	SURFACE i			
	Melt	Crucible	Encap	Enclosure
Melt	25	317	—	0
Crucible	361	2870	1305	8
Encapsulant	—	1323	331	6
Enclosure	145	1675	803	10
Emitted (2)	531	6185	2439	24
Absorbed (1)	342	4544	1660	2633
Net (2)-(1)	189	1641	779	-2609

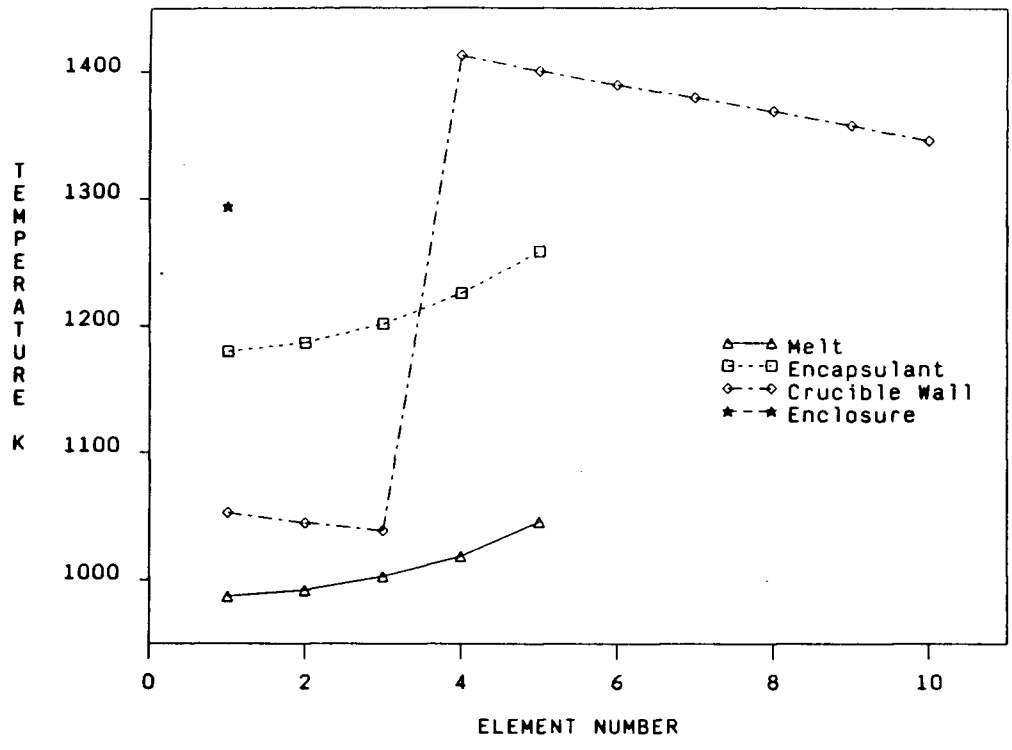

Figure 3.12: Effective ambient temperature versus element number for case–I / one surface enclosure.

- The crystal top loses heat to the enclosure (60%) and to the crucible wall, it absorbs heat from the crucible wall (47%) and the encapsulant (20%). The exchange with the other surfaces is 1–2 orders of magnitude lower.

- The enclosure absorbs heat mainly from the crucible, encapsulant and crystal wall. It also absorbs heat from the melt and itself, however that exchange is 5–7 times lower.

The effective ambient temperature versus element number is given in figure 3.13. The plot has the same general shape as that for the case of the full chamber. The temperatures are about (2–7) % higher than those of the full chamber case. The differences are expected since the geometry of the two systems is different. However, since the percentage difference range is low it can be accepted as a tradeoff to lower computing time. (The CPU time for this case is reduced by 63% from 628sec to 233sec). The temperature range here is (950–1450) K.

3.6.8 Analysis of Case–III

Table 3.18 gives the numerical results of the heat transfer between the surfaces for case—III. The net heat exchanged in the system is 1.6kW. The crucible, melt, encapsulant and crystal lose heat to the enclosure which is at 600K. The following is a brief description of the exchange of each surface seperately:

- The melt loses heat to the crucible (46%) and crystal wall (35%). It absorbs heat from the crucible wall (60%) and crystal (31%).

- The encapsulant loses heat to the crucible (39%), crystal wall (33%) and enclosure, while it absorbs heat mainly from the crucible (59%) and crystal (28%) walls . It also absorbs, through multiple reflections, heat generated from its surface.

Table 3.17: Heat transferred (in Watts) from surface i to surface j for case–II with one surface enclosure.

SURFACE j	SURFACE i					
	Melt	Crucible	Encap	Enclosure	Crystal Wall	Crystal Top
Melt	21	169	—	0	58	5
Crucible	174	1159	604	23	731	89
Encapsulant	—	1072	229	22	271	54
Enclosure	93	978	495	56	277	327
Crystal Wall	84	973	263	8	161	28
Crystal Top	11	142	61	13	35	40
Emitted (2)	383	4493	1652	122	1533	543
Absorbed (1)	253	2780	1648	2226	1517	302
Net (2)-(1)	130	1713	4	-2104	16	241

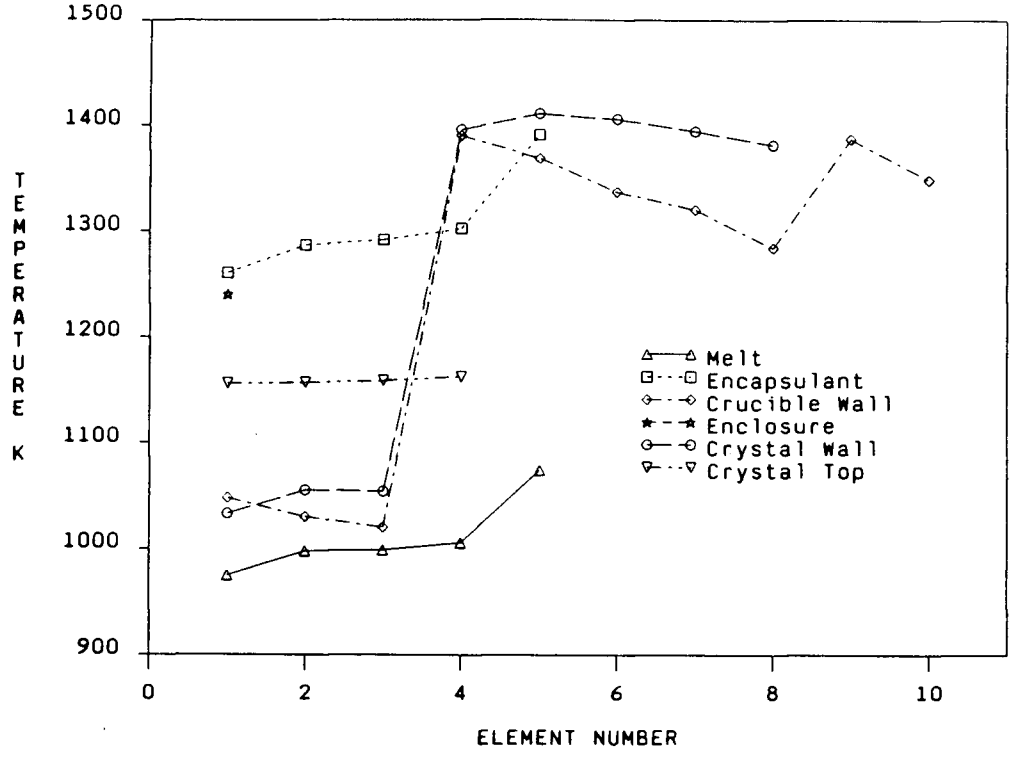

Figure 3.13: Effective ambient temperature versus element number for case–II / one surface enclosure.

- The crucible exchanges heat mainly with the encapsulant and crystal and itself. It also loses heat to the melt and enclosure that is 5–10 times lower than to the other surfaces.

- The enclosure absorbs heat from the crucible, encapsulant and crystal wall — all of the same order of magnitude.

- The crystal wall exchanges heat with the crucible (37% of total heat lost and 49% of total heat gained) and encapsulant (11% of lost and 15% of gained). It also loses heat to the enclosure (22%) and gains heat originating from its surface (28% - through multiple reflections).

- The crystal top loses heat mainly to the enclosure (46%) and it absorbs heat from the crystal wall (49%) through multiple reflections.

Figure 3.14 shows the effective ambient temperature versus the element number of each surface. The general shape of the curves is similar to the full chamber case. The temperature range is (900 - 1400) K. The effective ambient temperatures for this case are within one percent of those for case-III with five surfaces enclosure (except for the crystal top 10 nodes where the differences are higher, 8%). That is explained by the fact that the melt, encapsulant, crystal and crucible walls exchange a higher percentage of heat with each other than with the other surfaces. Again, the differences for this case are accepted as a trade off to lower computing time (CPU time is reduced by 63% from 704sec to 263sec).

3.7 Results of the simplified Case–III with Cutoff Wavelength 2.5 μm

The results obtained using a transparent/opaque cutoff wave length $\lambda = 2.5\mu m$ instead of $\lambda = 2.0\mu m$ are given in table 3.19. The effective ambient temperature is plotted

Table 3.18: Heat transferred from surface i to surface j for case-III with one surface enclosure in Watts.

SURFACE j	SURFACE i					
	Melt	Crucible	Encap	Enclosure	Crystal Wall	Crystal Top
Melt	18	122	—	0	64	0
Crucible	178	1093	647	15	1463	15
Encapsulant	—	910	176	11	433	10
Enclosure	49	437	252	27	848	75
Crytal Wall	133	1754	546	58	1010	55
Crystal Top	6	54	31	10	106	9
Emitted (2)	384	4370	1652	121	3924	164
Absorbed (1)	204	3411	1540	1688	3556	216
Net (2)-(1)	180	959	112	-1567	368	-52

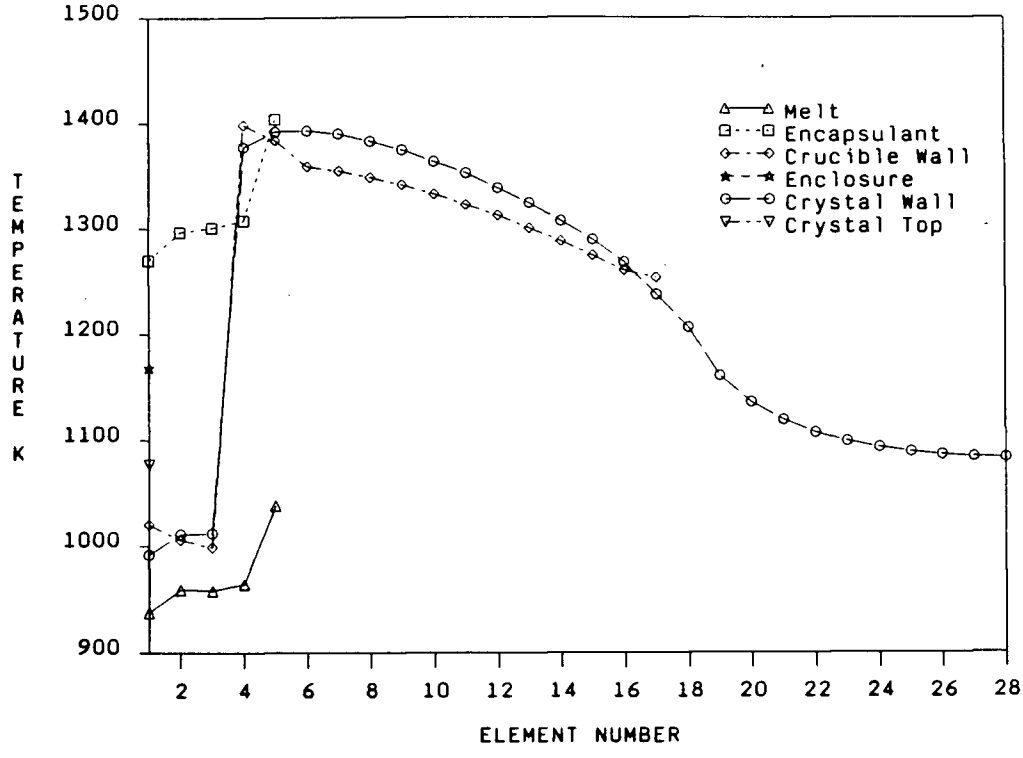

Figure 3.14: Effective ambient temperature versus element number for case–III / one surface enclosure.

versus element number in figure 3.15. It is clear that the effect of increasing the cutoff wavelength from $2\mu m$ to $2.5\mu m$ is the increase of the heat exchange with the melt surface and a decrease of exchange with the encapsulant surface. However, the exchange between the other surfaces did not change significantly (5–10 % difference only). Comparing figures 3.14 and 3.15 that show the effective ambient temperature, indicates that all the curves have the same general shape in both cases. However, the melt and encapsulant curves are closer in figure 3.15 than they are in figure 3.14 due to the increase (decrease) in the melt(encapsulant) heat transfer rate.

The effective ambient temperature effects the fluid flow in the melt which also effects the liquid/solid interface. It is therefore important to obtain the correct cutoff wave length for better modelling of the fluid flow and heat transfer in the crystal puller.

3.8 Comparison of the Results of the Full and Simplified Chambers

A comparison between the values of the heat transfer and equivilent ambient temperatures that are obtained for both chambers is done in order to decide the importance of including the full chamber. The reported results show that the melt, encapsulant, crucible and crystal walls exchange heat between each other by higher percentages than they do with the other surfaces. The other surfaces being the middle cylinder wall, top and lower annuli, and the top cylinder wall and top for the full chamber case. While for the simplified chamber, the other surfaces are simply the enclosure.

The comparison between the effective ambient temperatures $T_{k,a}$ of both chambers shows that those of the simplified chamber are generally 5% higher than those of the full chamber. The slight difference due to chamber geometry difference is expected and accepted. Also, the curves have the same trend as those of the full chamber case.

Table 3.19: Heat transferred from surface i to surface j for case-III with one surface enclosure in Watts for $\lambda = 2.5\mu m$.

SURFACE j	SURFACE i					
	Melt	Crucible	Encap	Enclosure	Crystal Wall	Crystal Top
Melt	28	189	—	0	102	0
Crucible	274	1251	527	16	1551	10
Encapsulant	—	747	138	10	345	6
Enclosure	76	440	190	27	708	49
Crytal Wall	209	1883	439	58	952	36
Crystal Top	10	55	24	10	88	6
Emitted (2)	597	4565	1318	121	3746	107
Absorbed (1)	319	3629	1248	1490	3577	193
Net (2)-(1)	278	936	72	-1369	169	-86

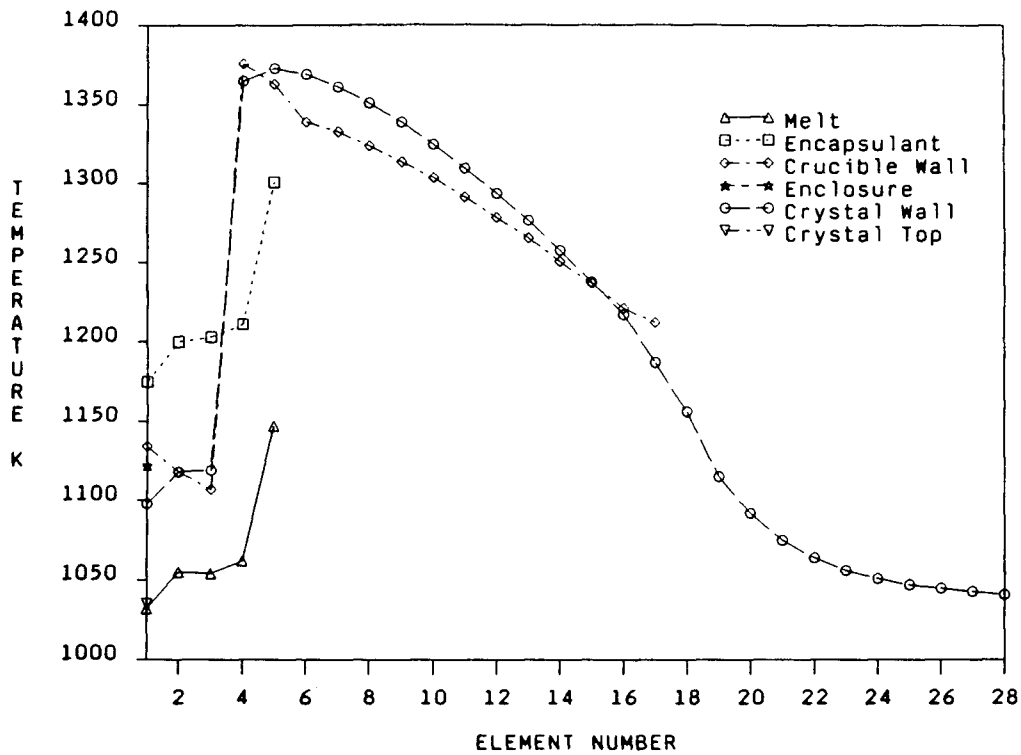

Figure 3.15: Effective ambient temperature versus element number for case–III / one surface enclosure and $\lambda = 2.5\mu m$.

3.9 Conclusions

Eventhough the results in this chapter are obtained using temperature distributions from previous numerical models, they still show the importance of a detailed radiative heat transfer model in GaAs crystal pullers. The effective ambient temperatures obtained for the surface elements show that the use of one ambient temperature for all surfaces introduces errors in the calculation of radiative heat transfer. The comparison between the results of the full and simplified chambers show that it is acceptable to use the simplified chamber as representative of the real crystal puller chamber when calculating heat transfer and fluid flow in the system. The comparison between the results of two cutoff wavelengths $\lambda = 2$ and 2.5 μm shows that it is important to determine which one is a better representative of the encapsulant absorptive property.

Chapter 4

Mathematical Modelling of Fluid and Heat Flow

4.1 Introduction

The fluid flow and heat transfer during the crystal growth process are governed by the conservation of mass, momentum and energy equations. Those equations are solved numerically using a control volume method that is described in this chapter. The modes of heat transfer that are present during the crystal growth are (a)forced convection due to crystal and crucible rotation, (b) natural convection due to heating at the crucible wall, (c) conduction, and (d) radiation . This chapter also compares the results obtained using the programme developed by Sabhapathy and Salcudean in [25, 26, 27] when a simplified radiative model is used (radiation to a uniform temperature ambient) versus the detailed radiative model (radiation to effective ambient temperatures) developed in the previous chapter. Only the effect of natural convection is considered here since the main objective of the exercise is the determination of the effect of the detailed radiative model.

4.2 Assumptions

The numerical results obtained are dependent on the following assumptions:

- Axisymmetrical and laminar flow in the melt and encapsulant.
- Cylindrical crucible and crystal whose axes coincide.

- No slip and non–penetration conditions at the crystal and crucible surfaces and also at the melt–encapsulant interface.
- Free slip at the encapsulant–gas interface.
- Zero radial velocity and zero radial gradient of the temperature at the axis of symmetry.
- Negligible convective heat loss from the encapsulant to the ambient gas and from the crystal to the gas.
- Planar melt surface and planar encapsulant surface.
- Boussinesq's approximation is used.

4.3 Governing Equations

The partial differential equations that govern the fluid flow and heat transfer in $GaAs$, B_2O_3 and Ar during the crystal growth of $GaAs$ are the mass, momentum and energy conservation equations. The equations can be written in general form for an axisymmetric flow in cylindrical coordinates as follows :

$$\frac{\partial}{\partial t}(\rho'\phi) + \frac{\partial}{\partial x}(\rho' u\phi) + \frac{1}{r}\frac{\partial}{\partial r}(\rho' rv\phi) = \frac{\partial}{\partial x}(\Gamma_\phi \frac{\partial \phi}{\partial x}) + \frac{1}{r}\frac{\partial}{\partial r}(r\Gamma_\phi \frac{\partial \phi}{\partial r}) + S_\phi \qquad (4.8)$$

where,

ϕ is the dependent variable,

Γ_ϕ is the exchange coefficient for the variable ϕ,

S_ϕ is the source term.

Table 4.3 defines the variables ϕ, Γ_ϕ and S_ϕ for each equation. The equation that governs the heat transfer in the crystal is :

$$\rho_s c_s u_p \frac{\partial T_s}{\partial x} = k_s(\frac{\partial^2 T_s}{\partial x^2} + \frac{1}{r}\frac{\partial}{\partial r}(r\frac{\partial T_s}{\partial r})) \qquad (4.9)$$

4.4 Boundary Conditions

The following boundary conditions are imposed on the system (see figure 4.16 for further clarification of the terms) :

- Bottom of the crucible:

  $x = 0, \quad r_c > r \geq 0,$

  $u = 0, \; v = 0, \; w = 0, \quad \frac{\partial T}{\partial x} = 0$

- Crucible wall upto melt surface:

  $h_m > x \geq 0, \quad r = r_c \; ,$

  $\frac{\partial u}{\partial r} = 0, \; v = 0, \; w = 0, \quad \frac{\partial T_m}{\partial r} = 0$

- Crucible wall between melt surface and encapsulant surface:

  $h_m + h_e > x \geq h_m, \quad r = r_c,$

  $u = 0, \; v = 0, \; w = 0, \quad T_m = T_c$

- Melt surface between the crystal and crucible :

  $x = h_m, \quad r_c > r > r_s,$

  $u = 0, \quad -k_m \frac{\partial T_m}{\partial x} = \epsilon_m \sigma (T_m^4 - T_{amb}^4)$

- Melt surface at the liquid/solid interface :

  $x = h_m, \quad r_s \geq r \geq 0,$

  $u = 0, \; v = 0, \; w = 0, \quad T = T_{melting}$

- Axis of symmetry upto the melt top :

  $h_m \geq x > 0, \quad r = 0,$

  $\frac{\partial u}{\partial r} = 0, \; v = 0, \; w = 0, \quad \frac{\partial T_m}{\partial r} = 0$

Table 4.20: Definition of the variables in the conservation equations.

Equation	ϕ	Γ_ϕ	S_ϕ
mass	1	0	0
x-mom	u	μ	$-\rho' g - \frac{\partial P}{\partial x} + \frac{\partial}{\partial x}(\mu \frac{\partial u}{\partial x}) + \frac{1}{r}\frac{\partial}{\partial r}(\mu r \frac{\partial v}{\partial x})$
r-mom	v	μ	$-\frac{\partial P}{\partial r} + \frac{\partial}{\partial x}(\mu \frac{\partial u}{\partial r}) - 2\mu \frac{v}{r^2} + \frac{1}{r}\frac{\partial}{\partial r}(r\mu \frac{\partial v}{\partial r}) + \rho' \frac{w^2}{r}$
$\theta - mom$	w	μ	$-\frac{w}{r^2}\frac{\partial}{\partial r}(r\mu) - \frac{\rho' vw}{r}$
Energy	T	$\frac{k}{C_p}$	0

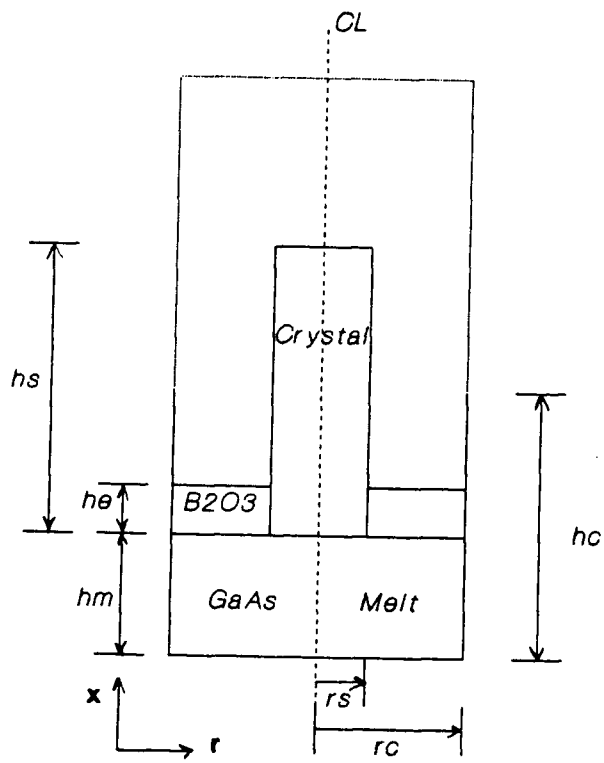

Figure 4.16: Schematic of the calculation domain showing all variables of the system.

- Axis of symmetry between melt top and crystal top :

  $h_m + h_s \geq x > h_m, \quad r = 0,$

  $\frac{\partial T_s}{\partial r} = 0$

- Encapsulant–crystal interface :

  $h_m + h_e > x \geq h_m, \quad r = r_s,$

  $u = 0,\ v = 0,\ w = 0, \quad -k_s \frac{\partial T_s}{\partial r} + k_e \frac{\partial T_e}{\partial r} = \epsilon_s \sigma (T_s^4 - T_{amb}^4)$

- Encapsulant—ambient interface :

  $x = h_m + h_e, \quad r_c > r > r_s,$

  $u = 0,\ \frac{\partial v}{\partial x} = 0,\ \frac{\partial w}{\partial x} = 0, \quad -k_e \frac{\partial T_e}{\partial x} = \epsilon_e \sigma (T_e^4 - T_{amb}^4)$

- Encapsulant–crucible interface :

  $h_m + h_e > x > h_m, \quad r = r_c,$

  $u = 0,\ v = 0,\ w = 0, \quad T_e = T_c$

- Crystal surface that is exposed to the ambient :

  $h_m + h_s \geq x > h_e + h_m, \quad r = r_s,$

  $u = u_p,\ v = 0,\ w = 0, \quad -k_s \frac{\partial T_s}{\partial r} = \epsilon_s \sigma (T_s^4 - T_{amb}^4)$

- Crystal top: $x = h_s + h_m, \quad r_s > r > 0,$

  $u = u_p,\ v = 0,\ w = 0, \quad -k_s \frac{\partial T_s}{\partial r} = \epsilon_s \sigma (T_s^4 - T_{amb}^4)$

- Release of latent heat at the crystal–melt interface :

  $2 \int_0^{r_s} (-k_m \frac{\partial T_m}{\partial x_i} + k_s \frac{\partial T_s}{\partial x}) r dr = u_p r_s^2 L \rho_s$

4.5 Solution Procedure

The partial differential equations introduced earlier are complex and cannot be solved analytically. The numerical solution procedure used in this work is based on the control

volume method. The control volume method requires that the solution domain be divided into a finite number of six–sided control volumes or cells. A grid-point is placed at the geometric centre of each control volume. This arrangement has the following advantages:

- The value of the general variable that is directly available at the centre of the cell is a good representation of the average value over the control volume and can be used without interpolation to calculate the source terms and physical properties.
- Discontinuities at the boundaries can be conveniently handled by locating boundary cells where discontinuities occur.

A staggered grid arrangement is used since it solves some of the problems introduced by non-staggered grids (like producing non-realistic solutions) [45]. The scalar quantities (pressure and temperature) and the velocity component w are calculated at the geometric centre of the control volume, while the velocity components *(u and v)* are calculated at the scalar cell surfaces. (see firgure 4.17). In this way, the velocities are directly available for the evaluation of convection through the boundaries of the control volume. Figure 4.18 shows clearly the control volumes used in the analysis.

4.5.1 Discretization of the Differential Equations

The finite volume equations are derived by the approximate integration of the general transport equation 4.8. The integral form of the differential equation for steady state conditions over a typical control volume for a general dependent variable ϕ can be written as:

$$\oint_A (\rho' \vec{u}\phi - \Gamma_\phi \nabla\phi)\vec{n}dA = \int_V S_\phi dV \tag{4.10}$$

where,

A and V are the control volume area and volume,

$\vec{n}$ is the outward normal unit vector,

Γ_ϕ is the diffusion coefficient of the variable ϕ.

The left hand side of equation 4.10 expresses the convective and diffusive inflow/outflow through the area A of the scalar cell. It can be rewritten for a cylindrical coordinate system as follows (see figure 4.19 for definition of the coordinate system and idealized geometry):

$$\begin{aligned}\oint_A(\rho'\vec{u}\phi - \Gamma_\phi\nabla\phi)\vec{n}dA = &\int_{x_s}^{x_n}(\rho'v\phi - \Gamma_\phi\frac{\partial\phi}{\partial r})_{r_e}dx \\ &- \int_{x_s}^{x_n}(\rho'v\phi - \Gamma_\phi\frac{\partial\phi}{\partial r})_{r_w}dx \\ &+ \int_{r_w}^{r_e}(\rho'u\phi - \Gamma_\phi\frac{\partial\phi}{\partial x})_{x_n}dr \\ &- \int_{r_w}^{r_e}(\rho'u\phi - \Gamma_\phi\frac{\partial\phi}{\partial x})_{x_s}dr \end{aligned} \tag{4.11}$$

The first two terms on the right hand side describe the total transport in the radial direction. They can be discretized as follows :

$$(\rho'v\phi_e - \Gamma_\phi\frac{\phi_E - \phi_P}{\delta r}) - (\rho'v\phi_w - \Gamma_\phi\frac{\phi_W - \phi_P}{\delta r}) \tag{4.12}$$

where δr is the grid spacing in the radial direction (see figure 4.17) , and e & w represent the east and west faces of the control volume.

The variables that are not available at the scalar cells surfaces must be determind by linear interpolation between neighbouring cells :

$$\rho'_e = f_e\rho'_P + (1 - f_e)\rho'_E \tag{4.13}$$

where f_e is a special weighting factor defined by :

$$f_e = 0.5\frac{\Delta r_P}{\delta r_P} \tag{4.14}$$

The total transport through the the east cell boundary consists of convective and diffusive fluxes; $C_e = (\rho'v\phi)_e$ and $D_e = (\Gamma_\phi\frac{\partial\phi}{\partial r})_e$. Due to the staggard grid arrangement, fluxes

are calculated at the scalar cell faces. However, the value of the variable ϕ is directly available only at the nodal points. There are a few possible approximation schemes to obtain the fluxes at the scalar cell boundaries.

The central difference scheme is one that assumes a piecewise–linear profile of the variable ϕ between nodal points. The convective flux can thus be expressed by :

$$C_e = (\rho' v)_e \frac{\phi_e + \phi_P}{2} \tag{4.15}$$

This formulation is second order accurate and gives satisfactory results for flows charaterized by low Peclet number, $Pe_e = ((\rho' v)_e / \frac{\Gamma_\phi}{\delta_r}$), that is flows dominated by diffusion. However, in cases when convection is much larger than diffusion, the central difference method leads to numerical instabilities and yields unrealistic results.

These difficulties can be overcome by using the upwind scheme approximation for convection dominated flows. The value of ϕ at the scalar cell face is assumed to be the same as the value of ϕ at the upwind grid point. The convective flux at the east scalar cell boundary is evaluated as:

$$C_e = (\rho' v)_e \phi_P \quad if \ v_e > 0 \tag{4.16}$$

$$C_e = (\rho' v)_e \phi_E \quad if \ v_e < 0 \tag{4.17}$$

The hybrid differencing scheme [45] combines the advantages of central differencing for small Peclet numbers $|Pe| < 2$ and upwind differencing for large Peclet numbers $|Pe| > 2$. As a result, the numerical stability and accuracy of the solution are enhanced.

The discretized term representing convective and diffusive transport across the east boundry Z_e can be approximated by :

$$Z_e = m_e(\phi - \frac{\delta_r}{Pe} \frac{\partial \phi}{\partial r})_e = m_e(1 - \gamma_e \phi_e + \gamma_e \phi_P) \tag{4.18}$$

where $m_e = \rho' u$ and the coefficient γ_e is defined for hybrid central/upwind differencing

scheme as :

$$\gamma_e = ((1-f) + max[-(1-f)Pe, fPe, 1]/Pe)_e \tag{4.19}$$

Assuming a linear dependence between the source term and the dependent variable ϕ, the right hand side of equation 4.10 can be rewritten as follows:

$$\int_V S_\phi dV = \int_{x_s}^{x_n} \int_{r_w}^{r_e} S_\phi r dr dx = S_c^\phi - S_P^\phi \phi_P \tag{4.20}$$

where,

S_c^ϕ is the constant part of the linearized source term,

S_P^ϕ is the coefficient of ϕ_P.

The final form of of the discretized transport equation can thus be written as follows:

$$m_e[(1-\gamma_e)\phi_E + \gamma_e\phi_P] + m_w[(1-\gamma_w)\phi_W + \gamma_w\phi_P] +$$
$$m_n[(1-\gamma_n)\phi_N + \gamma_n\phi_P] + m_s[(1-\gamma_s)\phi_S + \gamma_s\phi_P] = S_c^\phi - S_P\phi_P \tag{4.21}$$

For numerical convenience a compact form of the above equation will be introduced :

$$A_P\phi_P = A_E\phi_E + A_W\phi_W + A_N\phi_N + A_S\phi_S + S_c^\phi \tag{4.22}$$

which can also be written as :

$$A_P\phi_P = \sum_z A_z\phi_z + S_c^\phi \tag{4.23}$$

where the subscript z denotes the neighbouring grid points, that is E, W, N and S, and the coefficients A_z are defined as follows :

$$A_E = max[[C_e/2], D_e] - C_e/2 \tag{4.24}$$

$$A_W = max[[C_w/2], D_w] + C_w/2 \tag{4.25}$$

$$A_N = max[[C_n/2], D_n] - C_n/2 \tag{4.26}$$

$$A_S = max[[C_s/2], D_s] + C_s/2 \tag{4.27}$$

$$A_P = \sum_z A_z + S_P^\phi \tag{4.28}$$

4.5.2 Discretization of the Boundary Conditions

Imposed Temperatures and Velocities

The values of the variables that are known or assumed can be directly assigned at the boundary points. However, in the case of an internal grid point, the given value of any variable ϕ can be imposed via the source terms S_c and S_P in the following way :

$$S_c = \phi_{given} * 10^{30} \tag{4.29}$$

$$S_P = -10^{30} \tag{4.30}$$

Introducing these terms into the discretized governing equation 4.10 makes all other terms negligible and the equation simplifies to:

$$\phi_P S_P \approx -S_c \tag{4.31}$$

and this forces the following value to be returned by the numerical procedure:

$$\phi_P = -\frac{S_c}{S_P} = \phi_{given} \tag{4.32}$$

Free Surfacs

The free slip condition (zero velocity gradiant) is imposed by cancelling the respective flux terms; e.g. for the east boundary :

$$A_e^{\phi} = 0 \tag{4.33}$$

Axis of Symmetry

The zero radial gradient of the temperature at the axis of symmetry is imposed in the same manner as the zero velocity gradient at the free surface.

4.5.3 The Solution Algorithm

The SIMPLE (Semi Implicit for Pressure Linked Equations) algorithm of Patankar and Spalding [45] is used to solve the system of nonlinear coupled equations. This algorithm uses an iterative solution which involves the following steps :

1. The fields of dependent variables u, v, w, p, T, are guessed for the first iteration loop.

2. The momentum equations in the $r-$, $\theta-$, $x-$ directions are solved and the first estimates of the velocity field u^*, v^*, w^*, are obtained from the guessed pressure field.

3. A pressure correction equation is solved.

4. Corrections are made to the velocity components and pressure:

$$u = u^* + u' \tag{4.34}$$

$$v = v^* + v' \tag{4.35}$$

$$w = w^* + w' \tag{4.36}$$

$$p = p^* + p' \tag{4.37}$$

5. The equation for the scalar quatity T is solved.

6. The results are checked for convergence. If convergence is not attained then the new values of the dependent variables are used as the starting values, and the procedure from step 2 on is repeated.

4.5.4 Solution of the Linear Algebraic Equations

The general finite volume equation 4.10 can be rewritten using the indices (i, j) as follows :

$$A_{i,j}\phi_{i,j} = A_{i+1,j}\phi_{i+1,j} + A_{i-1,j}\phi_{i-1,j} + A_{i,j+1}\phi_{i,j+1} + A_{i,j-1}\phi_{i,j-1} + S_c^{\phi} \tag{4.38}$$

Figures 4.20 to 4.22 show control volume faces for the variables u, v and also the scalar variables defined at the grid node *'P' (I,J)*. The figures also show other variables as defined in the code.

It is possible in principle to solve the above system of equations by matrix inversion. However, this is a computationally costly operation. An alternative solution procedure is to solve the system using an iterative line by line method. For the line of constant i, equation 4.38 can be expressed as :

$$\phi_j = a_j\phi_{j+1} + b_j\phi_{j-1} + c_j \tag{4.39}$$

where ,

$$a_j = A_{i,j+1}/A_{i,j} \tag{4.40}$$

$$b_j = A_{i,j-1}/A_{i,j} \tag{4.41}$$

$$c_j = (A_{i+1,j}\phi_{i+1,j} + A_{i-1,j}\phi_{i-1,j} + S_c^{\phi})/A_{i,j} \tag{4.42}$$

The nonzero coefficients of the set of equations defined by equation 4.38 form a tri-diagonal matrix. Such a system of equations can be solved by a Gaussian–elimination method known as tri–diagonal matrix algorithm (TDMA) or Thomas–algorithm. When the values of ϕ on the line are found , the same procedure is carried out for all lines in the x–direction and can be repeated for the r– direction as well (see figure 4.23). The convergence of the above method is fast because the boundary conditions information is transmitted at once to the nodal points lying inside the solution domain.

4.5.5 Numerical Considerations

Underrelaxation

In order to handle nonlinearities in the iterative solution of the algebraic equations, it is necessary to underrelax or slow down the iteration process. The dependent variable, i.e. the temperature T, can be underrelaxed by the introduction of an underrelaxation factor α into the general discretized equation : $A_P T_P = \sum_z A_z T_z + S_c^T$. Thus the discretized equation can be written as follows :

$$\frac{A_P}{\alpha} T_P = \sum_z A_z T_z + S_c^T + (1-\alpha)\frac{A_P}{\alpha} T_P^* \tag{4.43}$$

where T_P^* is the value of T_P from the previous iteration. At convergence, $T_P^* = T_P$ and the equation with the underrelaxation factor is identical to the discretized equation.

In the present work, the following underrelaxation factors are used : $\alpha_u = 0.25$, $\alpha_v = 0.25$, $\alpha_w = 0.25$, $\alpha_p = 0.50$, $\alpha_T = 0.25$. The source term can be underrelaxed as follows :

$$S_c = \alpha S_c + (1-\alpha) S_c^* \tag{4.44}$$

where S_c^* is the source term from the previous iteration.

Another way of controlling convergence is by the use of the transient approach. The practice of solving a steady state problem via an unsteady formulation can be regarded as a special kind of underrelaxation.

Convergence Criteria

An iteration procedure is normally converged when further iteration does not produce any significant changes in the values of the dependent variables. In addition, it is necessary to have a convergence criterion which measures the degree to which a computed solution

satisfies the original set of transport equations. In the present work, this is done by using the 'residual source' method. The residual R_ϕ over one cell is defined as :

$$R_\phi = \sum_z A_z \phi_z + S_c^\phi - A_P \phi_P \tag{4.45}$$

and the sum of the residuals for the whole field is :

$$R_\phi^\Sigma = \sum_{field} |R_\phi| \tag{4.46}$$

At convergence R_ϕ^Σ becomes 0. For practical purposes, it is sufficient for the sum of the residuals to drop below a specified small number , i.e. :

$$R_\phi^\Sigma < R_\phi^{ref} \lambda \tag{4.47}$$

where R_ϕ^{ref} is the reference value for the variable ϕ, and λ is the level of convergence for all dependent variables (e.g. $\lambda = 0.0001$). The value of R_ϕ^Σ can be monitored during the iteration process and any unexpected behaviour can indicate the source of error in the programme. For example, a divergent behaviour could mean errors in the implementation of some of the boundary conditions.

False Source

In order to ensure convergence and stabilize the numerical behaviour of the solution, one may introduce into the finite volume equations the so called 'false source' term S_f defined by :

$$S_f = C_P(\phi^{i-1} - \phi^i) \tag{4.48}$$

where C_P is the mass imbalance for a control volume defined by:

$$C_P = |\sum_z m_z| = |m_e - m_w + m_n - m_s| \tag{4.49}$$

The false source term can be incorporated into the discretized equation as follows :

$$(A_P + C_P)\phi_P^i = \sum_z A_z\phi_z + S_c^\phi + C_P\phi_P^{i-1} \tag{4.50}$$

At convergence, C_P and S_f become 0 and have no effect on the final converged solution. The addition of a false source term allows avoiding the singularity problem which may arise during the iteration process when A_P takes on the value 0 (corresponding to zero ϕ transport into the cell).

False Diffusion

For high Peclet numbers ($|Pe| > 2$), the hybrid scheme reduces to the upwind scheme. The upwind scheme, though numerically stable, has the disadvantage of being only first order accurate and introduces a discretization error referred to as false diffusion. The effect of false diffusion is an artificial increase in the (physical) diffusion coefficients which results in smearing of the gradients in the flow field. The errors introduced in the solution can be quite important, particularly when the grid lines are inclined with respect to the local velocity vectors [46]. False diffusion can be limited by using (a) a fine mesh, (b) grid lines that are aligned with the flow direction, (c) discretization schemes accounting for the multidimensional nature of the flow and involving more neighbouring cells, and (d) a curvilinear coordinate system.

Numerical Errors and Instabilities

The most likely sources of numerical errors are : (a) unrealistic initial values and (b) grids that are too coarse. Numerical instabilities are often due to (a) inappropriate underrelaxation factors (usually too large), (b) too few sweeps in the iterative line–by–line method. The correct evaluation of numerical parameters can be based on previous experience or can be achieved through trial and error.

The errors in the results are usually caused by mistakes in the implementation of boundary conditions or wrong input data (e.g. physical properties or geometry).

4.6 Simplified Radiative Model Results

The system is assumed to be radiating to a uniform ambient at $1211K$. The stream functions and isotherms in the melt, encapsulant and crystal are shown in figures 4.24 and 4.25.

Figure 4.24 shows the stream lines in the melt and encapsulant. The melt flows upwards near the crucible wall due to heating at that surface. It is then cooled by the encapsulant and the crystal, falls towards the crucible base and is pushed towards the crucible wall. The flow near the crucible wall, base and near the encapsulant and crystal is one of the boundary layer type where high velocity and temperature gradients occur as can be seen clearly in figures 4.24 and 4.25. The flow velocity at the centre of the melt is lower than at the edges.

The flow in the encapsulant moves upwards near the crucible wall and is pushed towards the crystal where it is cooled and sinks downwards near the crystal. The flow velocity in the encapsulant is two orders of magnitude lower than that in the melt. Thus, conduction dominates convection in the encapsulant.

The crystal isotherms show a high gradient near the encapsulant region, however, the gradient decreases with increasing distance from the encapsulant top. The isotherms are curved near the crystal surface where radiative effects are greatest but they flatten out towards the centre.

The encapsulant isotherms are nearly flat except near the crucible wall where it is heated. At the encapsulant free surface, there is a high radial gradient of the temperature near the crucible wall due to heat gain from the wall and heat loss by radiation to the

ambient. The melt isotherms are highly concentrated near the melt-crystal-encapsulant junction and near the crucible wall where the highest rate of heat transfer takes place.

4.7 Detailed Radiative Model Results

The results obtained when a detailed radiative model is used are shown in figures 4.26 and 4.27. The melt flows in a manner similar to that described earlier: upwards near the crucible wall and downwards under the crystal. The central region has a lower velocity since it is away from the direct effects of heating and cooling. The encapsulant streamlines show a circular flow pattern.

The crystal isotherms show a high radial gradient near the upper half of the encapsulant region; they also have a steep slope in that region near the crystal surface. The temperature of the crystal surface decreases near the encapsulant–crystal interface away from the melt surface, however it starts increasing again above the encapsulant top due to exposure to a higher ambient temperature (reflected from higher heat absorption from the crucible wall and the encapsulant). The isotherms in the top half of the crystal are nearly flat.

The isotherms in the melt show high concentration near the melt-crystal-encapsulant junction and near the crucible wall where convective effects are greatest. The encapsulant isotherms show the domination of conduction in that layer; they also show a uniform gradient at the encapsulant-ambient interface.

4.8 Comparison between the Radiative Models

It is clear from the previous two sections that the temperature fields in the melt, encapsulant and crystal are affected by the introduction of a radiative model that takes into

account exchange between all surfaces. The field in the crystal is highly affected especially at the crystal surface where heat gain or loss by radiation occurs. It is also clear that the crystal temperature distribution resulting from the detailed model shows higher values in the top half (1336–1211)K than the simplified model (1261–1211)K. That is due to reduced heat loss to the surroundings shown by radiation to a higher ambient temperature.

The melt surface loses more heat by radiation when the detailed model is used since it is radiating to a lower ambient temperature distribution than the constant ambient temperature. The effect of that on the temperature distribution is clear where the isotherms are not as concentrated near the crystal. (Melt cooling drives the flow faster downwards). The temperature distribution of the encapsulant free surface changes significantly from one model to the other. In the simplified model, the gradient is high near the crucible wall ($\approx 150K/cm$) while it decreases drastically to ($\approx 20K/cm$) away from the crucible wall. When the detailed model is used, the gradient obtained is more uniform across the surface ($\approx 45K/cm$). That is due to including detailed calculations of heat exchange between the encapsulant and the crystal, crucible and ambient.

Eventhough, the analysis presented here included only the effects of natural convection, the exercise does evaluate the effect of including a detailed radiative model on the temperature distribution in the crystal, melt and encapsulant. Therefore, it can be concluded that for better representation of heat transfer during the crystal growth process, a detailed radiative model be used.

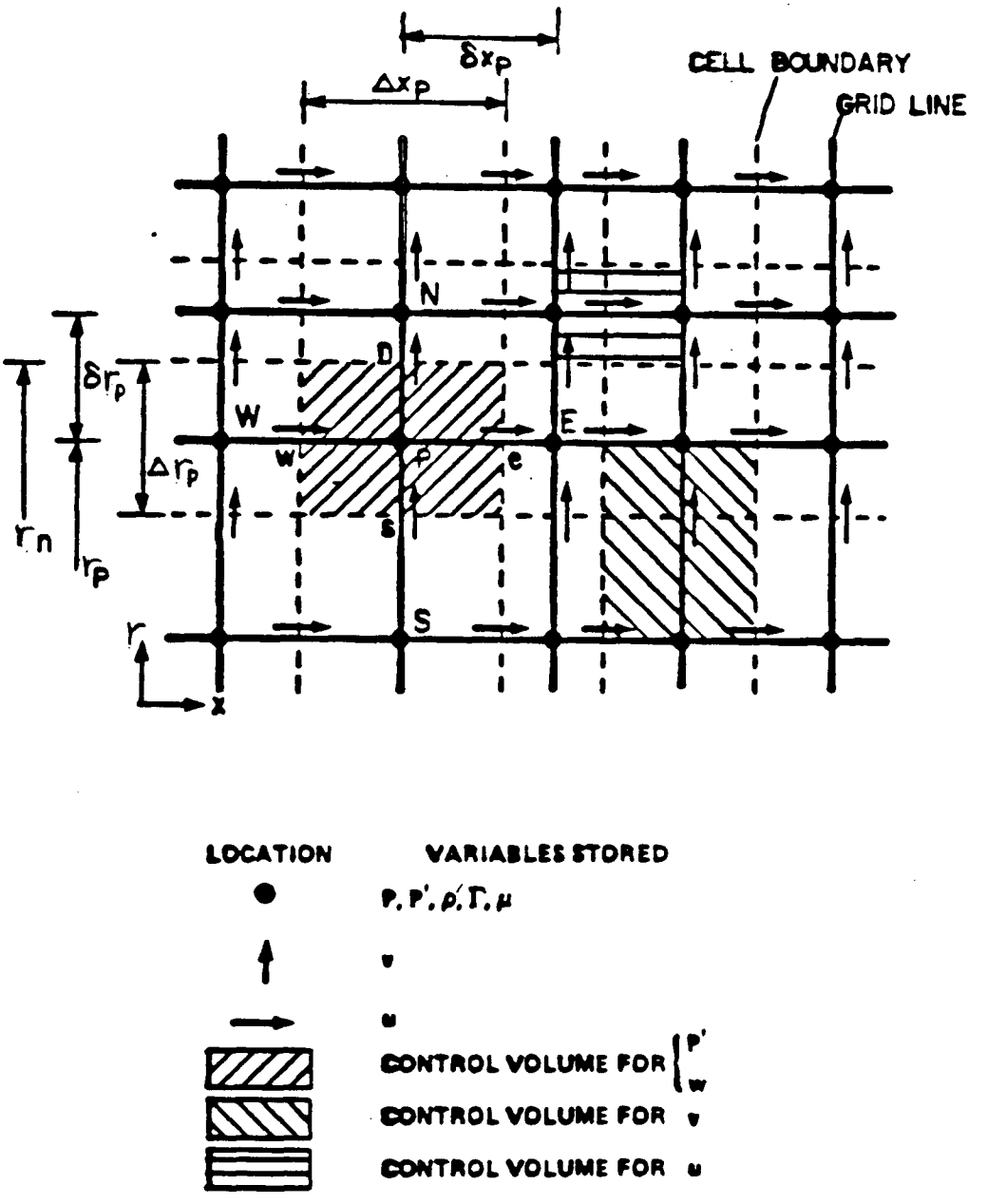

Figure 4.17: A finite volume grid in the (x–r)–plane.

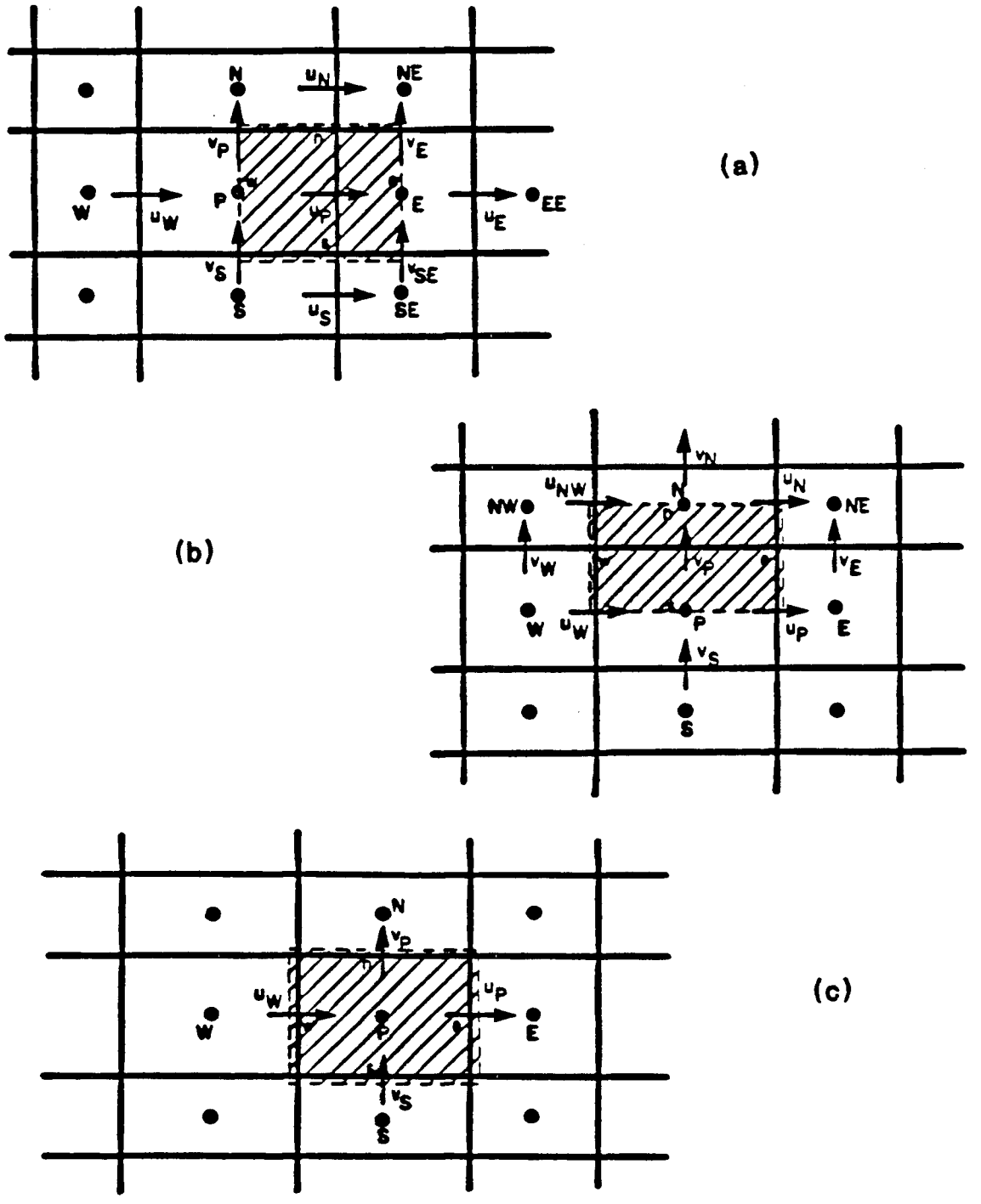

Figure 4.18: Control volume and notation for (a,b) u– and v–momentum analysis, and (c) transport of scalar quantity in θ–direction.

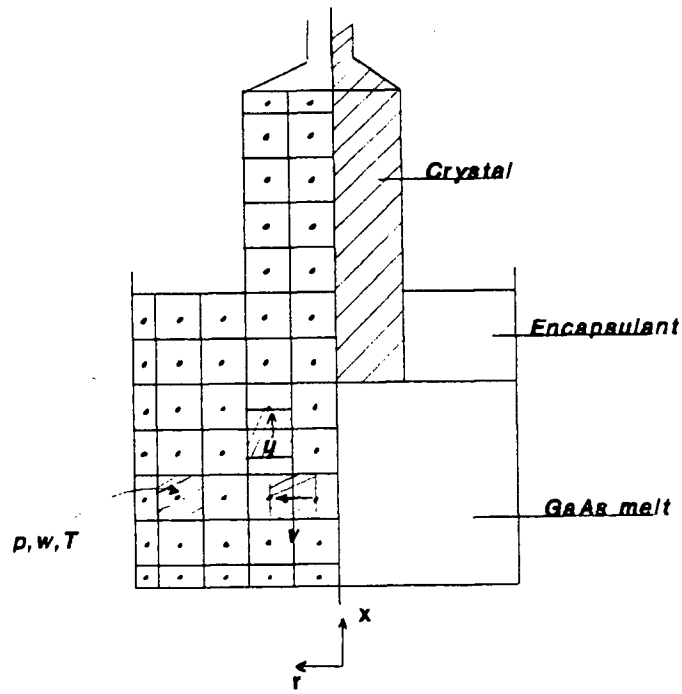

Figure 4.19: The coordinate system and idealized geometry.

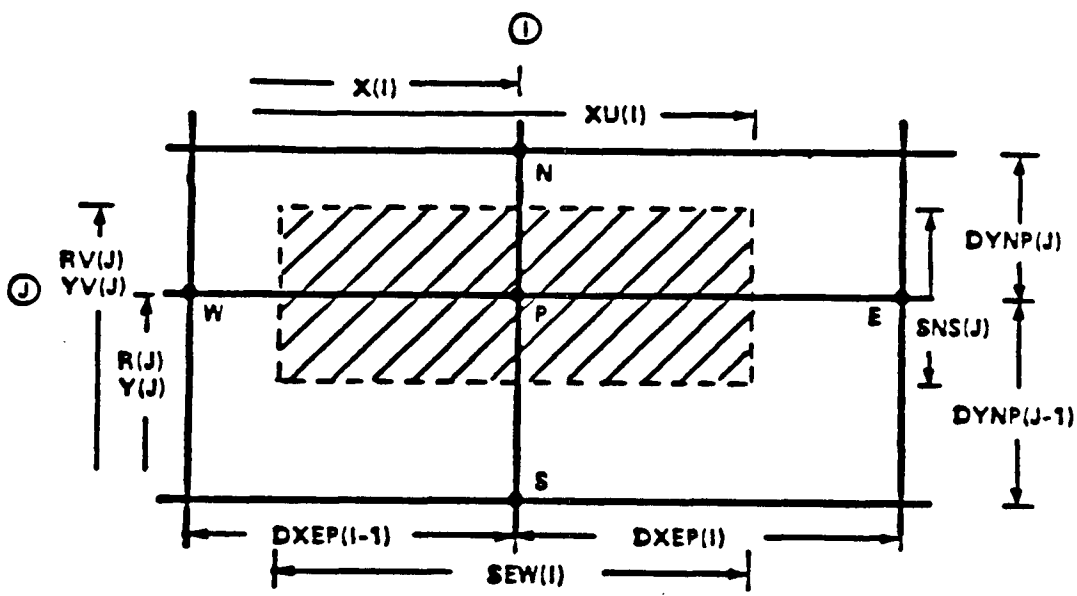

Figure 4.20: Control volume for all scalar varibles defined at the grid-node (I,J)

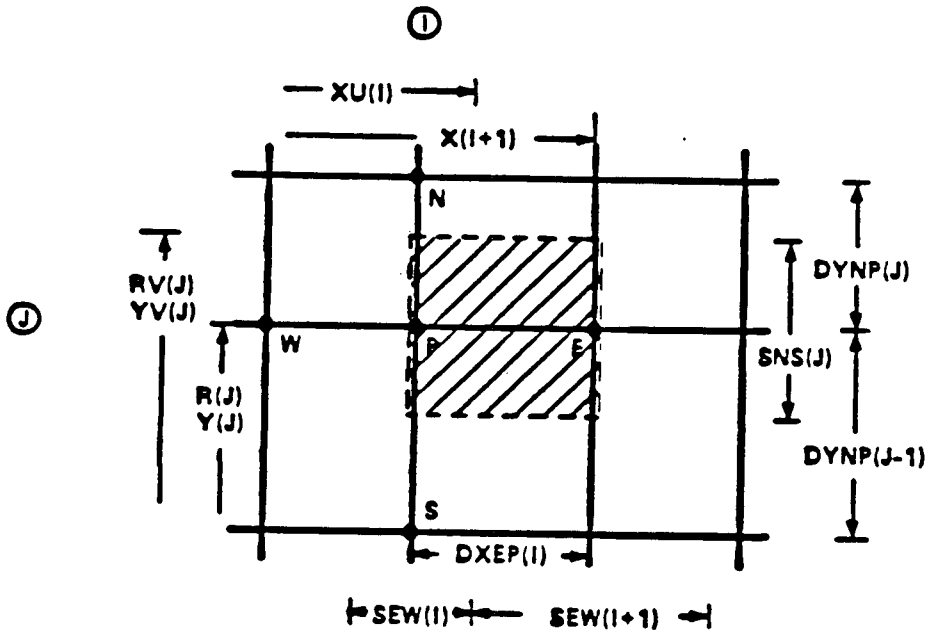

Figure 4.21: Control volume for u–velocity defined at the grid node (I,J)

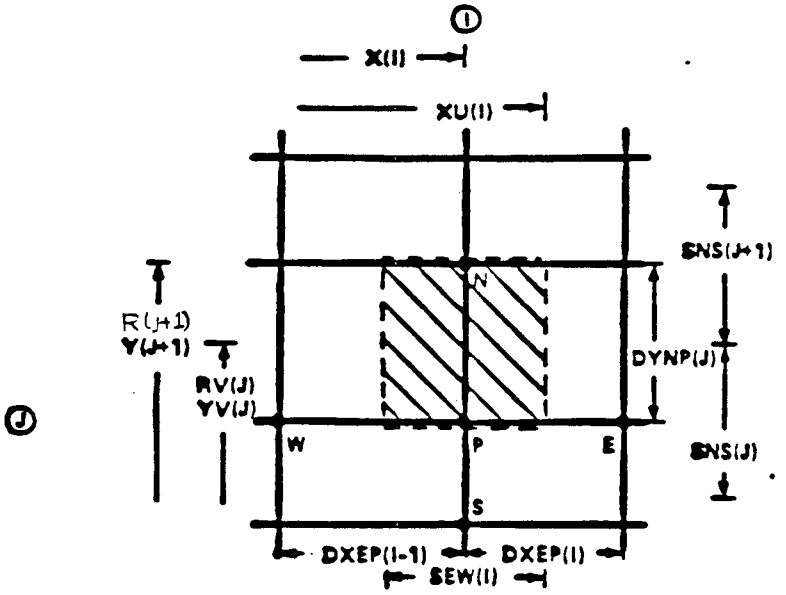

Figure 4.22: Control volume for v–velocity defined at the grid node (I,J)

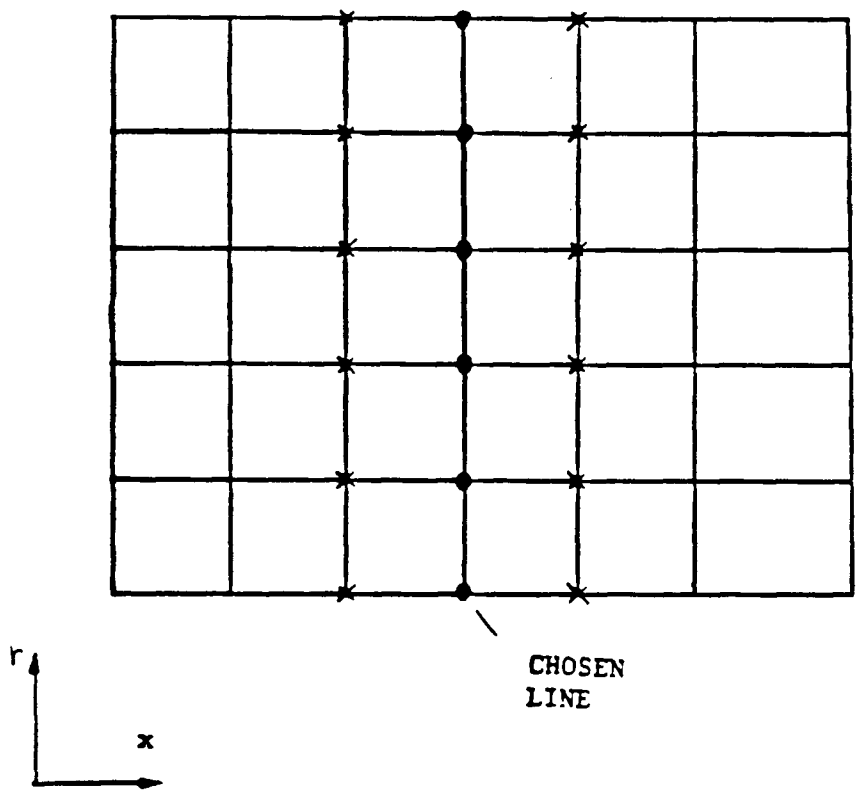

Figure 4.23: Representation of the line–by–line method.

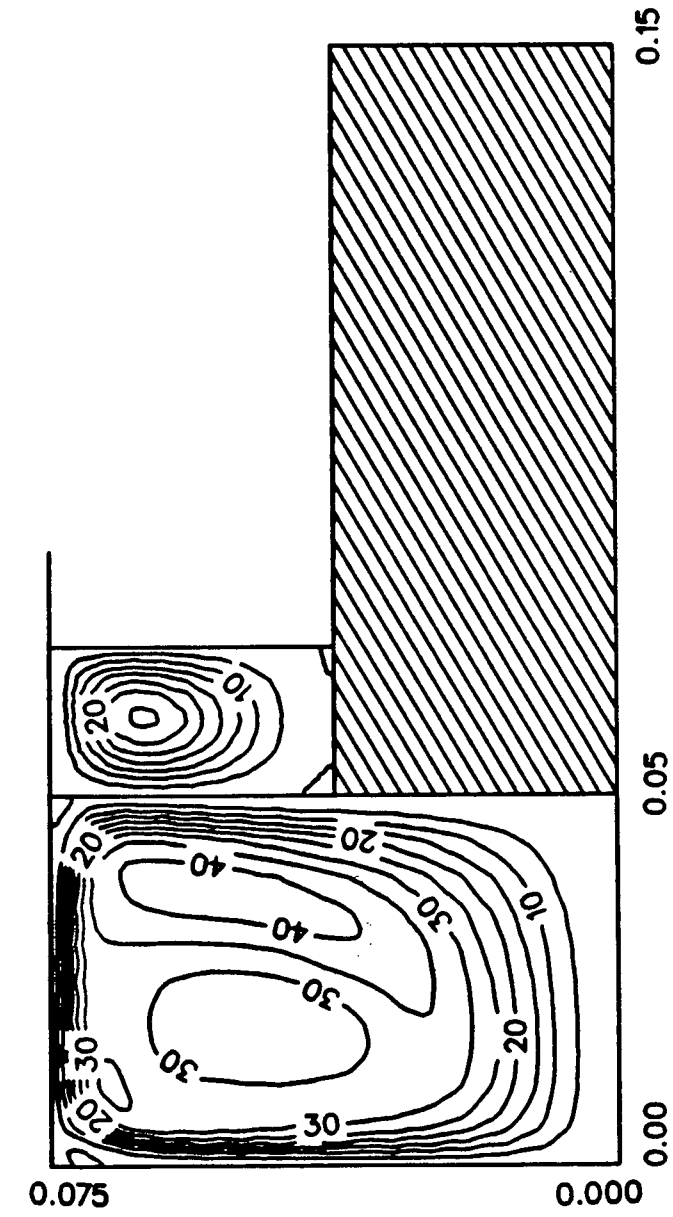

Figure 4.24: Stream functions of the melt and encapsulant – simplified radiative model. Ambient temperature = 1211K, crucible wall temperature = 1531K.

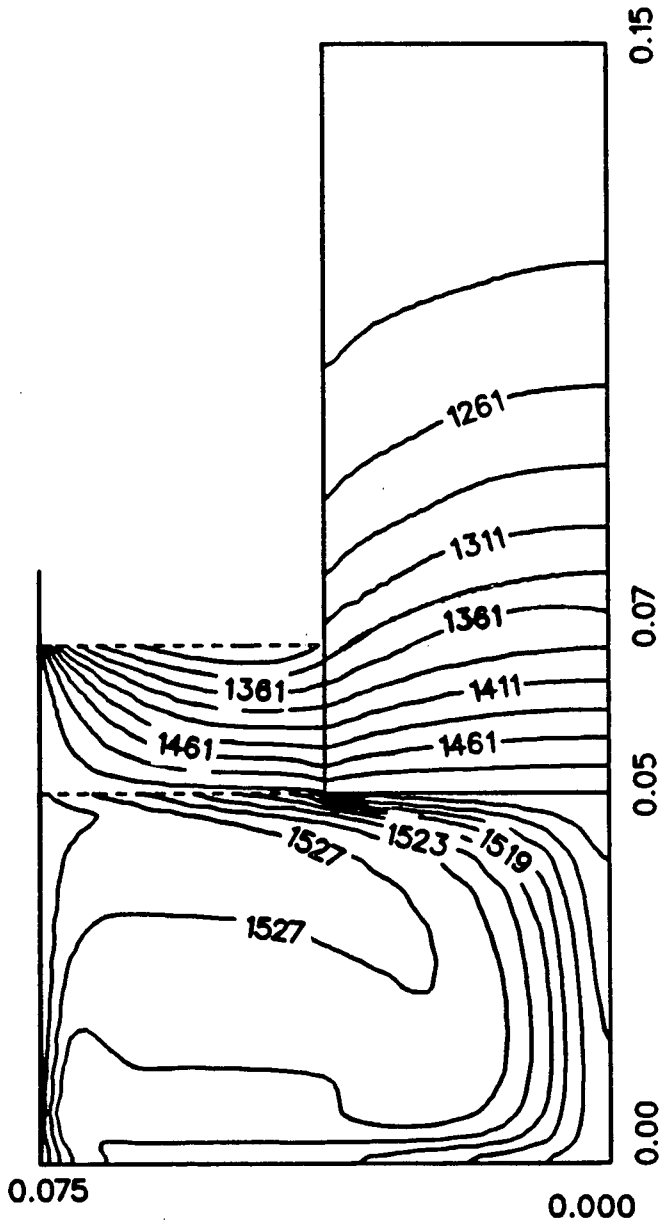

Figure 4.25: Melt, crystal and encapsulant isotherms – simplified radiative model. Ambient temperature = 1211K, crucible wall temperature = 1531K.

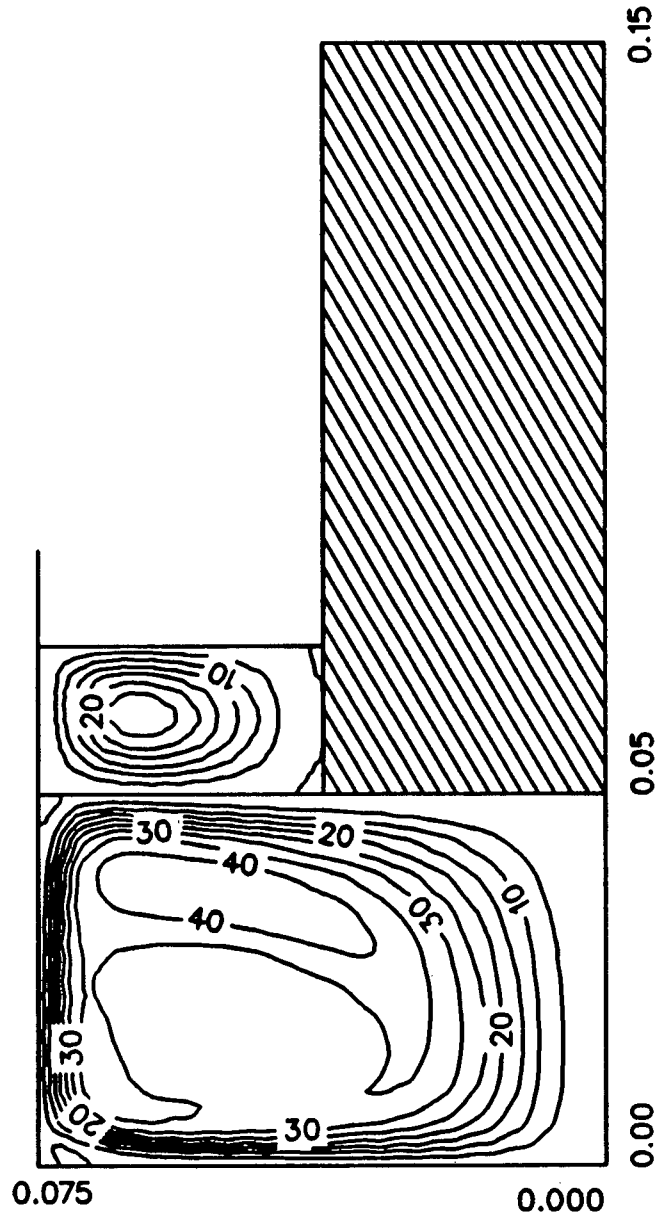

Figure 4.26: Melt and encapsulant stream functions – detailed radiative model. Crucible wall temperature = 1529K.

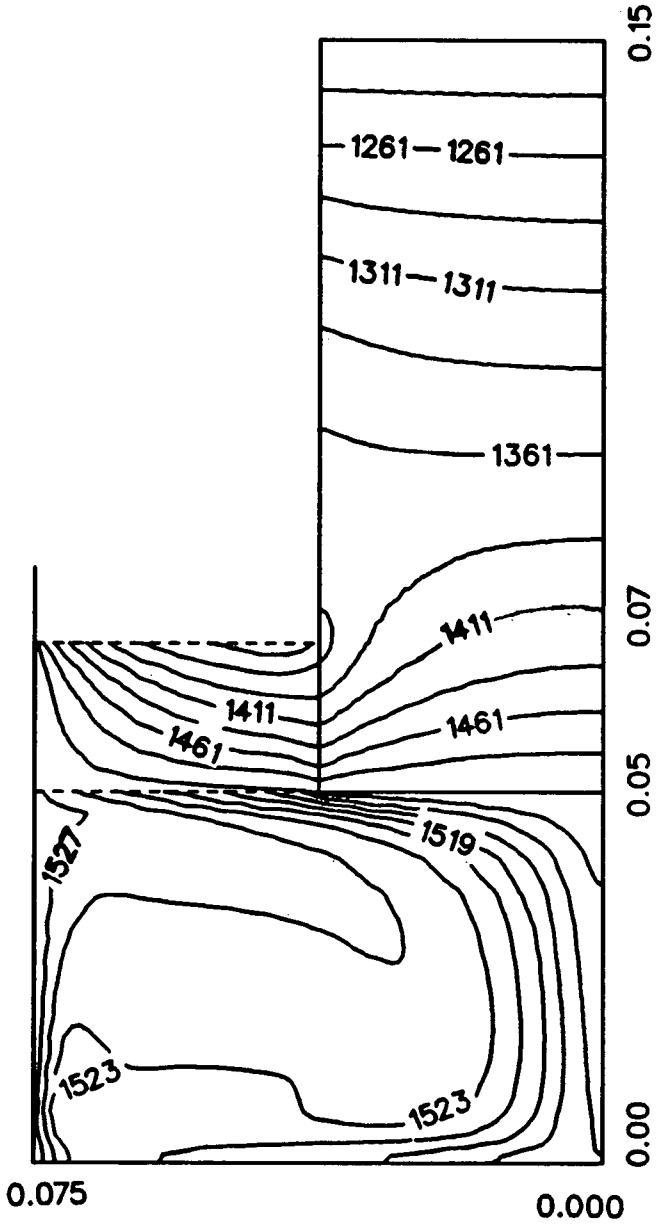

Figure 4.27: Melt, encapsulant and crystal isotherms – detailed radiative model. Crucible wall temperature = 1529K.

Chapter 5

Conclusions and Recommendations

5.1 Summary

This thesis presents a description of the LEC crystal growth process of *GaAs*. It defines the modes of heat transfer present in the system but concentrates on evaluating the radiative mode through the use of a simplified and a detailed model. It also presents an analysis of the effect each model has on the fluid flow and heat transfer in the whole system.

The conclusions drawn from the research and numerical work done are presented in the next section. In addition, some recommendations are suggested for better evaluation and understanding of the heat transfer that takes place during the crystal growing in LEC chambers.

5.2 Conclusions

The following points may be concluded from the work given in the previous chapters:

- Radiation is an important mode of heat transfer that must be included for proper modelling of the crystal growth process.
- The upper part of the growth chamber may be replaced by one isothermal surface for the numerical analysis purposes without significant loss of accurate representation of the real system.

- The use of a simplified radiative model where all surfaces are radiating to one ambient temperature does not evaluate the radiative heat transfer during the growth process correctly.

- A detailed radiative model changes the melt, encapsulant and crystal isotherms. The changes in the crystal isotherms are quite significant especially near the encapsulant top.

- The emissivities of $GaAs$ (solid and liquid), the encapsulant (B_2O_3), the crucible material (PBN) and stainless steel which forms the upper chamber surfaces are important factors in the determination of radiative heat transfer.

- Varying the cutoff wavelength of the encapsulant absorptive property from $2\mu m$ to $2.5\mu m$ effects the effective ambient temperature distribution of the melt, encapsulant and crystal.

5.3 Recommendations

The following recomendations are suggested for future numerical analysis work in the field of $GaAs$ crystal pulling :

- Evaluation of the emissivity of solid and liquid $GaAs$ so that the sources available now may be verified.

- Evaluation of the emissivity of the encapsulant B_2O_3 which is still not available in the literature.

- Evaluation of the absorptive property of the encapsulant B_2O_3 in order to verify the results available from [21].

- Making temperature measurements in the melt and encapsulant layers as possible, and near the crystal surface and crucible wall surface so that better boundary conditions can be imposed on the system when performing numerical simulations of the growth process.

Appendix A

Configuration Factors of the System

A.1 Introduction

This appendix gives the equations used to calculate configuration factors for the cases analysed. Configuration factor will be referred to as CF. The relationships are obtained from [44].

A.2 Configuration Factor Equations

The following is a list of the equations used in the programme written to calculate the radiative heat transfer in the GaAs crystal puller.

1. CF from the ring element on tube to ring element on coaxial annular element on circular fin. Figure A.28 shows r_1, r_2, dr and l. With the following definitions :

   $L = l/r_1$,

   $R = r_2/r_1$,

   $Z = 1 + R^2 + L^2$

   $a_1 = Z^2 - 4R^2$,

   $a_2 = R^2 - L^2 - 1$

   the equation is

   $$dF_{d1-d2} = \left(\frac{2LR}{\pi * a_1}\right)(R^2-1)^{1/2} + \frac{2 * a_2}{a_1^{1/2}} * tan^{-1}\left(\frac{(Z+2R)(R-1)}{(Z-2R)(R+1)}\right)^{1/2}\Big)(dr) \quad \text{(A.51)}$$

   This equation is used to calculate CF from a crystal element to a melt or encapsulant element, or from the crucible outer wall to a middle cylinder lower annulus element.

2. CF from the outer surface of cylinder to annular disk at end of cylinder. Figure A.29 shows the cylinder and disk and the variables R, r and l. With the following definitions :

   $A = l^2 - R^2 + r^2,$

   $B = l^2 + R^2 - r^2,$

   $C = l^2 + R^2 + r^2$

   $D = (\frac{C^2}{r^4} - 4(\frac{R}{r})^2)^{1/2},$

   $E = cos^{-1}(\frac{rA}{RB})$

   the equation defining CF is :

   $$F_{1-2} = \frac{1}{2\pi} * (cos^{-1}(\frac{A}{B}) - (\frac{r}{2l})(D * E + (\frac{A}{r^2})sin^{-1}(\frac{r}{R}) - (\pi/2)(\frac{B}{r^2}))) \quad \text{(A.52)}$$

   Surfaces 1 and 2 may be the crystal element #1 and the melt element #1, respectively. They may also be the crucible outer wall element #1 and the middle cylinder lower annulus element #1, respectively.

3. CF from an annular ring on a cylinder to an annular disk at the end of the cylinder. The variables r, R and x are as shown in figure A.30. Therefore, with the following definition of a, b, c, d, and e :

   $a = x^2 - R^2 + r^2$

   $b = x^2 + R^2 - r^2$

   $c = x^2 + R^2 + R^2$

   $d = \frac{c}{(c^2 - 4(Rr)^2)^{1/2}}$

   $e = ra/Rb$

   the CF equations is given by :

   $$F_{d1-2} = \frac{1}{2\pi}(cos^{-1}(a/b) - \frac{x}{r}(d * cos^{-1}(e) - cos^{-1}(r/R))) \quad \text{(A.53)}$$

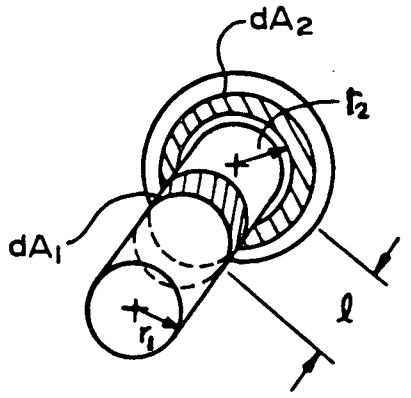

Figure A.28: Schematic showing ring element on tube and ring element on disk.

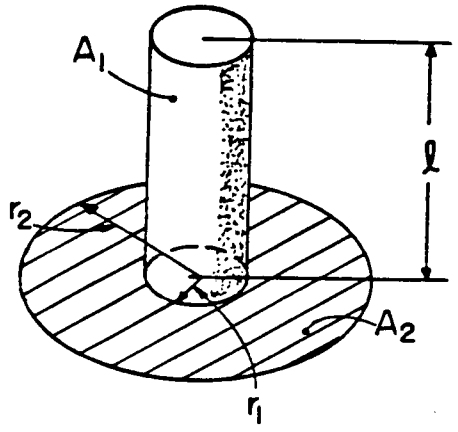

Figure A.29: Schematic showing surfaces 1-cylinder and 2-disk.

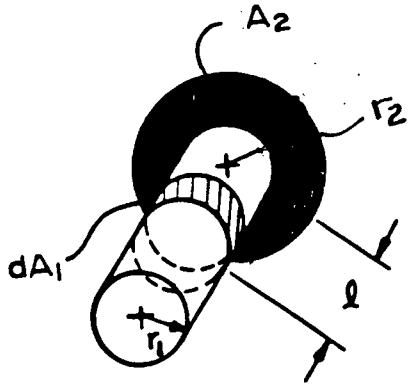

Figure A.30: Schematic showing ring on cylinder and disk connected at end of cylinder.

This equation may be used to calculate CF from a crystal element #(2–ns), to the melt element #1. It may also be used from a crucible outer wall element #(2–nco) to the middle cylinder lower annulus element #1.

4. CF from the inside surface of right circular cylinder to itself. Section and variables are shown in figure A.31. With the following definition : H = h/2r , the CF equation is :

$$F_{1-1} = 1 + H - (1 + H^2)^{1/2} \tag{A.54}$$

This equation will be useful in evaluating CF from the crucible wall to itself, from the middle cylinder wall to itself and from the top cylinder wall to itself.

5. CF from the base of a right circular cylinder to inside surface of cylinder. With the variable H = h/2r , where h and r are as shown in figure A.32, the equation is :

$$F_{1-2} = 2H((1 + H^2)^{1/2} - H) \tag{A.55}$$

The CF from the crucible wall or the the middle cylinder wall to the fictitious surface a_i (see section 3.3.2) may be calculated using the equation.

6. CF from a disk in cylinder base or top to inside of right circular cylinder. With the variables $R = r_2/r_1$ and $H = h/r_1$, where r_1, r_2 and h are as shown in figure A.33, the equation for the CF is :

$$F_{1-2} = \frac{1}{2}(1 - R^2 - H^2 + ((1 + R^2 + H^2)^2 - 4R^2)^{1/2}) \tag{A.56}$$

This equation is used to calculate CF from the middle cylinder wall to the crystal top.

7. CF from an annular ring on cylinder base or top to inside of right circular cylinder. The section and variables are shown in figure A.34. With the same definition of H

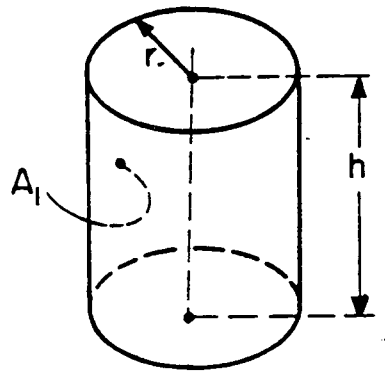

Figure A.31: Schematic showing surface-1.

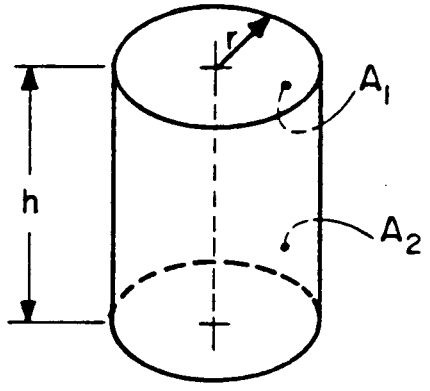

Figure A.32: Schematic showing surfaces 1 and 2 on a right circular cylinder.

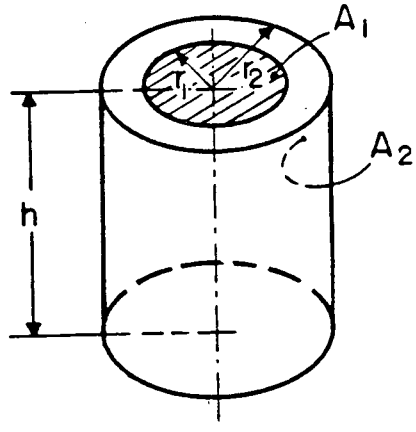

Figure A.33: Schematic showing surface-1, disk an base of cylinder, and surface-2

and R as in the previous point, and the following definition of a, b and c :

$a = R^2 - 1$

$b = (4R^2 + H^2)^{1/2}$

$c = ((1 + R^2 + H^2)^2 - 4R^2)^{1/2}$

the equation for the CF is :

$$F_{1-2} = \frac{1}{2}(1 + \frac{1}{a}(H * b - c)) \tag{A.57}$$

Surface 1 may be a melt, encapsulant or middle cylinder lower annulus element and surface 2 may be the crucible wall or the middle cylinder wall.

8. CF from the interior of right circular cylinder to finite annular ring in base.The variables r_1, r_2, l and a are as shown in figure A.35. Therefore, with the following definition of R, L and X :

   $R = r/a$,

   $L = l/a$,

   $X = (L^4 + 2L^2(1 + R^2) + (1 - R^2)^2)^{1/2}$

   The governing equation is :

$$F_{1-2} = \frac{1}{4L}(X_2 - X_1 + (R_2)^2 - (R_1)^2) \tag{A.58}$$

   This equation is used to calculate CF from the crucible wall to a melt or encapsulant element, or from the middle cylinder wall to a lower annulus element.

9. CF from the interior of a finite length right circular coaxial cylinder to itself. With the same definition of R and H as in the previous point (section shown in figure A.36), and the following definition of a, b, c, d and e :

   $a = \frac{2(R^2-1)^{1/2}}{H}$

   $b = \frac{(4R^2+H^2)^{1/2}}{H}$

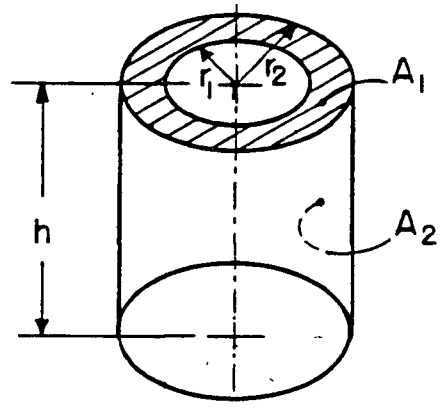

Figure A.34: Schematic showing surface-1, annular ring on base of cylinder, and surface-2.

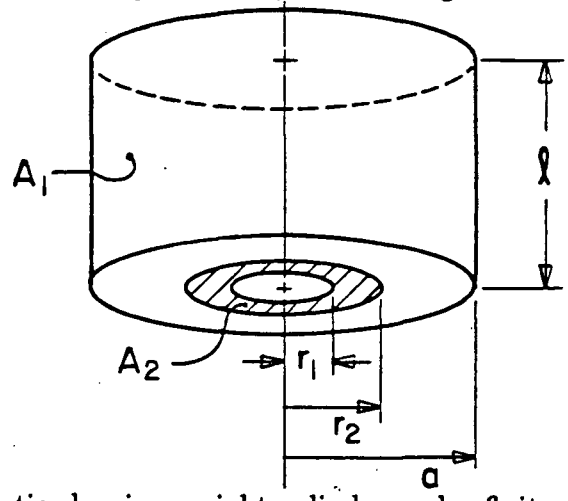

Figure A.35: Schematic showing a right cylinder and a finite annular ring on its base.

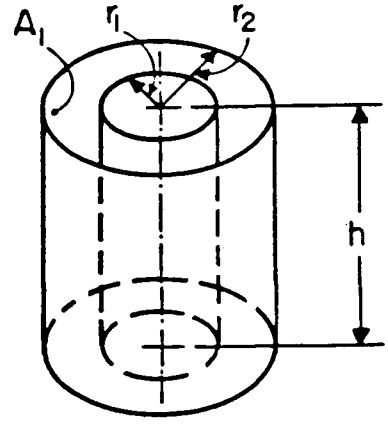

Figure A.36: Schematic showing surface-1 for which CF is calculated.

$c = \frac{4(R^2-1)+(H/R)^2(R^2-2)}{H^2+4(R^2-1)}$

$d = \frac{R^2-2}{R^2}$

$e = \frac{(4R^2+H^2)^{1/2}}{H} - 1$

the equation governing the configuration factor is :

$$F_{1-1} = 1 - \frac{1}{R} + \frac{1}{\pi}(\frac{2}{R} * tan^{-1}(a) - \frac{H}{2R}(b * sin^{-1}(c) - sin^{-1}(d) + \frac{\pi}{2} * e)) \quad (A.59)$$

Surface 1 may be either the crucible wall or the middle cylinder wall.

10. CF from the interior of the outer right circular cylinder of finite length to exterior of inner right circular coaxial cylinder. The section is shown in figure A.37. With the same definition of R and H and the following definition of a, b, c, d and e :

$a = H^2 - R^2 + 1$

$b = H^2 + R^2 - 1$

$c = H^2 + R^2 + 1$

$d = a/b$

$e = (c^2 - (2R)^2)^{1/2}$

$f = e * cos^{-1}(d/R)$

$g = a * sin^{-1}(1/R)$

the CF governing equation is :

$$F_{1-2} = \frac{1}{R}(1 - \frac{1}{\pi}(cos^{-1}(d) - \frac{1}{2H}(f + (g - \frac{\pi}{2} * b)))) \quad (A.60)$$

This equation may be used to calculate CF from the crucible or middle cylinder walls to the crystal wall.

11. CF from the interior of an outer right circular cylinder of finite length to the annular end enclosing space between the coaxial cylinders. The section is as shown in figure A.38. With the following definitions of H, R, a through i and k_1 through

k_5 :

$H = h/r_2, R = r_1/r_2$

$a = 1 - R^2 - H^2$

$b = 1 - R^2 + H^2$

$c = 1 + R^2 + H^2$

$d = 2R^2 - 1$

$e = (c^2 - 4R^2)^{1/2}$

$f = (4 + H^2)^{1/2}$

$g = (1 - R^2)^{1/2}$

$h = 1 - \frac{2(RH)^2}{4g^2+H^2}$

$i = R * a/b$

$k_1 = tan^{-1}(g/H) - tan^{-1}(2g/H)$

$k_2 = sin^{-1}(d) - sin^{-1}(R)$

$k_3 = \frac{\pi}{2} + sin^{-1}(R)$

$k_4 = \frac{\pi}{2} + sin^{-1}(i)$

$k_5 = \frac{\pi}{2} + sin^{-1}(h)$

the governing equation will be :

$$F_{1-2} = \frac{1}{\pi}(R * k_1 + \frac{H}{4} * k_2 + \frac{g^2}{4H} * k_3 - \frac{e}{4H} * k_4 + \frac{f}{4} * k_5) \qquad \text{(A.61)}$$

This equation is used to calculate CF from the crucible or middle cylinder walls to the fictitious surface a_i or the fictitious surface b_i.

12. CF from a differential element on annulus between coaxial cylinders to interior of outer cylinder as shown in figure A.39. The equation for this CF will have to be integrated over the whole annulus for it to be useful here. With the following definition of H, R, a, b, c, d and ω :

$H = h/r_2$

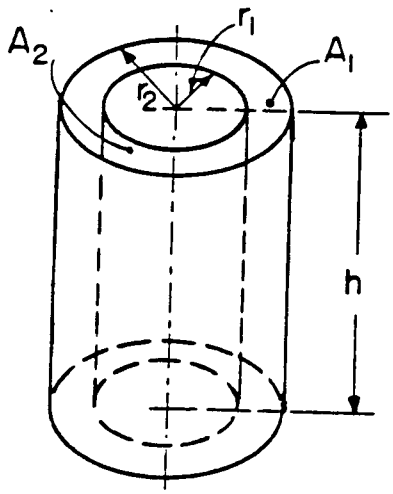

Figure A.37: Schematic showing surfaces 1 and 2 on two coaxial cylinders.

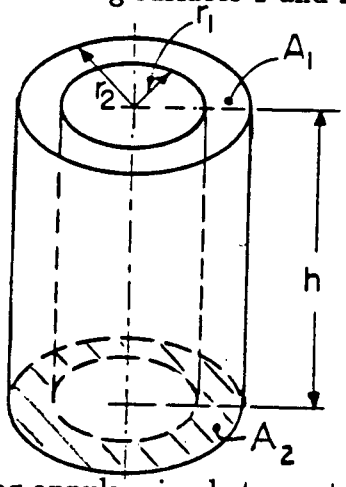

Figure A.38: Schematic showing annular ring between two coaxial cylinders to which CF is calculated.

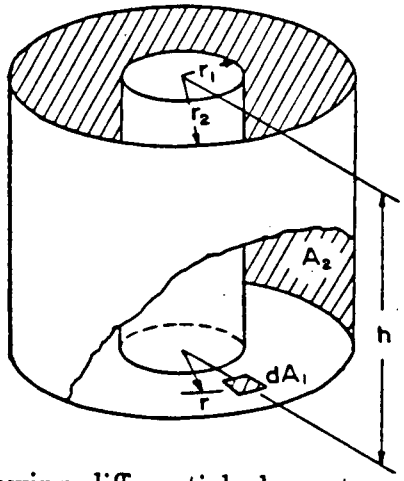

Figure A.39: Schematic showing differential element on annulus between two coaxial cylinders from which CF is calculated.

$R = r/r_2$

$a = 1 + R^2 + H^2$

$b = \frac{1+R}{1-R}$

$c = \frac{a-2}{\pi(a^2-4R^2)^{1/2}}$

$d = \frac{(a^2-4R^2)^{1/2}}{a-2R}$

$\omega = cos^{-1}(r_1/r) + cos^{-1}(r_1/r_2)$

the equation for the CF can be written as follows :

$$F_{d1-2} = \frac{1}{\pi} tan^{-1}(b * tan^{-1}(\frac{\omega}{2})) + c * tan^{-1}(d * tan^{-1}(\frac{\omega}{2})) \qquad \text{(A.62)}$$

After integrating this equation, it can be used to calculate CF from a melt or encapsulant element to the crucible wall. It can also be used for the configuration factor from a lower annulus element to the middle cylinder wall.

13. CF from the wall of the smaller radius cylinder to the wall of the other coaxial cylinder as shown in figure A.40. The variables R, H_1, H_2, L_1 and L_2 are defined as follows:

$R = r_1/r_2,$

$H_1 = h_1/r_1,$

$H_2 = h_2/r_1,$

$L_1 = R^2 + H_1^2,$

$L_2 = R^2 + H_2^2.$

The configuration factor is defined by :

$$F_{1-2} = \frac{(1 - L_2 + ((1 + L_2)^2 - 4R^2)^{1/2})}{4H_1} \qquad \text{(A.63)}$$

This equation is used for calculating CF from the top cylinder wall to the middle cylinder wall, and from the crucible wall to the middle cylinder wall.

14. CF from the interior of a circular cylinder of radius r_1 to a disk of radius r_2 as shown in figure A.41. With the following definition of R, H_1, H_2, X_1 and X_2 :

    $R = r_1/r_2,$

    $H_1 = h_1/r_2,$

    $H_2 = h_2/r_2,$

    $X_1 = H_1^2 + R^2 + 1,$

    $X_2 = H_2^2 + R^2 + 1$

    the CF equation is

$$F_{1-2} = \frac{X_1 - X_2 - (X_1^2 - 4R^2)^{1/2} + (X_2^2 - 4R^2)^{1/2}}{4R(H_2 - H_1)} \tag{A.64}$$

    This equation is used to calculate CF from the middle cylinder wall to the fictitious surface a_i at the crucible edge or at the top cylinder edge.

15. CF from the inside surface of a right cylinder to a coaxial disk of the same diameter seperated from the base of the cylinder as shown in figure A.42 . H_1, H_2, a_1, a_2, a_3 and a_4 are defined as follows :

    $H_1 = h_1/r,$

    $H_2 = h_2/r,$

    $a_1 = 1 + H_1/H_2,$

    $a_2 = H_1 + H_2^2$

    $a_3 = (4 + (H_1 + H_2)^2)^{1/2},$

    $a_4 = (4 + H_2^2)^{1/2} * H_2/H_1$

    and CF is defined as follows :

$$F_{1-2} = \frac{a_1 * a_3 - a_2 - a_4}{4} \tag{A.65}$$

    This equation calculates CF from the middle cylinder wall to a fictitious surface a_i or from the crucible wall to a fictitious surface a_i or b_i.

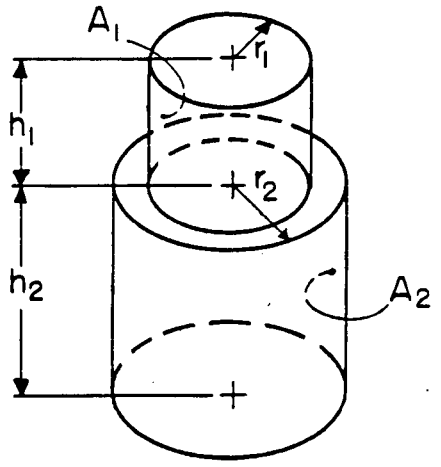

Figure A.40: Schematic showing two coaxial cylinders, one on top of the other for which CF is calculated.

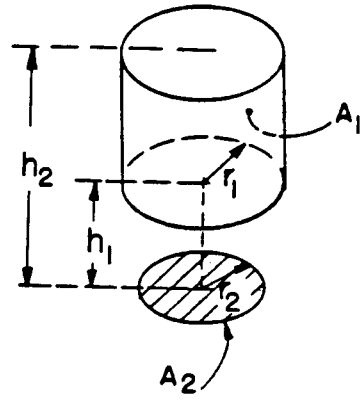

Figure A.41: Schematic showing surface-1, circular cylinder, and surface-2, disk of smaller radius.

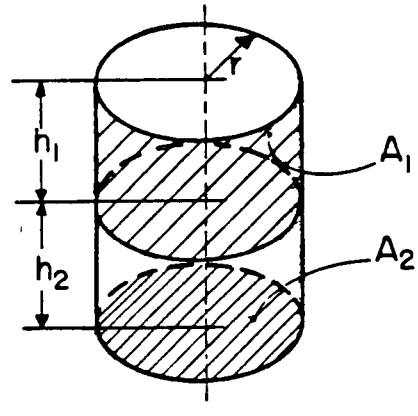

Figure A.42: Schematic showing surfaces 1 and 2 for which CF is calcualted.

16. CF between two parallel disks with centers along the same normal as is shown in figure A.43. The variables r_1, r_2 and h are as defined in the figure. With the following definition of R_1, R_2 and x :

    $R_1 = r_1/h,$

    $R_2 = r_2/h,$

    $x = 1 + (1 + R_2^2)/R_1^2$

    the equation of the CF will be defined as :

$$F_{1-2} = \frac{1}{2}(x - (x^2 - 4(r_2/r_1)^2)) \tag{A.66}$$

    This equation may be used to calculate CF from a fictitious surface a_i to another fictitious surface a_j.

A.3 Configuration Factor Calculation of Case–I

The following is a description of the configuration factor calculation for case–I of the simplified chamber. This case is chosen to illustrate the solution approach because it is the simplest case. All other cases are solved in a similar manner.

1. Equation A.54 is used to calculate CF from the crucible wall element to itself, F_{Ci-Ci}.

2. Equation A.55 is used to calculate CF from the fictitious surfaces 'a' and 'b' to the crucible elements. The reciprocity relationship is then used to calculate CF from the crucible wall elements to the fictitious surfaces. The CF from crucible element c_i to element c_{i+1} can be calculated by the following equation :

$$F_{Ci-Ci+1} = F_{Ci-ai} - F_{Ci-ai+1} \tag{A.67}$$

3. Equations A.57 and A.58 are used to calculate CF from the melt or encapsulant elements to the crucible wall elements. The reciprocity relation is then used to calculate CF from the crucible wall element to the melt or encapsulant elements.

4. CF from from each element to all other elements are summed up. The sum is then subtracted from one to obtain the CF from the each element to the enclosure.

Table A.21 gives the summation of CF from surface i to surface j that are obtained using the method described above. The total from each surface is equal to 1. All dimensions of the puller are as given in the main text (table 3.10).

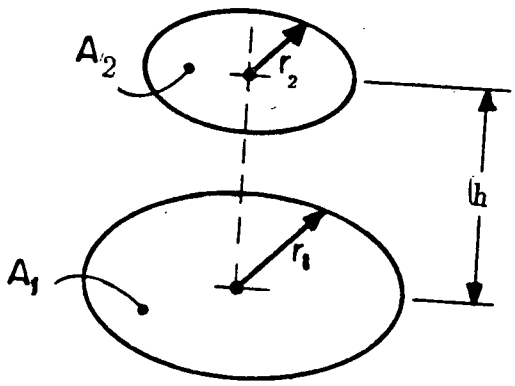

Figure A.43: Schematic showing two disks of different radii for which CF is calcualted.

Table A.21: CF summation from surface i to surface j for case–I of the simplified chamber.

ELEMENT # & SURFACE i	SURFACE j		
	ENCAPSULANT	CRUCIBLE	ENCLOSURE
ENCAPSULANT			
1	—	0.3348	0.6652
2	—	0.3596	0.6404
3	—	0.4123	0.5877
4	—	0.4964	0.5036
5	—	0.6073	0.3927
Crucible			
4	0.4756	0.2733	0.2511
5	0.4294	0.2905	0.2802
6	0.3868	0.3009	0.3123
7	0.3478	0.3043	0.3478
8	0.3868	0.3009	0.3868
9	0.2802	0.2905	0.4294
10	0.2511	0.2733	0.4756
ENCLOSURE			
1	0.1678	0.1655	0.6667
	MELT	CRUCIBLE	ENCLOSURE
MELT			
1	—	0.5050	0.4950
2	—	0.5250	0.4750
3	—	0.5644	0.4356
4	—	0.6210	0.3790
5	—	0.6891	0.3109
CRUCIBLE			
1	0.4756	0.3438	0.1805
2	0.4294	0.3691	0.2015
3	0.3868	0.3883	0.2249
4	0.3478	0.4011	0.2511
5	0.3123	0.4075	0.2802
6	0.2802	0.4075	0.3123
7	0.2511	0.4011	0.3478
8	0.2249	0.3883	0.3868
9	0.2015	0.3691	0.4294
10	0.1805	0.3438	0.4756
ENCLOSURE			
1	0.1273	0.2060	0.6667

Appendix B

Gebhart Factor Equations Derivation

B.1 Introduction

The derivation of the Gebhart factor equations of the system surfaces is given in this appendix. A detailed derivation is shown for only one surface being the melt. The equations of the other surfaces will be written in a similar manner as described in each section.

The genaral form of the Gebhart factor equation is given in the main text and is given again here for convenience [43].

$$\begin{aligned} G_{jk} &= F_{j-k}\epsilon_k + F_{j-1}\rho_1 G_{1-k} + F_{j-2}\rho_2 G_{2-k} \\ &\quad + \ldots\ldots + G_{j-k}\rho_k G_{k-k} + \ldots\ldots\ldots + F_{j-N}\rho_N G_{N-k} \end{aligned} \tag{B.68}$$

B.2 Melt Gebhart factor equations

The following set of equations are the Gebhart factor equations for the melt surface which is divided to nm elements. The variable i goes from 1 to nm in equation B.69 ; from 1 to nc for equation B.70 ; from 1 to nmc for equation B.71 ; from 1 to nla for equation B.72 ; from 1 to ns for equation B.77, from 1 to nst for equation B.76 and from 1 to nco for equation B.78 for each k. k goes from 1 to nm . These equations include the crystal surface elements, the crystal top and the outer surface of the crucible. However, for the case which does not include the crystal, the terms involving the crystal and outer crucible

will be eliminated. All other terms remain the same.

$$
\begin{aligned}
G_{m-m}(i,k) \;=\; & f_{m-m}(i,k)\epsilon_m \\
& + f_{m-m}(i,1)\rho_m G_{m-m}(1,k) + f_{m-m}(i,2)\rho_m G_{m-m}(2,k) \\
& + \ldots\ldots\ldots\ldots\ldots\ldots\ldots\ldots + f_{m-m}(i,nm)\rho_m G_{m-m}(nm,k) \\
& + f_{m-c}(i,1)\rho_c G_{c-m}(1,k) + f_{m-c}(i,2)\rho_c G_{c-m}(2,k) \\
& + \ldots\ldots\ldots\ldots\ldots\ldots\ldots\ldots + f_{m-c}(i,nc)\rho_c G_{c-m}(nc,k) \\
& + f_{m-co}(i,1)\rho_{co} G_{co-m}(1,k) + f_{m-co}(i,2)\rho_{co} G_{co-m}(2,k) \\
& + \ldots\ldots\ldots\ldots\ldots\ldots\ldots\ldots + f_{m-co}(i,nco)\rho_{co} G_{co-m}(nco,k) \\
& + f_{m-s}(i,1)\rho_s G_{s-m}(1,k) + f_{m-s}(i,2)\rho_s G_{s-m}(2,k) \\
& + \ldots\ldots\ldots\ldots\ldots\ldots\ldots\ldots + f_{m-s}(i,ns)\rho_s G_{s-m}(ns,k) \\
& + f_{m-mc}(i,1)\rho_{mc} G_{mc-m}(1,k) \\
& + f_{m-mc}(i,2)\rho_{mc} G_{mc-m}(2,k) \\
& + \ldots\ldots\ldots\ldots + f_{m-mc}(i,nmc)\rho_{mc} G_{mc-m}(nmc,k) \\
& + f_{m-mcla}(i,1)\rho_{mcla} G_{mcla-m}(1,k) \\
& + f_{m-mcla}(i,2)\rho_{mcla} G_{mcla-m}(2,k) \\
& + \ldots\ldots\ldots + f_{m-mcla}(i,nla)\rho_{mcla} G_{mcla-m}(nla,k) \\
& + f_{m-mcta}(i)\rho_{mcta} G_{mcta-m}(k) \\
& + f_{m-tcw}(i)\rho_{tcw} G_{tcw-m}(k) \\
& + f_{m-tct}(i)\rho_{tct} G_{tct-m}(k) \\
& + f_{m-st}(i,1)\rho_{st} G_{st-m}(1,k) + f_{m-st}(i,2)\rho_{st} G_{st-m}(2,k) \\
& + \ldots\ldots\ldots\ldots + f_{m-st}(i,nst)\rho_{st} G_{st-m}(nst,k)
\end{aligned}
\tag{B.69}
$$

$$
\begin{aligned}
G_{c-m}(i,k) \;=\; & f_{c-m}(i,k)\epsilon_m \\
& + f_{c-m}(i,1)\rho_m G_{m-m}(1,k) + f_{c-m}(i,2)\rho_m G_{m-m}(2,k) \\
& + \ldots\ldots\ldots\ldots + f_{c-m}(i,nm)\rho_m G_{m-m}(nm,k) \\
& + f_{c-c}(i,1)\rho_c G_{c-m}(1,k) + f_{c-c}(i,2)\rho_c G_{c-m}(2,k) \\
& + \ldots\ldots\ldots\ldots + f_{c-c}(i,nc)\rho_c G_{c-m}(nc,k) \\
& + f_{c-co}(i,1)\rho_{co} G_{co-m}(1,k) + f_{c-co}(i,2)\rho_{co} G_{co-m}(2,k) \\
& + \ldots\ldots\ldots\ldots + f_{c-co}(i,nco)\rho_{co} G_{co-m}(nc,k) \\
& + f_{c-s}(i,1)\rho_s G_{s-m}(1,k) + f_{c-s}(i,2)\rho_s G_{s-m}(2,k) \\
& + \ldots\ldots\ldots\ldots + f_{c-s}(i,ns)\rho_s G_{s-m}(nc,k) \\
& + f_{c-mc}(i,1)\rho_{mc} G_{mc-m}(1,k) \\
& + f_{c-mc}(i,2)\rho_{mc} G_{mc-m}(2,k) \\
& + \ldots\ldots\ldots\ldots + f_{c-mc}(i,nmc)\rho_{mc} G_{mc-m}(nmc,k) \\
& + f_{c-mcla}(i,1)\rho_{mcla} G_{mcla-m}(1,k) \\
& + f_{c-mcla}(i,2)\rho_{mcla} G_{mcla-m}(2,k) \\
& + \ldots\ldots\ldots\ldots + f_{c-mcla}(i,nla)\rho_{mcla} G_{mcla-m}(nla,k) \\
& + f_{c-mcta}(i)\rho_{mcta} G_{mcta-m}(k) \\
& + f_{c-tcw}(i)\rho_{tcw} G_{tcw-m}(k) \\
& + f_{c-tct}(i)\rho_{tct} G_{tct-m}(k) \\
& + f_{c-st}(i,1)\rho_{st} G_{st-m}(1,k) + f_{c-st}(i,2)\rho_{st} G_{st-m}(2,k) \\
& + \ldots\ldots\ldots\ldots + f_{c-st}(i,nst)\rho_{st} G_{st-m}(nc,k)
\end{aligned}
\tag{B.70}
$$

$$
\begin{aligned}
G_{mc-m}(i,k) \;=\; & f_{mc-m}(i,k)\epsilon_m \\
& + f_{mc-m}(i,1)\rho_m G_{m-m}(1,k) + f_{mc-m}(i,2)\rho_m G_{m-m}(2,k)
\end{aligned}
$$

$$
\begin{aligned}
&+\ldots\ldots\ldots\ldots + f_{mc-m}(i,nm)\rho_m G_{m-m}(nm,k) \\
&+f_{mc-c}(i,1)\rho_c G_{c-m}(1,k) + f_{mc-c}(i,2)\rho_c G_{c-m}(2,k) \\
&+\ldots\ldots\ldots\ldots + f_{mc-c}(i,nc)\rho_c G_{c-m}(nc,k) \\
&+f_{mc-co}(i,1)\rho_{co} G_{co-m}(1,k) + f_{mc-co}(i,2)\rho_{co} G_{co-m}(2,k) \\
&+\ldots\ldots\ldots\ldots + f_{mc-co}(i,nco)\rho_{co} G_{co-m}(nco,k) \\
&+f_{mc-s}(i,1)\rho_s G_{s-m}(1,k) + f_{mc-s}(i,2)\rho_s G_{s-m}(2,k) \\
&+\ldots\ldots\ldots\ldots + f_{mc-s}(i,ns)\rho_s G_{s-m}(ns,k) \\
&+f_{mc-mc}(i,1)\rho_{mc} G_{mc-m}(1,k) \\
&+f_{mc-mc}(i,2)\rho_{mc} G_{mc-m}(2,k) \\
&+\ldots\ldots\ldots\ldots + f_{mc-mc}(i,nmc)\rho_{mc} G_{mc-m}(nmc,k) \\
&+f_{mc-mcla}(i,1)\rho_{mcla} G_{mcla-m}(1,k) \\
&+f_{mc-mcla}(i,2)\rho_{mcla} G_{mcla-m}(2,k) \\
&+\ldots\ldots\ldots\ldots + f_{mc-mcla}(i,nla)\rho_{mcla} G_{mcla-m}(nla,k) \\
&+f_{mc-mcta}(i)\rho_{mcta} G_{mcta-m}(k) \\
&+f_{mc-tcw}(i)\rho_{tcw} G_{tcw-m}(k) \\
&+f_{mc-tct}(i)\rho_{tct} G_{tct-m}(k) \\
&+f_{mc-st}(i,1)\rho_{st} G_{st-m}(1,k) + f_{mc-st}(i,2)\rho_{st} G_{st-m}(2,k) \\
&+\ldots\ldots\ldots\ldots + f_{mc-st}(i,nst)\rho_{st} G_{st-m}(nst,k) \qquad \text{(B.71)}
\end{aligned}
$$

$$
\begin{aligned}
G_{mcla-m}(i,k) \;=\; & f_{mcla-m}(i,k)\epsilon_m \\
&+f_{mcla-m}(i,1)\rho_m G_{m-m}(1,k) + f_{mcla-m}(i,2)\rho_m G_{m-m}(2,k) \\
&+\ldots\ldots\ldots\ldots + f_{mcla-m}(i,nm)\rho_m G_{m-m}(nm,k) \\
&+f_{mcla-c}(i,1)\rho_c G_{c-m}(1,k) + f_{mcla-c}(i,2)\rho_c G_{c-m}(2,k)
\end{aligned}
$$

$$
\begin{aligned}
&+\ldots\ldots\ldots\ldots + f_{mcla-c}(i,nc)\rho_c G_{c-m}(nc,k) \\
&+f_{mcla-co}(i,1)\rho_{co} G_{co-m}(1,k) + f_{mcla-co}(i,2)\rho_{co} G_{co-m}(2,k) \\
&+\ldots\ldots\ldots\ldots + f_{mcla-co}(i,nco)\rho_{co} G_{co-m}(nco,k) \\
&+f_{mcla-s}(i,1)\rho_s G_{s-m}(1,k) + f_{mcla-s}(i,2)\rho_s G_{s-m}(2,k) \\
&+\ldots\ldots\ldots\ldots + f_{mcla-s}(i,ns)\rho_s G_{s-m}(ns,k) \\
&+f_{mcla-mc}(i,1)\rho_{mc} G_{mc-m}(1,k) \\
&+f_{mcla-mc}(i,2)\rho_{mc} G_{mc-m}(2,k) \\
&+\ldots\ldots\ldots\ldots + f_{mcla-mc}(i,nmc)\rho_{mc} G_{mc-m}(nmc,k) \\
&+f_{mcla-mcla}(i,1)\rho_{mcla} G_{mcla-m}(1,k) \\
&+f_{mcla-mcla}(i,2)\rho_{mcla} G_{mcla-m}(2,k) \\
&+\ldots\ldots\ldots\ldots + f_{mcla-mcla}(i,nla)\rho_{mcla} G_{mcla-m}(nla,k) \\
&+f_{mcla-mcta}(i)\rho_{mcta} G_{mcta-m}(k) \\
&+f_{mcla-tcw}(i)\rho_{tcw} G_{tcw-m}(k) \\
&+f_{mcla-tct}(i)\rho_{tct} G_{tct-m}(k) \\
&+f_{mcla-st}(i,1)\rho_{st} G_{st-m}(1,k) + f_{mcla-st}(i,2)\rho_{st} G_{st-m}(2,k) \\
&+\ldots. + f_{mcla-st}(i,nst)\rho_{st} G_{st-m}(nst,k)
\end{aligned}
\tag{B.72}
$$

$$
\begin{aligned}
G_{mcta-m}(k) \;=\; & f_{mcta-m}(k)\epsilon_m \\
&+f_{mcta-m}(1)\rho_m G_{m-m}(1,k) + f_{mcta-m}(2)\rho_m G_{m-m}(2,k) \\
&+\ldots\ldots\ldots\ldots + f_{mcta-m}(nm)\rho_m G_{m-m}(nm,k) \\
&+f_{mcta-c}(1)\rho_c G_{c-m}(1,k) + f_{mcta-c}(2)\rho_c G_{c-m}(2,k) \\
&+\ldots\ldots\ldots\ldots + f_{mcta-c}(nc)\rho_c G_{c-m}(nc,k) \\
&+f_{mcta-co}(1)\rho_{co} G_{co-m}(1,k) + f_{mcta-co}(2)\rho_{co} G_{co-m}(2,k)
\end{aligned}
$$

$$
\begin{aligned}
&+\ldots\ldots\ldots\ldots + f_{mcta-co}(nco)\rho_{co}G_{co-m}(nco,k)\\
&+f_{mcta-s}(1)\rho_{s}G_{s-m}(1,k)\\
&+f_{mcta-s}(2)\rho_{s}G_{s-m}(2,k)\\
&+\ldots\ldots\ldots\ldots + f_{mcta-s}(ns)\rho_{s}G_{s-m}(ns,k)\\
&+f_{mcta-mc}(1)\rho_{mc}G_{mc-m}(1,k)\\
&+f_{mcta-mc}(2)\rho_{mc}G_{mc-m}(2,k)\\
&+\ldots\ldots\ldots\ldots + f_{mcta-mc}(nmc)\rho_{mc}G_{mc-m}(nmc,k)\\
&+f_{mcta-mcla}(1)\rho_{mcla}G_{mcla-m}(1,k)\\
&+f_{mcta-mcla}(2)\rho_{mcla}G_{mcla-m}(2,k)\\
&+\ldots\ldots\ldots\ldots + f_{mcta-mcla}(nla)\rho_{mcla}G_{mcla-m}(nla,k)\\
&+f_{mcta-mcta}(1)\rho_{mcta}G_{mcta-m}(k)\\
&+f_{mcta-tcw}(1)\rho_{tcw}G_{tcw-m}(k)\\
&+f_{mcta-tct}(1)\rho_{tct}G_{tct-m}(k)\\
&+f_{mcta-st}(1)\rho_{st}G_{st-m}(1,k) + f_{mcta-st}(2)\rho_{st}G_{st-m}(2,k)\\
&+\ldots\ldots\ldots\ldots + f_{mcta-st}(nst)\rho_{st}G_{st-m}(nst,k)
\end{aligned}
\tag{B.73}
$$

$$
\begin{aligned}
G_{tcw-m}(k) \;=\;& f_{tcw-m}(k)\epsilon_{m}\\
&+f_{tcw-m}(1)\rho_{m}G_{m-m}(1,k) + f_{tcw-m}(2)\rho_{m}G_{m-m}(2,k)\\
&+\ldots\ldots\ldots\ldots + f_{tcw-m}(nm)\rho_{m}G_{m-m}(nm,k)\\
&+f_{tcw-c}(1)\rho_{c}G_{c-m}(1,k) + f_{tcw-c}(2)\rho_{c}G_{c-m}(2,k)\\
&+\ldots\ldots\ldots\ldots + f_{tcw-c}(nc)\rho_{c}G_{c-m}(nc,k)\\
&+f_{tcw-co}(1)\rho_{co}G_{co-m}(1,k) + f_{tcw-co}(2)\rho_{co}G_{co-m}(2,k)\\
&+\ldots\ldots\ldots\ldots + f_{tcw-co}(nco)\rho_{co}G_{co-m}(nco,k)
\end{aligned}
$$

$$
\begin{aligned}
&+f_{tcw-s}(1)\rho_s G_{s-m}(1,k) + f_{tcw-s}(2)\rho_s G_{s-m}(2,k)\\
&+\ldots\ldots\ldots\ldots + f_{tcw-s}(ns)\rho_s G_{s-m}(ns,k)\\
&+f_{tcw-mc}(1)\rho_{mc} G_{mc-m}(1,k)\\
&+f_{tcw-mc}(2)\rho_{mc} G_{mc-m}(2,k)\\
&+\ldots\ldots\ldots\ldots + f_{tcw-mc}(nmc)\rho_{mc} G_{mc-m}(nmc,k)\\
&+f_{tcw-mcla}(1)\rho_{mcla} G_{mcla-m}(1,k)\\
&+f_{tcw-mcla}(2)\rho_{mcla} G_{mcla-m}(2,k)\\
&+\ldots\ldots\ldots\ldots + f_{tcw-mcla}(nla)\rho_{mcla} G_{mcla-m}(nla,k)\\
&+f_{tcw-mcta}(1)\rho_{mcta} G_{mcta-m}(k)\\
&+f_{tcw-tcw}(1)\rho_{tcw} G_{tcw-m}(k)\\
&+f_{tcw-tct}(1)\rho_{tct} G_{tct-m}(k)\\
&+f_{tcw-st}(1)\rho_{st} G_{st-m}(1,k) + f_{tcw-st}(2)\rho_{st} G_{st-m}(2,k)\\
&+\ldots\ldots\ldots\ldots + f_{tcw-st}(nst)\rho_{st} G_{st-m}(nst,k)
\end{aligned}
\tag{B.74}
$$

$$
\begin{aligned}
G_{tct-m}(k) \;=\; & f_{tct-m}(k)\epsilon_m\\
&+f_{tct-m}(1)\rho_m G_{m-m}(1,k) + f_{tct-m}(2)\rho_m G_{m-m}(2,k)\\
&+\ldots\ldots\ldots\ldots + f_{tct-m}(nm)\rho_m G_{m-m}(nm,k)\\
&+f_{tct-c}(1)\rho_c G_{c-m}(1,k) + f_{tct-c}(2)\rho_c G_{c-m}(2,k)\\
&+\ldots\ldots\ldots\ldots + f_{tct-c}(nc)\rho_c G_{c-m}(nc,k)\\
&+f_{tct-co}(1)\rho_{co} G_{co-m}(1,k) + f_{tct-co}(2)\rho_{co} G_{co-m}(2,k)\\
&+\ldots\ldots\ldots\ldots + f_{tct-co}(nco)\rho_{co} G_{co-m}(nco,k)\\
&+f_{tct-s}(1)\rho_s G_{s-m}(1,k) + f_{tct-s}(2)\rho_s G_{s-m}(2,k)\\
&+\ldots\ldots\ldots\ldots + f_{tct-s}(ns)\rho_s G_{s-m}(ns,k)
\end{aligned}
$$

$$
\begin{aligned}
&+f_{tct-mc}(1)\rho_{mc}G_{mc-m}(1,k)\\
&+f_{tct-mc}(2)\rho_{mc}G_{mc-m}(2,k)\\
&+\ldots\ldots\ldots\ldots+f_{tct-mc}(nmc)\rho_{mc}G_{mc-m}(nmc,k)\\
&+f_{tct-mcla}(1)\rho_{mcla}G_{mcla-m}(1,k)\\
&+f_{tct-mcla}(2)\rho_{mcla}G_{mcla-m}(2,k)\\
&+\ldots\ldots\ldots\ldots+f_{tct-mcla}(nla)\rho_{mcla}G_{mcla-m}(nla,k)\\
&+f_{tct-mcta}(1)\rho_{mcta}G_{mcta-m}(k)\\
&+f_{tct-tcw}(1)\rho_{tcw}G_{tcw-m}(k)\\
&+f_{tct-tct}(1)\rho_{tct}G_{tct-m}(k)\\
&+f_{tct-st}(1)\rho_{st}G_{st-m}(1,k)+f_{tct-st}(2)\rho_{st}G_{st-m}(2,k)\\
&+\ldots\ldots\ldots\ldots+f_{tct-st}(nst)\rho_{st}G_{st-m}(nst,k)
\end{aligned}
\tag{B.75}
$$

$$
\begin{aligned}
G_{st-m}(i,k) \;=\; & f_{st-m}(i,k)\epsilon_m\\
&+f_{st-m}(i,1)\rho_m G_{m-m}(1,k)+f_{st-m}(i,2)\rho_m G_{m-m}(2,k)\\
&+\ldots\ldots\ldots\ldots+f_{st-m}(i,nm)\rho_m G_{m-m}(nm,k)\\
&+f_{st-c}(i,1)\rho_c G_{c-m}(1,k)+f_{st-c}(i,2)\rho_c G_{c-m}(2,k)\\
&+\ldots\ldots\ldots\ldots+f_{st-c}(i,nc)\rho_c G_{c-m}(nc,k)\\
&+f_{st-co}(i,1)\rho_{co}G_{co-m}(1,k)+f_{st-co}(i,2)\rho_{co}G_{co-m}(2,k)\\
&+\ldots\ldots\ldots\ldots+f_{st-co}(i,nco)\rho_{co}G_{co-m}(nco,k)\\
&+f_{st-s}(i,1)\rho_m G_{s-m}(1,k)+f_{st-s}(i,2)\rho_m G_{s-m}(2,k)\\
&+\ldots\ldots\ldots\ldots+f_{st-s}(i,nm)\rho_m G_{s-m}(nm,k)\\
&+f_{st-mc}(i,1)\rho_{mc}G_{mc-m}(1,k)\\
&+f_{st-mc}(i,2)\rho_{mc}G_{mc-m}(2,k)
\end{aligned}
$$

$$
\begin{aligned}
&+\ldots\ldots\ldots\ldots + f_{st-mc}(i,nmc)\rho_{mc}G_{mc-m}(nmc,k)\\
&+f_{st-mcla}(i,1)\rho_{mcla}G_{mcla-m}(1,k) + f_{st-mcla}(i,2)\rho_{mcla}G_{mcla-m}(2,k)\\
&+\ldots\ldots\ldots\ldots + f_{st-mcla}(i,nla)\rho_{mcla}G_{mcla-m}(nla,k)\\
&+f_{st-mcta}(i)\rho_{mcta}G_{mcta-m}(k)\\
&+f_{st-tcw}(i)\rho_{tcw}G_{tcw-m}(k)\\
&+f_{st-tct}(i)\rho_{tct}G_{tct-m}(k)\\
&+f_{st-st}(i,1)\rho_{m}G_{st-m}(1,k) + f_{st-st}(i,2)\rho_{m}G_{st-m}(2,k)\\
&+\ldots\ldots\ldots\ldots + f_{st-st}(i,nm)\rho_{m}G_{st-m}(nm,k)
\end{aligned}
\tag{B.76}
$$

$$
\begin{aligned}
G_{s-m}(i,k) \;=\; & f_{s-m}(i,k)\epsilon_{m}\\
&+f_{s-m}(i,1)\rho_{m}G_{m-m}(1,k) + f_{s-m}(i,2)\rho_{m}G_{m-m}(2,k)\\
&+\ldots\ldots\ldots\ldots + f_{s-m}(i,nm)\rho_{m}G_{m-m}(nm,k)\\
&+f_{s-c}(i,1)\rho_{c}G_{c-m}(1,k) + f_{s-c}(i,2)\rho_{c}G_{c-m}(2,k)\\
&+\ldots\ldots\ldots\ldots + f_{s-c}(i,nc)\rho_{c}G_{c-m}(nc,k)\\
&+f_{s-co}(i,1)\rho_{co}G_{co-m}(1,k) + f_{s-co}(i,2)\rho_{co}G_{co-m}(2,k)\\
&+\ldots\ldots\ldots\ldots + f_{s-co}(i,nco)\rho_{co}G_{co-m}(nco,k)\\
&+f_{s-s}(i,1)\rho_{m}G_{s-m}(1,k) + f_{s-s}(i,2)\rho_{m}G_{s-m}(2,k)\\
&+\ldots\ldots\ldots\ldots + f_{s-s}(i,nm)\rho_{m}G_{s-m}(nm,k)\\
&+f_{s-mc}(i,1)\rho_{mc}G_{mc-m}(1,k)\\
&+f_{s-mc}(i,2)\rho_{mc}G_{mc-m}(2,k)\\
&+\ldots\ldots\ldots\ldots + f_{s-mc}(i,nmc)\rho_{mc}G_{mc-m}(nmc,k)\\
&+f_{s-mcla}(i,1)\rho_{mcla}G_{mcla-m}(1,k)\\
&+f_{s-mcla}(i,2)\rho_{mcla}G_{mcla-m}(2,k)
\end{aligned}
$$

$$
\begin{aligned}
&+\ldots\ldots\ldots\ldots + f_{s-mcla}(i,nla)\rho_{mcla}G_{mcla-m}(nla,k)\\
&+f_{s-mcta}(i)\rho_{mcta}G_{mcta-m}(k)\\
&+f_{s-tcw}(i)\rho_{tcw}G_{tcw-m}(k)\\
&+f_{s-tct}(i)\rho_{tct}G_{tct-m}(k)\\
&+f_{s-st}(i,1)\rho_m G_{s-m}(1,k) + f_{s-st}(i,2)\rho_m G_{s-m}(2,k)\\
&+\ldots\ldots\ldots\ldots + f_{s-st}(i,nm)\rho_m G_{s-m}(nm,k) \qquad \text{(B.77)}
\end{aligned}
$$

$$
\begin{aligned}
G_{co-m}(i,k) \;=\; & f_{co-m}(i,k)\epsilon_m\\
&+f_{co-m}(i,1)\rho_m G_{m-m}(1,k) + f_{co-m}(i,2)\rho_m G_{m-m}(2,k)\\
&+\ldots\ldots\ldots\ldots + f_{co-m}(i,nm)\rho_m G_{m-m}(nm,k)\\
&+f_{co-c}(i,1)\rho_c G_{c-m}(1,k) + f_{co-c}(i,2)\rho_c G_{c-m}(2,k)\\
&+\ldots\ldots\ldots\ldots + f_{co-c}(i,nc)\rho_c G_{c-m}(nc,k)\\
&+f_{co-co}(i,1)\rho_{co} G_{co-m}(1,k) + f_{co-co}(i,2)\rho_{co} G_{co-m}(2,k)\\
&+\ldots\ldots\ldots\ldots + f_{co-co}(i,nco)\rho_{co} G_{co-m}(nco,k)\\
&+f_{co-s}(i,1)\rho_s G_{s-m}(1,k) + f_{co-s}(i,2)\rho_s G_{s-m}(2,k)\\
&+\ldots\ldots\ldots\ldots + f_{co-s}(i,ns)\rho_s G_{s-m}(ns,k)\\
&+f_{co-mc}(i,1)\rho_{mc} G_{mc-m}(1,k)\\
&+f_{co-mc}(i,2)\rho_{mc} G_{mc-m}(2,k)\\
&+\ldots\ldots\ldots\ldots + f_{co-mc}(i,nmc)\rho_{mc} G_{mc-m}(nmc,k)\\
&+f_{co-mcla}(i,1)\rho_{mcla} G_{mcla-m}(1,k)\\
&+f_{co-mcla}(i,2)\rho_{mcla} G_{mcla-m}(2,k)\\
&+\ldots\ldots\ldots\ldots + f_{co-mcla}(i,nla)\rho_{mcla} G_{mcla-m}(nla,k)\\
&+f_{co-mcta}(i)\rho_{mcta} G_{mcta-m}(k)
\end{aligned}
$$

$$+f_{co-tcw}(i)\rho_{tcw}G_{tcw-m}(k)$$
$$+f_{co-tct}(i)\rho_{tct}G_{tct-m}(k)$$
$$+f_{co-st}(i,1)\rho_{st}G_{st-m}(1,k)+f_{co-st}(i,2)\rho_{st}G_{st-m}(2,k)$$
$$+.....+f_{co-st}(i,nst)\rho_{st}G_{st-m}(nst,k) \qquad \text{(B.78)}$$

These equations will be solved simultaneously for the Gebhart factors G_{i-j} where j represents the melt element k and i represents each other surface. The system that is produced by these equations can be written in matrix form as follows:

$$\left[\ \mathbf{A}\ \right]\left(\ \mathbf{x}\ \right)=\left[\ \mathbf{b}\ \right]$$

where [**A**] is a square matrix of size $N*N$ where N $= nm+nc+nmc+ns+nla+nco+nst+3$ if the crystal, crystal top and outer crucible wall are included. If the system is solved for the encapsulant instead of the melt, nm will be replaced by ne , and N will be reduced by twice times the number of elements of the crystal that are below the encapsulant surface. Otherwise, N will be either equal to ($nm+nc+nmc+nla+3$) or ($nm+nc+nmc+nla+3+ns+nst$). (**x**) is a column matrix of size $N*1$ that represents the Gebhart factors, and [**b**] is a column matrix of size $N*1$ which represents the right hand side of the equation.The matrix is solved using routines available on the VAX-VMS system. The matrices [**A**], (**x**) and [**b**] are given next. The matrix [**A**] is large and will

therefore be written as a $8 * 8$ matrix where each element represents a matrix.

$$\left[\mathbf{A} \right] = \begin{bmatrix} \mathbf{A1} & \mathbf{A2} & \mathbf{A3} & \mathbf{A4} & \mathbf{A5} & \mathbf{A6} & \mathbf{A7} & \mathbf{A8} \\ \mathbf{B1} & \mathbf{B2} & \mathbf{B3} & \mathbf{B4} & \mathbf{B5} & \mathbf{B6} & \mathbf{B7} & \mathbf{B8} \\ \mathbf{C1} & \mathbf{C2} & \mathbf{C3} & \mathbf{C4} & \mathbf{C5} & \mathbf{C6} & \mathbf{C7} & \mathbf{C8} \\ \mathbf{D1} & \mathbf{D2} & \mathbf{D3} & \mathbf{D4} & \mathbf{D5} & \mathbf{D6} & \mathbf{D7} & \mathbf{D8} \\ \mathbf{E1} & \mathbf{E2} & \mathbf{E3} & \mathbf{E4} & \mathbf{E5} & \mathbf{E6} & \mathbf{E7} & \mathbf{E8} \\ \mathbf{F1} & \mathbf{F2} & \mathbf{F3} & \mathbf{F4} & \mathbf{F5} & \mathbf{F6} & \mathbf{F7} & \mathbf{F8} \\ \mathbf{G1} & \mathbf{G2} & \mathbf{G3} & \mathbf{G4} & \mathbf{G5} & \mathbf{G6} & \mathbf{G7} & \mathbf{G8} \\ \mathbf{H1} & \mathbf{H2} & \mathbf{H3} & \mathbf{H4} & \mathbf{H5} & \mathbf{H6} & \mathbf{H7} & \mathbf{H8} \end{bmatrix}$$

where **A1, A2 ... A8, B1, B2 ... B8, C1,C2 ... C8, D1, D2 ... D8, E1, E2 ... E8, F1, F2 ... F8, G1, G2 ... G8** and **H1, H2 ... H8** are as follows.

$$\mathbf{A1} = \begin{pmatrix} f_{m-m}(1,1)\rho_m - 1 & f_{m-m}(1,2)\rho_m & \ldots\ldots & f_{m-m}(1,nm)\rho_m \\ f_{m-m}(2,1)\rho_m & f_{m-m}(2,2)\rho_m - 1 & \ldots\ldots & f_{m-m}(2,nm)\rho_m \\ \ldots\ldots & \ldots\ldots & \ldots\ldots & \ldots\ldots \\ \ldots\ldots & \ldots\ldots & \ldots\ldots & \ldots\ldots \\ f_{m-m}(nm,1)\rho_m & f_{m-m}(nm,2)\rho_m & \ldots\ldots & f_{m-m}(nm,nm)\rho_m - 1 \end{pmatrix}$$

$$\mathbf{A2} = \begin{pmatrix} f_{m-c}(1,1)\rho_c & f_{m-c}(1,2)\rho_c & \ldots\ldots\ldots\ldots & f_{m-c}(1,nc)\rho_c \\ f_{m-c}(2,1)\rho_c & f_{m-c}(2,2)\rho_c & \ldots\ldots\ldots\ldots & f_{m-c}(2,nc)\rho_c \\ \ldots\ldots & \ldots\ldots & \ldots\ldots\ldots\ldots & \ldots\ldots \\ \ldots\ldots & \ldots\ldots & \ldots\ldots\ldots\ldots & \ldots\ldots \\ f_{m-c}(nm,1)\rho_c & f_{m-c}(nm,2)\rho_c & \ldots\ldots\ldots\ldots & f_{m-c}(nm,nc)\rho_c \end{pmatrix}$$

$$\mathbf{A3} = \begin{pmatrix} f_{m-mc}(1,1)\rho_{mc} & f_{m-mc}(1,2)\rho_{mc} & \ldots\ldots & f_{m-mc}(1,nmc)\rho_{mc} \\ f_{m-mc}(2,1)\rho_{mc} & f_{m-mc}(2,2)\rho_{mc} & \ldots\ldots & f_{m-mc}(2,nmc)\rho_{mc} \\ \ldots\ldots & \ldots\ldots & \ldots\ldots & \ldots\ldots \\ \ldots\ldots & \ldots\ldots & \ldots\ldots & \ldots\ldots \\ f_{m-mc}(nm,1)\rho_{mc} & f_{m-mc}(nm,2)\rho_{mc} & \ldots\ldots & f_{m-mc}(nm,nmc)\rho_{mc} \end{pmatrix}$$

$$\mathbf{A4} = \begin{pmatrix} f_{m-mcla}(1,1)\rho_{mcla} & f_{m-mcla}(1,2)\rho_{mcla} & \ldots\ldots & f_{m-mcla}(1,nla)\rho_{mcla} \\ f_{m-mcla}(2,1)\rho_{mcla} & f_{m-mcla}(2,2)\rho_{mcla} & \ldots\ldots & f_{m-mcla}(2,nla)\rho_{mcla} \\ \ldots\ldots & \ldots\ldots & \ldots\ldots & \ldots\ldots \\ \ldots\ldots & \ldots\ldots & \ldots\ldots & \ldots\ldots \\ f_{m-mcla}(nm,1)\rho_{mcla} & f_{m-mcla}(nm,2)\rho_{mcla} & \ldots\ldots & f_{m-mcla}(nm,nla)\rho_{mcla} \end{pmatrix}$$

$$\mathbf{A5} = \begin{pmatrix} f_{m-mcta}(1)\rho_{mcta} & f_{m-tcw}(1)\rho_{tcw} & f_{m-tct}(1)\rho_{tct} \\ f_{m-mcta}(2)\rho_{mcta} & f_{m-tcw}(2)\rho_{tcw} & f_{m-tct}(2)\rho_{tct} \\ \ldots\ldots & \ldots\ldots & \ldots\ldots \\ \ldots\ldots & \ldots\ldots & \ldots\ldots \\ f_{m-mcta}(nm)\rho_{mcta} & f_{m-tcw}(nm)\rho_{tcw} & f_{m-tct}(nm)\rho_{tct} \end{pmatrix}$$

$$\mathbf{A6} = \begin{pmatrix} f_{m-s}(1,1)\rho_s & f_{m-s}(1,2)\rho_s & \ldots\ldots & f_{m-s}(1,ns)\rho_s \\ f_{m-s}(2,1)\rho_s & f_{m-s}(2,2)\rho_s & \ldots\ldots & f_{m-s}(2,ns)\rho_s \\ \ldots\ldots & \ldots\ldots & \ldots\ldots & \ldots\ldots \\ \ldots\ldots & \ldots\ldots & \ldots\ldots & \ldots\ldots \\ f_{m-s}(nm,1)\rho_s & f_{m-s}(nm,2)\rho_s & \ldots\ldots & f_{m-s}(nm,ns)\rho_s \end{pmatrix}$$

$$\mathbf{A7} = \begin{pmatrix} f_{m-co}(1,1)\rho_{co} & f_{m-co}(1,2)\rho_{co} & \ldots\ldots\ldots & f_{m-co}(1,nco)\rho_{co} \\ f_{m-co}(2,1)\rho_{co} & f_{m-co}(2,2)\rho_{co} & \ldots\ldots\ldots & f_{m-co}(2,nco)\rho_{co} \\ \ldots\ldots\ldots\ldots & \ldots\ldots\ldots\ldots & \ldots\ldots\ldots & \ldots\ldots\ldots\ldots \\ \ldots\ldots\ldots\ldots & \ldots\ldots\ldots\ldots & \ldots\ldots\ldots & \ldots\ldots\ldots\ldots \\ f_{m-co}(nm,1)\rho_{co} & f_{m-co}(nm,2)\rho_{co} & \ldots\ldots\ldots & f_{m-co}(nm,nco)\rho_{co} \end{pmatrix}$$

$$\mathbf{A8} = \begin{pmatrix} f_{m-st}(1,1)\rho_{st} & f_{m-st}(1,2)\rho_{st} & \ldots\ldots\ldots\ldots & f_{m-st}(1,nst)\rho_{st} \\ f_{m-st}(2,1)\rho_{st} & f_{m-st}(2,2)\rho_{st} & \ldots\ldots\ldots\ldots & f_{m-st}(2,nst)\rho_{st} \\ \ldots\ldots\ldots\ldots & \ldots\ldots\ldots\ldots & \ldots\ldots\ldots\ldots & \ldots\ldots\ldots\ldots \\ \ldots\ldots\ldots\ldots & \ldots\ldots\ldots\ldots & \ldots\ldots\ldots\ldots & \ldots\ldots\ldots\ldots \\ f_{m-st}(nm,1)\rho_{st} & f_{m-st}(nm,2)\rho_{st} & \ldots\ldots\ldots\ldots & f_{m-st}(nm,nst)\rho_{st} \end{pmatrix}$$

$$\mathbf{B1} = \begin{pmatrix} f_{c-m}(1,1)\rho_{m} & f_{c-m}(1,2)\rho_{m} & \ldots\ldots\ldots\ldots & f_{c-m}(1,nm)\rho_{m} \\ f_{c-m}(2,1)\rho_{m} & f_{c-m}(2,2)\rho_{m} & \ldots\ldots\ldots\ldots & f_{c-m}(2,nm)\rho_{m} \\ \ldots\ldots\ldots & \ldots\ldots\ldots & \ldots\ldots\ldots\ldots & \ldots\ldots\ldots \\ \ldots\ldots\ldots & \ldots\ldots\ldots & \ldots\ldots\ldots\ldots & \ldots\ldots\ldots \\ f_{c-m}(nc,1)\rho_{m} & f_{c-m}(nc,2)\rho_{m} & \ldots\ldots\ldots\ldots & f_{c-m}(nc,nm)\rho_{m} \end{pmatrix}$$

$$\mathbf{B2} = \begin{pmatrix} f_{c-c}(1,1)\rho_{c} - 1 & f_{c-c}(1,2)\rho_{c} & \ldots\ldots\ldots & f_{c-c}(1,nc)\rho_{c} \\ f_{c-c}(2,1)\rho_{c} & f_{c-c}(2,2)\rho_{c} - 1 & \ldots\ldots\ldots & f_{c-c}(2,nc)\rho_{c} \\ \ldots\ldots\ldots & \ldots\ldots\ldots & \ldots\ldots\ldots & \ldots\ldots\ldots \\ \ldots\ldots\ldots & \ldots\ldots\ldots & \ldots\ldots\ldots & \ldots\ldots\ldots \\ f_{c-c}(nc,1)\rho_{c} & f_{c-c}(nc,2)\rho_{c} & \ldots\ldots\ldots & f_{c-c}(nc,nc)\rho_{c} - 1 \end{pmatrix}$$

$$\mathbf{B3} = \begin{pmatrix} f_{c-mc}(1,1)\rho_{mc} & f_{c-mc}(1,2)\rho_{mc} & \ldots\ldots & f_{c-mc}(1,nmc)\rho_{mc} \\ f_{c-mc}(2,1)\rho_{mc} & f_{c-mc}(2,2)\rho_{mc} & \ldots\ldots & f_{c-mc}(2,nmc)\rho_{mc} \\ \ldots\ldots\ldots & \ldots\ldots\ldots & \ldots\ldots & \ldots\ldots\ldots \\ \ldots\ldots\ldots & \ldots\ldots\ldots & \ldots\ldots & \ldots\ldots\ldots \\ f_{c-mc}(nc,1)\rho_{mc} & f_{c-mc}(nc,2)\rho_{mc} & \ldots\ldots & f_{c-mc}(nc,nmc)\rho_{mc} \end{pmatrix}$$

$$\mathbf{B4} = \begin{pmatrix} f_{c-mcla}(1,1)\rho_{mcla} & f_{c-mcla}(1,2)\rho_{mcla} & \ldots\ldots & f_{c-mcla}(1,nla)\rho_{mcla} \\ f_{c-mcla}(2,1)\rho_{mcla} & f_{c-mcla}(2,2)\rho_{mcla} & \ldots\ldots & f_{c-mcla}(2,nla)\rho_{mcla} \\ \ldots\ldots\ldots\ldots & \ldots\ldots\ldots\ldots & \ldots\ldots & \ldots\ldots\ldots\ldots \\ \ldots\ldots\ldots\ldots & \ldots\ldots\ldots\ldots & \ldots\ldots & \ldots\ldots\ldots\ldots \\ f_{c-mcla}(nc,1)\rho_{mcla} & f_{c-mcla}(nc,2)\rho_{mcla} & \ldots\ldots & f_{c-mcla}(nc,nla)\rho_{mcla} \end{pmatrix}$$

$$\mathbf{B5} = \begin{pmatrix} f_{c-mcta}(1)\rho_{mcta} & f_{c-tcw}(1)\rho_{tcw} & f_{c-tct}(1)\rho_{tct} \\ f_{c-mcta}(2)\rho_{mcta} & f_{c-tcw}(2)\rho_{tcw} & f_{c-tct}(2)\rho_{tct} \\ \ldots\ldots\ldots\ldots\ldots & \ldots\ldots\ldots\ldots\ldots & \ldots\ldots\ldots\ldots\ldots \\ \ldots\ldots\ldots\ldots\ldots & \ldots\ldots\ldots\ldots\ldots & \ldots\ldots\ldots\ldots\ldots \\ f_{c-mcta}(nc)\rho_{mcta} & f_{c-tcw}(nc)\rho_{tcw} & f_{c-tct}(nc)\rho_{tct} \end{pmatrix}$$

$$\mathbf{B6} = \begin{pmatrix} f_{c-s}(1,1)\rho_s & f_{c-s}(1,2)\rho_s & \ldots\ldots\ldots\ldots & f_{c-s}(1,ns)\rho_s \\ f_{c-s}(2,1)\rho_s & f_{c-s}(2,2)\rho_s & \ldots\ldots\ldots\ldots & f_{c-s}(2,ns)\rho_s \\ \ldots\ldots\ldots\ldots & \ldots\ldots\ldots\ldots & \ldots\ldots\ldots\ldots & \ldots\ldots\ldots\ldots \\ \ldots\ldots\ldots\ldots & \ldots\ldots\ldots\ldots & \ldots\ldots\ldots\ldots & \ldots\ldots\ldots\ldots \\ f_{c-s}(nc,1)\rho_s & f_{c-s}(nc,2)\rho_s & \ldots\ldots\ldots\ldots & f_{c-s}(nc,ns)\rho_s \end{pmatrix}$$

$$\mathbf{B7} = \begin{pmatrix} f_{c-co}(1,1)\rho_{co} & f_{c-co}(1,2)\rho_{co} & \ldots\ldots\ldots\ldots & f_{c-co}(1,nco)\rho_{co} \\ f_{c-co}(2,1)\rho_{co} & f_{c-co}(2,2)\rho_{co} & \ldots\ldots\ldots\ldots & f_{c-co}(2,nco)\rho_{co} \\ \ldots\ldots\ldots\ldots & \ldots\ldots\ldots\ldots & \ldots\ldots\ldots\ldots & \ldots\ldots\ldots\ldots \\ \ldots\ldots\ldots\ldots & \ldots\ldots\ldots\ldots & \ldots\ldots\ldots\ldots & \ldots\ldots\ldots\ldots \\ f_{c-co}(nc,1)\rho_{co} & f_{c-co}(nc,2)\rho_{co} & \ldots\ldots\ldots\ldots & f_{c-co}(nc,nco)\rho_{co} \end{pmatrix}$$

$$\mathbf{B8} = \begin{pmatrix} f_{c-st}(1,1)\rho_{st} & f_{c-st}(1,2)\rho_{st} & \ldots\ldots\ldots\ldots & f_{c-st}(1,nst)\rho_{st} \\ f_{c-st}(2,1)\rho_{st} & f_{c-st}(2,2)\rho_{st} & \ldots\ldots\ldots\ldots & f_{c-st}(2,nst)\rho_{st} \\ \ldots\ldots\ldots\ldots & \ldots\ldots\ldots\ldots & \ldots\ldots\ldots\ldots & \ldots\ldots\ldots\ldots \\ \ldots\ldots\ldots\ldots & \ldots\ldots\ldots\ldots & \ldots\ldots\ldots\ldots & \ldots\ldots\ldots\ldots \\ f_{c-st}(nc,1)\rho_{st} & f_{c-st}(nc,2)\rho_{st} & \ldots\ldots\ldots\ldots & f_{c-st}(nc,nst)\rho_{st} \end{pmatrix}$$

$$\mathbf{C1} = \begin{pmatrix} f_{mc-m}(1,1)\rho_m & f_{mc-m}(1,2)\rho_m & \ldots\ldots & f_{mc-m}(1,nm)\rho_m \\ f_{mc-m}(2,1)\rho_m & f_{mc-m}(2,2)\rho_m & \ldots\ldots & f_{mc-m}(2,nm)\rho_m \\ \ldots\ldots\ldots & \ldots\ldots\ldots & \ldots\ldots & \ldots\ldots \\ \ldots\ldots\ldots & \ldots\ldots\ldots & \ldots\ldots & \ldots\ldots \\ f_{mc-m}(nmc,1)\rho_m & f_{mc-m}(nmc,2)\rho_m & \ldots\ldots & f_{mc-m}(nmc,nm)\rho_m \end{pmatrix}$$

$$\mathbf{C2} = \begin{pmatrix} f_{mc-c}(1,1)\rho_c & f_{mc-c}(1,2)\rho_c & \ldots\ldots\ldots\ldots & f_{mc-c}(1,nc)\rho_c \\ f_{mc-c}(2,1)\rho_c & f_{mc-c}(2,2)\rho_c & \ldots\ldots\ldots\ldots & f_{mc-c}(2,nc)\rho_c \\ \ldots\ldots\ldots & \ldots\ldots\ldots & \ldots\ldots\ldots\ldots & \ldots\ldots\ldots \\ \ldots\ldots\ldots & \ldots\ldots\ldots & \ldots\ldots\ldots\ldots & \ldots\ldots\ldots \\ f_{mc-c}(nmc,1)\rho_c & f_{mc-c}(nmc,2)\rho_c & \ldots\ldots\ldots\ldots & f_{mc-c}(nmc,nc)\rho_c \end{pmatrix}$$

$$\mathbf{C3} = \begin{pmatrix} f_{mc-mc}(1,1)\rho_{mc} - 1 & f_{mc-mc}(1,2)\rho_{mc} & \ldots\ldots & f_{mc-mc}(1,nmc)\rho_{mc} \\ f_{mc-mc}(2,1)\rho_{mc} & f_{mc-mc}(2,2)\rho_{mc} - 1 & \ldots\ldots & f_{mc-mc}(2,nmc)\rho_{mc} \\ \ldots\ldots\ldots & \ldots\ldots\ldots & \ldots\ldots & \ldots\ldots\ldots \\ \ldots\ldots\ldots & \ldots\ldots\ldots & \ldots\ldots & \ldots\ldots\ldots \\ f_{mc-mc}(nmc,1)\rho_{mc} & f_{mc-mc}(nmc,2)\rho_{mc} & \ldots\ldots & f_{mc-mc}(nmc,nmc)\rho_{mc} - 1 \end{pmatrix}$$

$$\mathbf{C4} = \begin{pmatrix} f_{mc-mcla}(1,1)\rho_{mcla} & f_{mc-mcla}(1,2)\rho_{mcla} & \ldots\ldots & f_{mc-mcla}(1,nla)\rho_{mcla} \\ f_{mc-mcla}(2,1)\rho_{mcla} & f_{mc-mcla}(2,2)\rho_{mcla} & \ldots\ldots & f_{mc-mcla}(2,nla)\rho_{mcla} \\ \ldots\ldots\ldots\ldots & \ldots\ldots\ldots\ldots & \ldots\ldots & \ldots\ldots\ldots\ldots \\ \ldots\ldots\ldots\ldots & \ldots\ldots\ldots\ldots & \ldots\ldots & \ldots\ldots\ldots\ldots \\ f_{mc-mcla}(nmc,1)\rho_{mcla} & f_{mc-mcla}(nmc,2)\rho_{mcla} & \ldots\ldots & f_{mc-mcla}(nmc,nla)\rho_{mcla} \end{pmatrix}$$

$$\mathbf{C5} = \begin{pmatrix} f_{mc-mcta}(1)\rho_{mcta} & f_{mc-tcw}(1)\rho_{tcw} & f_{mc-tct}(1)\rho_{tct} \\ f_{mc-mcta}(2)\rho_{mcta} & f_{mc-tcw}(2)\rho_{tcw} & f_{mc-tct}(2)\rho_{tct} \\ \ldots\ldots\ldots\ldots\ldots & \ldots\ldots\ldots\ldots & \ldots\ldots\ldots\ldots \\ \ldots\ldots\ldots\ldots\ldots & \ldots\ldots\ldots\ldots & \ldots\ldots\ldots\ldots \\ f_{mc-mcta}(nmc)\rho_{mcta} & f_{mc-tcw}(nmc)\rho_{tcw} & f_{mc-tct}(nmc)\rho_{tct} \end{pmatrix}$$

$$\mathbf{C6} = \begin{pmatrix} f_{mc-s}(1,1)\rho_s & f_{mc-s}(1,2)\rho_s & \ldots\ldots & f_{mc-s}(1,ns)\rho_s \\ f_{mc-s}(2,1)\rho_s & f_{mc-s}(2,2)\rho_s & \ldots\ldots & f_{mc-s}(2,ns)\rho_s \\ \ldots\ldots\ldots\ldots & \ldots\ldots\ldots\ldots & \ldots\ldots & \ldots\ldots\ldots\ldots \\ \ldots\ldots\ldots\ldots & \ldots\ldots\ldots\ldots & \ldots\ldots & \ldots\ldots\ldots\ldots \\ f_{mc-s}(nmc,1)\rho_s & f_{mc-s}(nmc,2)\rho_s & \ldots\ldots & f_{mc-s}(nmc,ns)\rho_s \end{pmatrix}$$

$$\mathbf{C7} = \begin{pmatrix} f_{mc-co}(1,1)\rho_{co} & f_{mc-co}(1,2)\rho_{co} & \ldots\ldots & f_{mc-co}(1,nco)\rho_{co} \\ f_{mc-co}(2,1)\rho_{co} & f_{mc-co}(2,2)\rho_{co} & \ldots\ldots & f_{mc-co}(2,nco)\rho_{co} \\ \ldots\ldots\ldots\ldots & \ldots\ldots\ldots\ldots & \ldots\ldots & \ldots\ldots\ldots\ldots \\ \ldots\ldots\ldots\ldots & \ldots\ldots\ldots\ldots & \ldots\ldots & \ldots\ldots\ldots\ldots \\ f_{mc-co}(nmc,1)\rho_{co} & f_{mc-co}(nmc,2)\rho_{co} & \ldots\ldots & f_{mc-co}(nmc,nco)\rho_{co} \end{pmatrix}$$

$$\mathbf{C8} = \begin{pmatrix} f_{mc-st}(1,1)\rho_{st} & f_{mc-st}(1,2)\rho_{st} & \ldots\ldots & f_{mc-st}(1,nst)\rho_{st} \\ f_{mc-st}(2,1)\rho_{st} & f_{mc-st}(2,2)\rho_{st} & \ldots\ldots & f_{mc-st}(2,nst)\rho_{st} \\ \ldots\ldots\ldots\ldots & \ldots\ldots\ldots\ldots & \ldots\ldots & \ldots\ldots\ldots\ldots \\ \ldots\ldots\ldots\ldots & \ldots\ldots\ldots\ldots & \ldots\ldots & \ldots\ldots\ldots\ldots \\ f_{mc-st}(nmc,1)\rho_{st} & f_{mc-st}(nmc,2)\rho_{st} & \ldots\ldots & f_{mc-st}(nmc,nst)\rho_{st} \end{pmatrix}$$

$$\mathbf{D1} = \begin{pmatrix} f_{mcla-m}(1,1)\rho_m & f_{mcla-m}(1,2)\rho_m & \ldots\ldots\ldots & f_{mcla-m}(1,nm)\rho_m \\ f_{mcla-m}(2,1)\rho_m & f_{mcla-m}(2,2)\rho_m & \ldots\ldots\ldots & f_{mcla-m}(2,nm)\rho_m \\ \ldots\ldots\ldots & \ldots\ldots\ldots & \ldots\ldots\ldots & \ldots\ldots\ldots \\ \ldots\ldots\ldots & \ldots\ldots\ldots & \ldots\ldots\ldots & \ldots\ldots\ldots \\ f_{mcla-m}(nla,1)\rho_m & f_{mcla-m}(nla,2)\rho_m & \ldots\ldots\ldots & f_{mcla-m}(nla,nm)\rho_m \end{pmatrix}$$

$$\mathbf{D2} = \begin{pmatrix} f_{mcla-c}(1,1)\rho_c & f_{mcla-c}(1,2)\rho_c & \ldots\ldots\ldots\ldots & f_{mcla-c}(1,nc)\rho_c \\ f_{mcla-c}(2,1)\rho_c & f_{mcla-c}(2,2)\rho_c & \ldots\ldots\ldots\ldots & f_{mcla-c}(2,nc)\rho_c \\ \ldots\ldots\ldots & \ldots\ldots\ldots & \ldots\ldots\ldots\ldots & \ldots\ldots\ldots\ldots \\ \ldots\ldots\ldots & \ldots\ldots\ldots & \ldots\ldots\ldots\ldots & \ldots\ldots\ldots\ldots \\ f_{mcla-c}(nla,1)\rho_c & f_{mcla-c}(nla,2)\rho_c & \ldots\ldots\ldots\ldots & f_{mcla-c}(nla,nc)\rho_c \end{pmatrix}$$

$$\mathbf{D3} = \begin{pmatrix} f_{mcla-mc}(1,1)\rho_{mc} & f_{mcla-mc}(1,2)\rho_{mc} & \ldots\ldots & f_{mcla-mc}(1,nmc)\rho_{mc} \\ f_{mcla-mc}(2,1)\rho_{mc} & f_{mcla-mc}(2,2)\rho_{mc} & \ldots\ldots & f_{mcla-mc}(2,nmc)\rho_{mc} \\ \ldots\ldots & \ldots\ldots & \ldots\ldots & \ldots\ldots \\ \ldots\ldots & \ldots\ldots & \ldots\ldots & \ldots\ldots \\ f_{mcla-mc}(nla,1)\rho_{mc} & f_{mcla-mc}(nla,2)\rho_{mc} & \ldots\ldots & f_{mcla-mc}(nla,nmc)\rho_{mc} \end{pmatrix}$$

$$\mathbf{D4} = \begin{pmatrix} f_{mcla-mcla}(1,1)\rho_{mcla}-1 & f_{mcla-mcla}(1,2)\rho_{mcla} & \ldots & f_{mcla-mcla}(1,nla)\rho_{mcla} \\ f_{mcla-mcla}(2,1)\rho_{mcla} & f_{mcla-mcla}(2,2)\rho_{mcla}-1 & \ldots & f_{mcla-mcla}(2,nla)\rho_{mcla} \\ \ldots\ldots & \ldots\ldots & \ldots & \ldots\ldots \\ \ldots\ldots & \ldots\ldots & \ldots & \ldots\ldots \\ f_{mcla-mcla}(nla,1)\rho_{mcla} & f_{mcla-mcla}(nla,2)\rho_{mcla} & \ldots & f_{mcla-mcla}(nla,nla)\rho_{mcla}-1 \end{pmatrix}$$

$$\mathbf{D5} = \begin{pmatrix} f_{mcla-mcta}(1)\rho_{mcta} & f_{mcla-tcw}(1)\rho_{tcw} & f_{mcla-tct}(1)\rho_{tct} \\ f_{mcla-mcta}(2)\rho_{mcta} & f_{mcla-tcw}(2)\rho_{tcw} & f_{mcla-tct}(2)\rho_{tct} \\ \ldots\ldots & \ldots\ldots & \ldots\ldots \\ \ldots\ldots & \ldots\ldots & \ldots\ldots \\ f_{mcla-mcta}(nla)\rho_{mcta} & f_{mcla-tcw}(nla)\rho_{tcw} & f_{mcla-tct}(nla)\rho_{tct} \end{pmatrix}$$

$$\mathbf{D6} = \begin{pmatrix} f_{mcla-s}(1,1)\rho_s & f_{mcla-s}(1,2)\rho_s & \ldots\ldots & f_{mcla-s}(1,ns)\rho_s \\ f_{mcla-s}(2,1)\rho_s & f_{mcla-s}(2,2)\rho_s & \ldots\ldots & f_{mcla-s}(2,ns)\rho_s \\ \ldots\ldots & \ldots\ldots & \ldots\ldots & \ldots\ldots \\ \ldots\ldots & \ldots\ldots & \ldots\ldots & \ldots\ldots \\ f_{mcla-s}(nla,1)\rho_s & f_{mcla-s}(nla,2)\rho_s & \ldots\ldots & f_{mcla-s}(nla,ns)\rho_s \end{pmatrix}$$

$$\mathbf{D7} = \begin{pmatrix} f_{mcla-co}(1,1)\rho_{co} & f_{mcla-co}(1,2)\rho_{co} & \ldots & f_{mcla-co}(1,nco)\rho_{co} \\ f_{mcla-co}(2,1)\rho_{co} & f_{mcla-co}(2,2)\rho_{co} & \ldots & f_{mcla-co}(2,nco)\rho_{co} \\ \ldots\ldots\ldots\ldots & \ldots\ldots\ldots\ldots & \ldots & \ldots\ldots\ldots\ldots \\ \ldots\ldots\ldots\ldots & \ldots\ldots\ldots\ldots & \ldots & \ldots\ldots\ldots\ldots \\ f_{mcla-co}(nla,1)\rho_{co} & f_{mcla-co}(nla,2)\rho_{co} & \ldots & f_{mcla-co}(nla,nco)\rho_{co} \end{pmatrix}$$

$$\mathbf{D8} = \begin{pmatrix} f_{mcla-st}(1,1)\rho_{st} & f_{mcla-st}(1,2)\rho_{st} & \ldots\ldots\ldots & f_{mcla-st}(1,nst)\rho_{st} \\ f_{mcla-st}(2,1)\rho_{st} & f_{mcla-st}(2,2)\rho_{st} & \ldots\ldots\ldots & f_{mcla-st}(2,nst)\rho_{st} \\ \ldots\ldots\ldots\ldots & \ldots\ldots\ldots\ldots & \ldots\ldots\ldots & \ldots\ldots\ldots\ldots \\ \ldots\ldots\ldots\ldots & \ldots\ldots\ldots\ldots & \ldots\ldots\ldots & \ldots\ldots\ldots\ldots \\ f_{mcla-st}(nla,1)\rho_{st} & f_{mcla-st}(nla,2)\rho_{st} & \ldots\ldots\ldots & f_{mcla-st}(nla,nst)\rho_{st} \end{pmatrix}$$

$$\mathbf{E1} = \begin{pmatrix} f_{mcta-m}(1)\rho_m & f_{mcta-m}(2)\rho_m & \ldots\ldots\ldots\ldots\ldots & f_{mcta-m}(nm)\rho_m \\ f_{tcw-m}(1)\rho_m & f_{tcw-m}(2)\rho_m & \ldots\ldots\ldots\ldots\ldots & f_{tcw-m}(nm)\rho_m \\ f_{tct-m}(1)\rho_m & f_{tct-m}(2)\rho_m & \ldots\ldots\ldots\ldots\ldots & f_{tct-m}(nm)\rho_m \end{pmatrix}$$

$$\mathbf{E2} = \begin{pmatrix} f_{mcta-c}(1)\rho_c & f_{mcta-c}(2)\rho_c & \ldots\ldots\ldots\ldots\ldots & f_{mcta-c}(nc)\rho_c \\ f_{tcw-c}(1)\rho_c & f_{tcw-c}(2)\rho_c & \ldots\ldots\ldots\ldots\ldots & f_{tcw-c}(nc)\rho_c \\ f_{tct-c}(1)\rho_c & f_{tct-c}(2)\rho_c & \ldots\ldots\ldots\ldots\ldots & f_{tct-c}(nc)\rho_c \end{pmatrix}$$

$$\mathbf{E3} = \begin{pmatrix} f_{mcta-mc}(1)\rho_{mc} & f_{mcta-mc}(2)\rho_{mc} & \ldots\ldots\ldots\ldots & f_{mcta-mc}(nmc)\rho_{mc} \\ f_{tcw-mc}(1)\rho_{mc} & f_{tcw-mc}(2)\rho_{mc} & \ldots\ldots\ldots\ldots & f_{tcw-mc}(nmc)\rho_{mc} \\ f_{tct-mc}(1)\rho_{mc} & f_{tct-mc}(2)\rho_{mc} & \ldots\ldots\ldots\ldots & f_{tct-mc}(nmc)\rho_{mc} \end{pmatrix}$$

$$\mathbf{E4} = \begin{pmatrix} f_{mcta-mcla}(1)\rho_{mcla} & f_{mcta-mcla}(2)\rho_{mcla} & \cdots\cdots & f_{mcta-mcla}(nla)\rho_{mcla} \\ f_{tcw-mcla}(1)\rho_{mcla} & f_{tcw-mcla}(2)\rho_{mcla} & \cdots\cdots & f_{tcw-mcla}(nla)\rho_{mcla} \\ f_{tct-mcla}(1)\rho_{mcla} & f_{tct-mcla}(2)\rho_{mcla} & \cdots\cdots & f_{tct-mcla}(nla)\rho_{mcla} \end{pmatrix}$$

$$\mathbf{E5} = \begin{pmatrix} f_{mcta-mcta}\rho_{mcta} - 1 & f_{mcta-tcw}\rho_{tcw} & f_{mcta-tct}\rho_{tct} \\ f_{tcw-mcta}\rho_{mcta} & f_{tcw-tcw}\rho_{tcw} - 1 & f_{tcw-tct}\rho_{tct} \\ f_{tct-mcta}\rho_{mcta} & f_{tct-tcw}\rho_{tcw} & f_{tct-tct}\rho_{tct} - 1 \end{pmatrix}$$

$$\mathbf{E6} = \begin{pmatrix} f_{mcta-s}(1)\rho_s & f_{mcta-s}(2)\rho_s & \cdots\cdots & f_{mcta-s}(ns)\rho_s \\ f_{tcw-s}(1)\rho_s & f_{tcw-s}(2)\rho_s & \cdots\cdots & f_{tcw-s}(ns)\rho_s \\ f_{tct-s}(1)\rho_s & f_{tct-s}(2)\rho_s & \cdots\cdots & f_{tct-s}(ns)\rho_s \end{pmatrix}$$

$$\mathbf{E7} = \begin{pmatrix} f_{mcta-co}(1)\rho_{co} & f_{mcta-co}(2)\rho_{co} & \cdots\cdots & f_{mcta-co}(nco)\rho_{co} \\ f_{tcw-co}(1)\rho_{co} & f_{tcw-co}(2)\rho_{co} & \cdots\cdots & f_{tcw-co}(nco)\rho_{co} \\ f_{tct-co}(1)\rho_{co} & f_{tct-co}(2)\rho_{co} & \cdots\cdots & f_{tct-co}(nco)\rho_{co} \end{pmatrix}$$

$$\mathbf{E8} = \begin{pmatrix} f_{mcta-st}(1)\rho_{st} & f_{mcta-st}(2)\rho_{st} & \cdots\cdots & f_{mcta-st}(nst)\rho_{st} \\ f_{tcw-st}(1)\rho_{st} & f_{tcw-st}(2)\rho_{st} & \cdots\cdots & f_{tcw-st}(nst)\rho_{st} \\ f_{tct-st}(1)\rho_{st} & f_{tct-st}(2)\rho_{st} & \cdots\cdots & f_{tct-st}(nst)\rho_{st} \end{pmatrix}$$

$$\mathbf{F1} = \begin{pmatrix} f_{s-m}(1,1)\rho_m & f_{s-m}(1,2)\rho_m & \ldots\ldots\ldots\ldots & f_{s-m}(1,nm)\rho_m \\ f_{s-m}(2,1)\rho_m & f_{s-m}(2,2)\rho_m & \ldots\ldots\ldots\ldots & f_{s-m}(2,nm)\rho_m \\ \ldots\ldots & \ldots\ldots & \ldots\ldots\ldots\ldots & \ldots\ldots \\ \ldots\ldots & \ldots\ldots & \ldots\ldots\ldots\ldots & \ldots\ldots \\ f_{s-m}(ns,1)\rho_m & f_{s-m}(ns,2)\rho_m & \ldots\ldots\ldots\ldots & f_{s-m}(ns,nm)\rho_m \end{pmatrix}$$

$$\mathbf{F2} = \begin{pmatrix} f_{s-c}(1,1)\rho_c & f_{s-c}(1,2)\rho_c & \ldots\ldots\ldots\ldots & \ldots\ldots & f_{s-c}(1,nc)\rho_c \\ f_{s-c}(2,1)\rho_c & f_{s-c}(2,2)\rho_c & \ldots\ldots\ldots\ldots & \ldots\ldots & f_{s-c}(2,nc)\rho_c \\ \ldots\ldots & \ldots\ldots & \ldots\ldots\ldots\ldots & \ldots\ldots & \ldots\ldots \\ \ldots\ldots & \ldots\ldots & \ldots\ldots\ldots\ldots & \ldots\ldots & \ldots\ldots \\ f_{s-c}(ns,1)\rho_c & f_{s-c}(ns,2)\rho_c & \ldots\ldots\ldots\ldots & \ldots\ldots & f_{s-c}(ns,nc)\rho_c \end{pmatrix}$$

$$\mathbf{F3} = \begin{pmatrix} f_{s-mc}(1,1)\rho_{mc} & f_{s-mc}(1,2)\rho_{mc} & \ldots\ldots\ldots & f_{s-mc}(1,nmc)\rho_{mc} \\ f_{s-mc}(2,1)\rho_{mc} & f_{s-mc}(2,2)\rho_{mc} & \ldots\ldots\ldots & f_{s-mc}(2,nmc)\rho_{mc} \\ \ldots\ldots & \ldots\ldots & \ldots\ldots & \ldots\ldots \\ \ldots\ldots & \ldots\ldots & \ldots\ldots & \ldots\ldots \\ f_{s-mc}(ns,1)\rho_{mc} & f_{s-mc}(ns,2)\rho_{mc} & \ldots\ldots\ldots & f_{s-mc}(ns,nmc)\rho_{mc} \end{pmatrix}$$

$$\mathbf{F4} = \begin{pmatrix} f_{s-mcla}(1,1)\rho_{mcla} & f_{s-mcla}(1,2)\rho_{mcla} & \ldots\ldots & f_{s-mcla}(1,nla)\rho_{mcla} \\ f_{s-mcla}(2,1)\rho_{mcla} & f_{s-mcla}(2,2)\rho_{mcla} & \ldots\ldots & f_{s-mcla}(2,nla)\rho_{mcla} \\ \ldots\ldots & \ldots\ldots & \ldots\ldots & \ldots\ldots \\ \ldots\ldots & \ldots\ldots & \ldots\ldots & \ldots\ldots \\ f_{s-mcla}(ns,1)\rho_{mcla} & f_{s-mcla}(ns,2)\rho_{mcla} & \ldots\ldots & f_{s-mcla}(ns,nla)\rho_{mcla} \end{pmatrix}$$

$$\mathbf{F5} = \begin{pmatrix} f_{s-mcta}(1)\rho_{mcta} & f_{s-tcw}(1)\rho_{tcw} & f_{s-tct}(1)\rho_{tct} \\ f_{s-mcta}(2)\rho_{mcta} & f_{s-tcw}(2)\rho_{tcw} & f_{s-tct}(2)\rho_{tct} \\ \ldots\ldots\ldots\ldots & \ldots\ldots\ldots\ldots & \ldots\ldots\ldots\ldots \\ \ldots\ldots\ldots\ldots & \ldots\ldots\ldots\ldots & \ldots\ldots\ldots\ldots \\ f_{s-mcta}(ns)\rho_{mcta} & f_{s-tcw}(ns)\rho_{tcw} & f_{s-tct}(ns)\rho_{tct} \end{pmatrix}$$

$$\mathbf{F6} = \begin{pmatrix} f_{s-s}(1,1)\rho_s - 1 & f_{s-s}(1,2)\rho_s & \ldots\ldots\ldots\ldots & f_{s-s}(1,ns)\rho_s \\ f_{s-s}(2,1)\rho_s & f_{s-s}(2,2)\rho_s - 1 & \ldots\ldots\ldots\ldots & f_{s-s}(2,ns)\rho_s \\ \ldots\ldots\ldots\ldots & \ldots\ldots\ldots\ldots & \ldots\ldots\ldots\ldots & \ldots\ldots\ldots\ldots \\ \ldots\ldots\ldots\ldots & \ldots\ldots\ldots\ldots & \ldots\ldots\ldots\ldots & \ldots\ldots\ldots\ldots \\ f_{s-s}(ns,1)\rho_s & f_{s-s}(ns,2)\rho_s & \ldots\ldots\ldots\ldots & f_{s-s}(ns,ns)\rho_s - 1 \end{pmatrix}$$

$$\mathbf{F7} = \begin{pmatrix} f_{s-co}(1,1)\rho_{co} & f_{s-co}(1,2)\rho_{co} & \ldots\ldots\ldots\ldots & f_{s-co}(1,nco)\rho_{co} \\ f_{s-co}(2,1)\rho_{co} & f_{s-co}(2,2)\rho_{co} & \ldots\ldots\ldots\ldots & f_{s-co}(2,nco)\rho_{co} \\ \ldots\ldots\ldots\ldots & \ldots\ldots\ldots\ldots & \ldots\ldots\ldots\ldots & \ldots\ldots\ldots\ldots \\ \ldots\ldots\ldots\ldots & \ldots\ldots\ldots\ldots & \ldots\ldots\ldots\ldots & \ldots\ldots\ldots\ldots \\ f_{s-co}(ns,1)\rho_{co} & f_{s-co}(ns,2)\rho_{co} & \ldots\ldots\ldots\ldots & f_{s-co}(ns,nco)\rho_{co} \end{pmatrix}$$

$$\mathbf{F8} = \begin{pmatrix} f_{s-st}(1,1)\rho_{st} & f_{s-st}(1,2)\rho_{st} & \ldots\ldots\ldots\ldots & f_{s-st}(1,nst)\rho_{st} \\ f_{s-st}(2,1)\rho_{st} & f_{s-st}(2,2)\rho_{st} & \ldots\ldots\ldots\ldots & f_{s-st}(2,nst)\rho_{st} \\ \ldots\ldots\ldots\ldots & \ldots\ldots\ldots\ldots & \ldots\ldots\ldots\ldots & \ldots\ldots\ldots\ldots \\ \ldots\ldots\ldots\ldots & \ldots\ldots\ldots\ldots & \ldots\ldots\ldots\ldots & \ldots\ldots\ldots\ldots \\ f_{s-st}(ns,1)\rho_{st} & f_{s-st}(ns,2)\rho_{st} & \ldots\ldots\ldots\ldots & f_{s-st}(ns,nst)\rho_{st} \end{pmatrix}$$

$$\mathbf{G1} = \begin{pmatrix} f_{co-m}(1,1)\rho_m & f_{co-m}(1,2)\rho_m & \ldots\ldots\ldots\ldots & f_{co-m}(1,nm)\rho_m \\ f_{co-m}(2,1)\rho_m & f_{co-m}(2,2)\rho_m & \ldots\ldots\ldots\ldots & f_{co-m}(2,nm)\rho_m \\ \ldots\ldots & \ldots\ldots & \ldots\ldots\ldots\ldots & \ldots\ldots \\ \ldots\ldots & \ldots\ldots & \ldots\ldots\ldots\ldots & \ldots\ldots \\ f_{co-m}(nco,1)\rho_m & f_{co-m}(nco,2)\rho_m & \ldots\ldots\ldots\ldots & f_{co-m}(nco,nm)\rho_m \end{pmatrix}$$

$$\mathbf{G2} = \begin{pmatrix} f_{co-c}(1,1)\rho_c & f_{co-c}(1,2)\rho_c & \ldots\ldots\ldots\ldots\ldots & f_{co-c}(1,nc)\rho_c \\ f_{co-c}(2,1)\rho_c & f_{co-c}(2,2)\rho_c & \ldots\ldots\ldots\ldots\ldots & f_{co-c}(2,nc)\rho_c \\ \ldots\ldots\ldots & \ldots\ldots\ldots & \ldots\ldots\ldots\ldots\ldots & \ldots\ldots\ldots \\ \ldots\ldots\ldots & \ldots\ldots\ldots & \ldots\ldots\ldots\ldots\ldots & \ldots\ldots\ldots \\ f_{co-c}(nco,1)\rho_c & f_{co-c}(nco,2)\rho_c & \ldots\ldots\ldots\ldots\ldots & f_{co-c}(nco,nc)\rho_c \end{pmatrix}$$

$$\mathbf{G3} = \begin{pmatrix} f_{co-mc}(1,1)\rho_{mc} & f_{co-mc}(1,2)\rho_{mc} & \ldots\ldots\ldots & f_{co-mc}(1,nmc)\rho_{mc} \\ f_{co-mc}(2,1)\rho_{mc} & f_{co-mc}(2,2)\rho_{mc} & \ldots\ldots\ldots & f_{co-mc}(2,nmc)\rho_{mc} \\ \ldots\ldots\ldots & \ldots\ldots\ldots & \ldots\ldots\ldots & \ldots\ldots\ldots \\ \ldots\ldots\ldots & \ldots\ldots\ldots & \ldots\ldots\ldots & \ldots\ldots\ldots \\ f_{co-mc}(nco,1)\rho_{mc} & f_{co-mc}(nco,2)\rho_{mc} & \ldots\ldots\ldots & f_{co-mc}(nco,nmc)\rho_{mc} \end{pmatrix}$$

$$\mathbf{G4} = \begin{pmatrix} f_{co-mcla}(1,1)\rho_{mcla} & f_{co-mcla}(1,2)\rho_{mcla} & \ldots\ldots\ldots & f_{co-mcla}(1,nla)\rho_{mcla} \\ f_{co-mcla}(2,1)\rho_{mcla} & f_{co-mcla}(2,2)\rho_{mcla} & \ldots\ldots\ldots & f_{co-mcla}(2,nla)\rho_{mcla} \\ \ldots\ldots\ldots\ldots & \ldots\ldots\ldots\ldots & \ldots\ldots\ldots & \ldots\ldots\ldots\ldots \\ \ldots\ldots\ldots\ldots & \ldots\ldots\ldots\ldots & \ldots\ldots\ldots & \ldots\ldots\ldots\ldots \\ f_{co-mcla}(nco,1)\rho_{mcla} & f_{co-mcla}(nco,2)\rho_{mcla} & \ldots\ldots\ldots & f_{co-mcla}(nco,nla)\rho_{mcla} \end{pmatrix}$$

$$\mathbf{G5} = \begin{pmatrix} f_{co-mcta}(1)\rho_{mcta} & f_{co-tcw}(1)\rho_{tcw} & f_{co-tct}(1)\rho_{tct} \\ f_{co-mcta}(2)\rho_{mcta} & f_{co-tcw}(2)\rho_{tcw} & f_{co-tct}(2)\rho_{tct} \\ \ldots\ldots\ldots\ldots & \ldots\ldots\ldots\ldots & \ldots\ldots\ldots\ldots \\ \ldots\ldots\ldots\ldots & \ldots\ldots\ldots\ldots & \ldots\ldots\ldots\ldots \\ f_{co-mcta}(nco)\rho_{mcta} & f_{co-tcw}(nco)\rho_{tcw} & f_{co-tct}(nco)\rho_{tct} \end{pmatrix}$$

$$\mathbf{G6} = \begin{pmatrix} f_{co-s}(1,1)\rho_s & f_{co-s}(1,2)\rho_s & \ldots\ldots\ldots\ldots & f_{co-s}(1,ns)\rho_s \\ f_{co-s}(2,1)\rho_s & f_{co-s}(2,2)\rho_s & \ldots\ldots\ldots\ldots & f_{co-s}(2,ns)\rho_s \\ \ldots\ldots\ldots\ldots & \ldots\ldots\ldots\ldots & \ldots\ldots\ldots\ldots & \ldots\ldots\ldots\ldots \\ \ldots\ldots\ldots\ldots & \ldots\ldots\ldots\ldots & \ldots\ldots\ldots\ldots & \ldots\ldots\ldots\ldots \\ f_{co-s}(nco,1)\rho_s & f_{co-s}(nco,2)\rho_s & \ldots\ldots\ldots\ldots & f_{co-s}(nco,ns)\rho_s \end{pmatrix}$$

$$\mathbf{G7} = \begin{pmatrix} f_{co-co}(1,1)\rho_{co}-1 & f_{co-co}(1,2)\rho_{co} & \ldots & f_{co-co}(1,nco)\rho_{co} \\ f_{co-co}(2,1)\rho_{co} & f_{co-co}(2,2)\rho_{co}-1 & \ldots & f_{co-co}(2,nco)\rho_{co} \\ \ldots\ldots\ldots\ldots & \ldots\ldots\ldots\ldots & \ldots & \ldots\ldots\ldots\ldots \\ \ldots\ldots\ldots\ldots & \ldots\ldots\ldots\ldots & \ldots & \ldots\ldots\ldots\ldots \\ f_{co-co}(nco,1)\rho_{co} & f_{co-co}(nco,2)\rho_{co} & \ldots & f_{co-co}(nco,nco)\rho_{co}-1 \end{pmatrix}$$

$$\mathbf{G8} = \begin{pmatrix} f_{co-st}(1,1)\rho_{st} & f_{co-st}(1,2)\rho_{st} & \ldots\ldots\ldots\ldots & \ldots & f_{co-st}(1,nst)\rho_{st} \\ f_{co-st}(2,1)\rho_{st} & f_{co-st}(2,2)\rho_{st} & \ldots\ldots\ldots\ldots & \ldots & f_{co-st}(2,nst)\rho_{st} \\ \ldots\ldots\ldots\ldots & \ldots\ldots\ldots\ldots & \ldots\ldots\ldots\ldots & \ldots & \ldots\ldots\ldots\ldots \\ \ldots\ldots\ldots\ldots & \ldots\ldots\ldots\ldots & \ldots\ldots\ldots\ldots & \ldots & \ldots\ldots\ldots\ldots \\ f_{co-st}(nco,1)\rho_{st} & f_{co-st}(nco,2)\rho_{st} & \ldots\ldots\ldots\ldots & \ldots & f_{co-st}(nco,nst)\rho_{st} \end{pmatrix}$$

$$\mathbf{H1} = \begin{pmatrix} f_{st-m}(1,1)\rho_m & f_{st-m}(1,2)\rho_m & \ldots\ldots\ldots\ldots & \ldots\ldots & f_{st-m}(1,nm)\rho_m \\ f_{st-m}(2,1)\rho_m & f_{st-m}(2,2)\rho_m & \ldots\ldots\ldots\ldots & \ldots\ldots & f_{st-m}(2,nm)\rho_m \\ \ldots\ldots\ldots & \ldots\ldots\ldots & \ldots\ldots\ldots\ldots & \ldots\ldots & \ldots\ldots \\ \ldots\ldots\ldots & \ldots\ldots\ldots & \ldots\ldots\ldots\ldots & \ldots\ldots & \ldots\ldots \\ f_{st-m}(nst,1)\rho_m & f_{st-m}(nst,2)\rho_m & \ldots\ldots\ldots\ldots & \ldots\ldots & f_{st-m}(nst,nm)\rho_m \end{pmatrix}$$

$$\mathbf{H2} = \begin{pmatrix} f_{st-c}(1,1)\rho_c & f_{st-c}(1,2)\rho_c & \ldots\ldots\ldots\ldots & \ldots\ldots & f_{st-c}(1,nc)\rho_c \\ f_{st-c}(2,1)\rho_c & f_{st-c}(2,2)\rho_c & \ldots\ldots\ldots\ldots & \ldots\ldots & f_{st-c}(2,nc)\rho_c \\ \ldots\ldots\ldots & \ldots\ldots\ldots & \ldots\ldots\ldots\ldots & \ldots\ldots & \ldots\ldots\ldots \\ \ldots\ldots\ldots & \ldots\ldots\ldots & \ldots\ldots\ldots\ldots & \ldots\ldots & \ldots\ldots\ldots \\ f_{st-c}(nst,1)\rho_c & f_{st-c}(nst,2)\rho_c & \ldots\ldots\ldots\ldots & \ldots\ldots & f_{st-c}(nst,nc)\rho_c \end{pmatrix}$$

$$\mathbf{H3} = \begin{pmatrix} f_{st-mc}(1,1)\rho_{mc} & f_{st-mc}(1,2)\rho_{mc} & \ldots\ldots\ldots & f_{st-mc}(1,nmc)\rho_{mc} \\ f_{st-mc}(2,1)\rho_{mc} & f_{st-mc}(2,2)\rho_{mc} & \ldots\ldots\ldots & f_{st-mc}(2,nmc)\rho_{mc} \\ \ldots\ldots\ldots & \ldots\ldots\ldots\ldots & \ldots\ldots\ldots & \ldots\ldots\ldots \\ \ldots\ldots\ldots\ldots & \ldots\ldots\ldots\ldots & \ldots\ldots\ldots & \ldots\ldots\ldots \\ f_{st-mc}(nst,1)\rho_{mc} & f_{st-mc}(nst,2)\rho_{mc} & \ldots\ldots\ldots & f_{st-mc}(nst,nmc)\rho_{mc} \end{pmatrix}$$

$$\mathbf{H4} = \begin{pmatrix} f_{st-mcla}(1,1)\rho_{mcla} & f_{st-mcla}(1,2)\rho_{mcla} & \ldots\ldots & f_{st-mcla}(1,nla)\rho_{mcla} \\ f_{st-mcla}(2,1)\rho_{mcla} & f_{st-mcla}(2,2)\rho_{mcla} & \ldots\ldots & f_{st-mcla}(2,nla)\rho_{mcla} \\ \ldots\ldots\ldots\ldots & \ldots\ldots\ldots\ldots & \ldots\ldots & \ldots\ldots\ldots\ldots \\ \ldots\ldots\ldots\ldots & \ldots\ldots\ldots\ldots & \ldots\ldots & \ldots\ldots\ldots\ldots \\ f_{st-mcla}(nst,1)\rho_{mcla} & f_{st-mcla}(nst,2)\rho_{mcla} & \ldots\ldots & f_{st-mcla}(nst,nla)\rho_{mcla} \end{pmatrix}$$

$$\mathbf{H5} = \begin{pmatrix} f_{st-mcta}(1)\rho_{mcta} & f_{st-tcw}(1)\rho_{tcw} & f_{st-tct}(1)\rho_{tct} \\ f_{st-mcta}(2)\rho_{mcta} & f_{st-tcw}(2)\rho_{tcw} & f_{st-tct}(2)\rho_{tct} \\ \cdots\cdots\cdots & \cdots\cdots\cdots & \cdots\cdots\cdots \\ \cdots\cdots\cdots & \cdots\cdots\cdots & \cdots\cdots\cdots \\ f_{st-mcta}(nst)\rho_{mcta} & f_{st-tcw}(nst)\rho_{tcw} & f_{st-tct}(nst)\rho_{tct} \end{pmatrix}$$

$$\mathbf{H6} = \begin{pmatrix} f_{st-s}(1,1)\rho_s & f_{st-s}(1,2)\rho_s & \cdots\cdots & f_{st-s}(1,ns)\rho_s \\ f_{st-s}(2,1)\rho_s & f_{st-s}(2,2)\rho_s & \cdots\cdots & f_{st-s}(2,ns)\rho_s \\ \cdots\cdots & \cdots\cdots & \cdots\cdots & \cdots\cdots \\ \cdots\cdots & \cdots\cdots & \cdots\cdots & \cdots\cdots \\ f_{st-s}(nst,1)\rho_s & f_{st-s}(nst,2)\rho_s & \cdots\cdots & f_{st-s}(nst,ns)\rho_s \end{pmatrix}$$

$$\mathbf{H7} = \begin{pmatrix} f_{st-co}(1,1)\rho_{co} & f_{st-co}(1,2)\rho_{co} & \cdots\cdots & f_{st-co}(1,nco)\rho_{co} \\ f_{st-co}(2,1)\rho_{co} & f_{st-co}(2,2)\rho_{co} & \cdots\cdots & f_{st-co}(2,nco)\rho_{co} \\ \cdots\cdots & \cdots\cdots & \cdots\cdots & \cdots\cdots \\ \cdots\cdots & \cdots\cdots & \cdots\cdots & \cdots\cdots \\ f_{st-co}(nst,1)\rho_{co} & f_{st-co}(nst,2)\rho_{co} & \cdots\cdots & f_{st-co}(nst,nco)\rho_{co} \end{pmatrix}$$

$$\mathbf{H8} = \begin{pmatrix} f_{st-st}(1,1)\rho_{st} - 1 & f_{st-st}(1,2)\rho_{st} & \cdots\cdots & f_{st-st}(1,nst)\rho_{st} \\ f_{st-st}(2,1)\rho_{st} & f_{st-st}(2,2)\rho_{st} - 1 & \cdots\cdots & f_{st-st}(2,nst)\rho_{st} \\ \cdots\cdots & \cdots\cdots & \cdots\cdots & \cdots\cdots \\ \cdots\cdots & \cdots\cdots & \cdots\cdots & \cdots\cdots \\ f_{st-st}(ns,1)\rho_{st} & f_{st-st}(ns,2)\rho_{st} & \cdots\cdots & f_{st-st}(nst,nst)\rho_{st} - 1 \end{pmatrix}$$

The column matrix (**x**), as stated earlier, represents the Gebhart factors that must be evaluated. (**x**) will depend on the particular surface under consideration. It will be given here for a general case and for one specific case, that being the melt. Therefore, in general, (**x**) will have the form:

$$\left(\mathbf{x} \right) = \begin{pmatrix} G_{1,j} \\ G_{2,j} \\ G_{3,j} \\ \cdots \\ G_{j,j} \\ \cdots \\ G_{k-1,j} \\ G_{k,j} \end{pmatrix}$$

For the specific case of the melt (x) will be a long matrix. Therefore, it will be divided to 8 smaller column matrices that are as follows :

$$\left(\mathbf{x} \right) = \begin{pmatrix} \mathbf{x1} \\ \mathbf{x2} \\ \mathbf{x3} \\ \mathbf{x4} \\ \mathbf{x5} \\ \mathbf{x6} \\ \mathbf{x7} \\ \mathbf{x8} \end{pmatrix}$$

where **x1, x2,..... x8** are as defined below.

$$\mathbf{x1} = \begin{pmatrix} G_{m-m}(1,k) \\ G_{m-m}(2,k) \\ \cdots \\ G_{m-m}(k,k) \\ \cdots \\ G_{m-m}(nm,k) \end{pmatrix}, \mathbf{x2} = \begin{pmatrix} G_{c-m}(1,k) \\ G_{c-m}(2,k) \\ \cdots \\ \cdots \\ \cdots \\ G_{c-m}(nc,k) \end{pmatrix}, \mathbf{x3} = \begin{pmatrix} G_{mc-m}(1,k) \\ G_{mc-m}(2,k) \\ \cdots \\ \cdots \\ \cdots \\ G_{mc-m}(nmc,k) \end{pmatrix}$$

$$\mathbf{x4} = \begin{pmatrix} G_{mcla-m}(1,k) \\ G_{mcla-m}(2,k) \\ \cdots \\ G_{mcla-m}(nla,k) \end{pmatrix}, \mathbf{x5} = \begin{pmatrix} G_{mcta-m}(k) \\ G_{tcw-m}(k) \\ G_{tct-m}(k) \end{pmatrix}, \mathbf{x6} = \begin{pmatrix} G_{s-m}(1,k) \\ G_{s-m}(2,k) \\ \cdots \\ G_{s-m}(ns,k) \end{pmatrix}$$

$$\mathbf{x7} = \begin{pmatrix} G_{co-m}(1,k) \\ G_{co-m}(2,k) \\ \cdots \\ G_{co-m}(nco,k) \end{pmatrix}, \mathbf{x8} = \begin{pmatrix} G_{st-m}(1,k) \\ G_{st-m}(2,k) \\ \cdots \\ G_{st-m}(nst,k) \end{pmatrix}$$

The right hand side [b] is given by:

$$\left[\ \mathbf{b}\ \right] = \begin{bmatrix} \mathbf{b1} \\ \mathbf{b2} \\ \mathbf{b3} \\ \mathbf{b4} \\ \mathbf{b5} \\ \mathbf{b6} \\ \mathbf{b7} \\ \mathbf{b8} \end{bmatrix}$$

b1, b2 ..... b8 are defined next for the the melt surface.

$$\mathbf{b1} = \begin{bmatrix} f_{m-m}(1,k)\epsilon_m \\ f_{m-m}(2,k)\epsilon_m \\ \cdots\cdots \\ f_{m-m}(nm,k)\epsilon_m \end{bmatrix}, \mathbf{b2} = \begin{bmatrix} f_{c-m}(1,k)\epsilon_m \\ f_{c-m}(2,k)\epsilon_m \\ \cdots\cdots \\ f_{c-m}(nc,k)\epsilon_m \end{bmatrix}, \mathbf{b3} = \begin{bmatrix} f_{mc-m}(1,k)\epsilon_m \\ f_{mc-m}(2,k)\epsilon_m \\ \cdots\cdots \\ f_{mc-m}(nmc,k)\epsilon_m \end{bmatrix}$$

$$\mathbf{b4} = \begin{bmatrix} f_{mcla-m}(1,k)\epsilon_m \\ f_{mcla-m}(2,k)\epsilon_m \\ \cdots\cdots \\ f_{mcla-m}(nla,k)\epsilon_m \end{bmatrix}, \mathbf{b5} = \begin{bmatrix} f_{mcta-m}(k)\epsilon_m \\ f_{tcw-m}(k)\epsilon_m \\ f_{tct-m}(k)\epsilon_m \end{bmatrix}, \mathbf{b6} = \begin{bmatrix} f_{s-m}(1,k)\epsilon_m \\ f_{s-m}(2,k)\epsilon_m \\ \cdots\cdots \\ f_{s-m}(ns,k)\epsilon_m \end{bmatrix}$$

$$\mathbf{b7} = \begin{bmatrix} f_{co-m}(1,k)\epsilon_m \\ f_{co-m}(2,k)\epsilon_m \\ ..... \\ f_{co-m}(nco,k)\epsilon_m \end{bmatrix}, \mathbf{b8} = \begin{bmatrix} f_{st-m}(1,k)\epsilon_m \\ f_{st-m}(2,k)\epsilon_m \\ ..... \\ f_{st-m}(nst,k)\epsilon_m \end{bmatrix}$$

Since the surface considered here is the melt, then k will vary from 1 to nm. Therefore, the system will be solved nm times to determine the Gebhart factors for all melt elements. The matrix [**A**] is the same for the whole system. However, (**x**) and [**b**] are not. The fact that the matrix [**A**] is the same for all surfaces reduces the computation time required considerably. The method of solution for the other surfaces is similar to that for the melt and is described next.

B.3 Gebhart factor equations for the crucible inner wall

The equations for the crucible elements will be similar to the melt elements' equations. The 'm' subscript will be replaced by 'c' in the 'G_{i-m}' variable and in the product of ϵ_m and f_{i-m}. Also, k will vary from 1 to nc, which is the number of elements of the crucible. The subscript 'm' in the matrices (**x**) and [**b**] will be replaced by 'c'.

B.4 Gebhart factor equations for the middle cylinder wall

The 'm' subscript in this case will be replaced by 'mc' in 'G_{i-m}', and in the product of ϵ_m and f_{i-m}. k will vary from 1 to nmc - the number of elements of the middle cylinder. The subsript 'm' will be replaced by 'mc' in the matrices (**x**) and [**b**].

B.5 Gebhart factor equations for the crystal and the crystal top

The 'm' subscript in this case will be replaced by 's' for the crystal case and by 'st' for the crystal top case in 'G_{i-m}', and in the product of ϵ_m and f_{i-m}. k will vary from 1 to ns - the number of elements of the crystal, and from 1 to nst - the number of elements of the crystal top when calculating the crystal top factors. 'm' will be replaced by 's' or by 'st' in the matrices (x) and [b].

B.6 Gebhart factor equations for the crucible outer wall

The 'm' subscript in this case will be replaced by 'co' in 'G_{i-m}' and in the product of ϵ_m and f_{i-m}. k will vary from 1 to nco - the number of elements of the outer crucible wall. The subscript 'm' will be replaced by 'nco' in the matrices (x) and [b].

B.7 Gebhart factor equations for the middle cylinder lower annulus

The 'm' subscript in this case will be replaced by 'mcla' in 'G_{i-m}' and in the product of ϵ_m and f_{i-m}. k will vary from 1 to nla - the number of elements of the lower annulus. In the matrices (x) and [b], the subscript 'm' will be replaced by 'mcla'.

B.8 Gebhart factor equations for the middle cylinder top annulus, top cylinder wall, top cylinder top

The 'm' subscript in this case will be replaced by 'mcta', 'tcw' and 'tct' in 'G_{i-m}' and in the product of ϵ_m and f_{i-m} for the middle cylinder top equations, the top cylinder wall equations and the top cylinder top equations, respectively. The variable k will be equal to 1 since there is only one element on each surface. For the case of calculating the Gebhart factors for the top chamber that is composed of $mcta, tcw, tct$, the subscript

'm' in both matrices (x) and [b] will be replaced by 'mcta ' when calculating the middle cylinder top factors and so on for the other two surfaces.

B.9 Gebhart factor equations for the encapsulant

The encapsulant surface is considered for the case when the radiation emitted from the melt is at a wave length greater than $2\mu m$. Since at that wavelength, the encapsulant is considered opaque. Therefore, the Gebhart factor equations are written in the same manner as those for the melt except that the 'm' subscript is replaced by 'e' in all the equations and matrices. The subscript 'm' in the other surfaces' equations and matrices is also replaced by 'e'. The crucible and crystal elements that are below the encapsulant surface will not be considered as part of the system.

Appendix C

Programme Flow Chart

C.1 General

This appendix gives the flow chart of the programme that is used in calculating the configuration factors and the Gebhart factors. The flow chart is divided tofour sections and given in figures C.44 to C.47. Figure C.44 gives the flow chart of the main section of the programme in which the case is chosen, the surfaces are divided to elements and then the main subroutine is called for encapsulant surface (cases 12, 22 or 32). Depending on which case is calculated the main subroutine is called again for melt surface calculations (cases 1, 2 or 3). The numbers 1, 2 and 3 refer to the cases described in chapter-3. Figures C.45 to C.47 show the flow chart of the main subroutine.

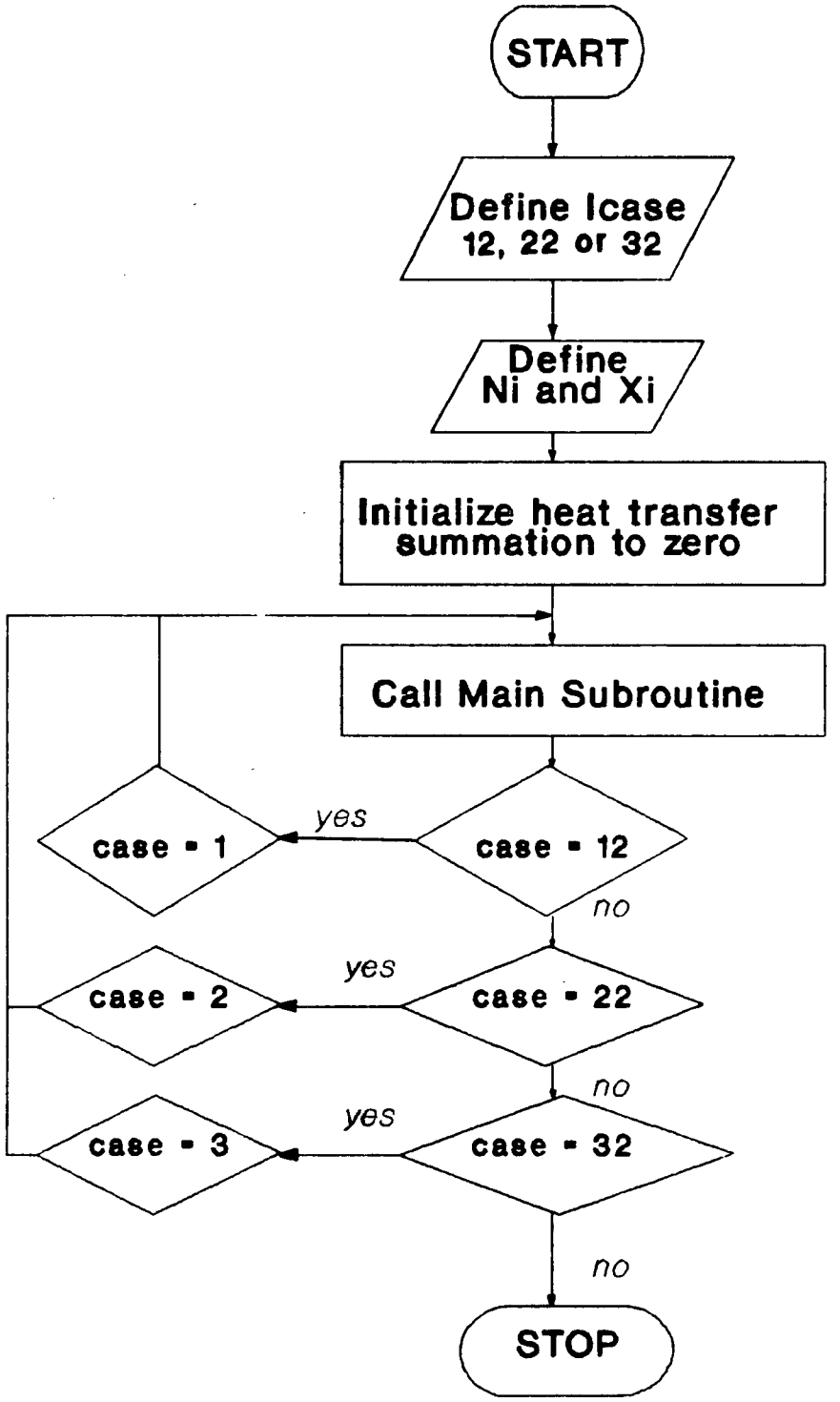

Figure C.45: Main programme flow chart.

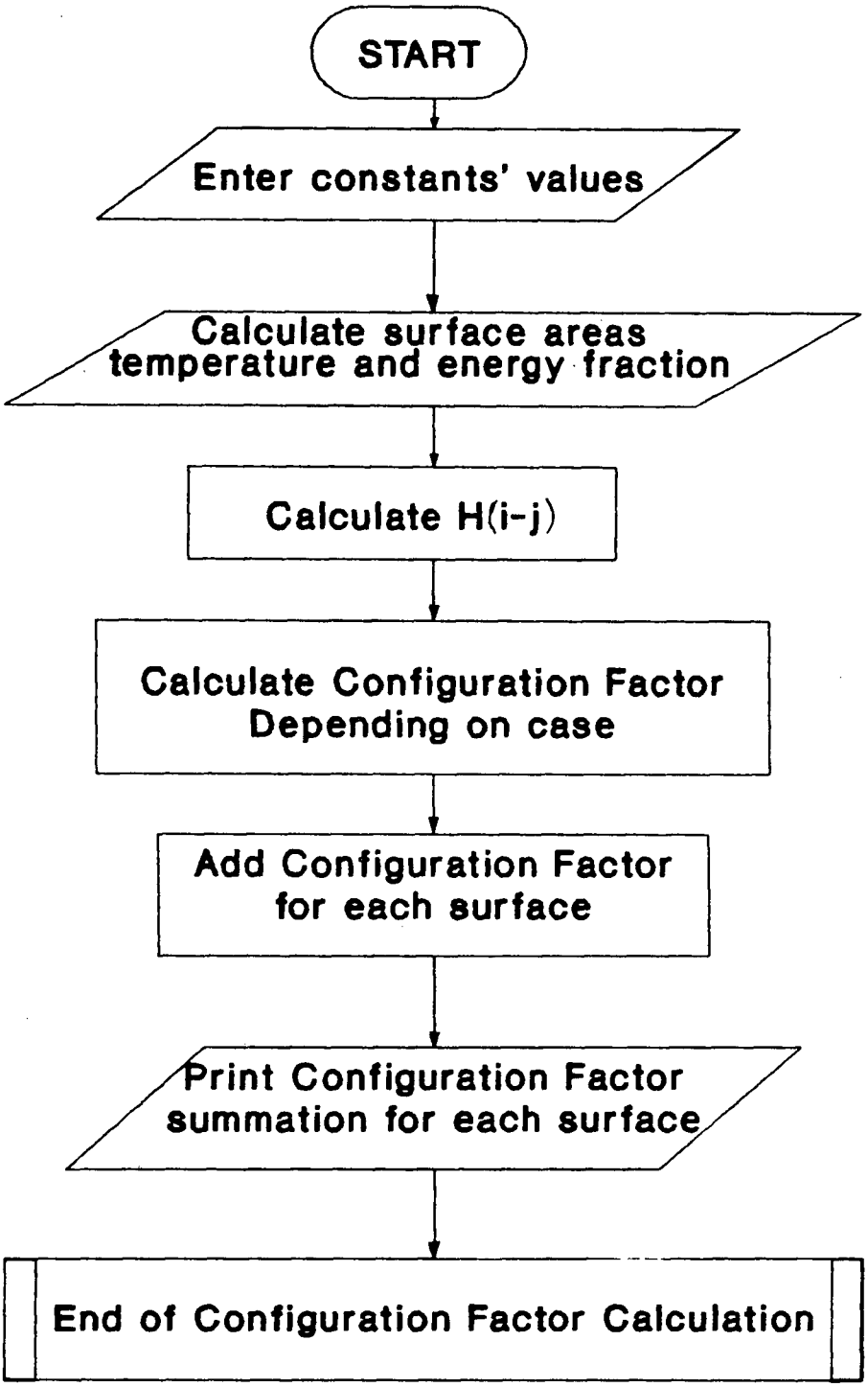

Figure C.46: Main subroutine flow chart.

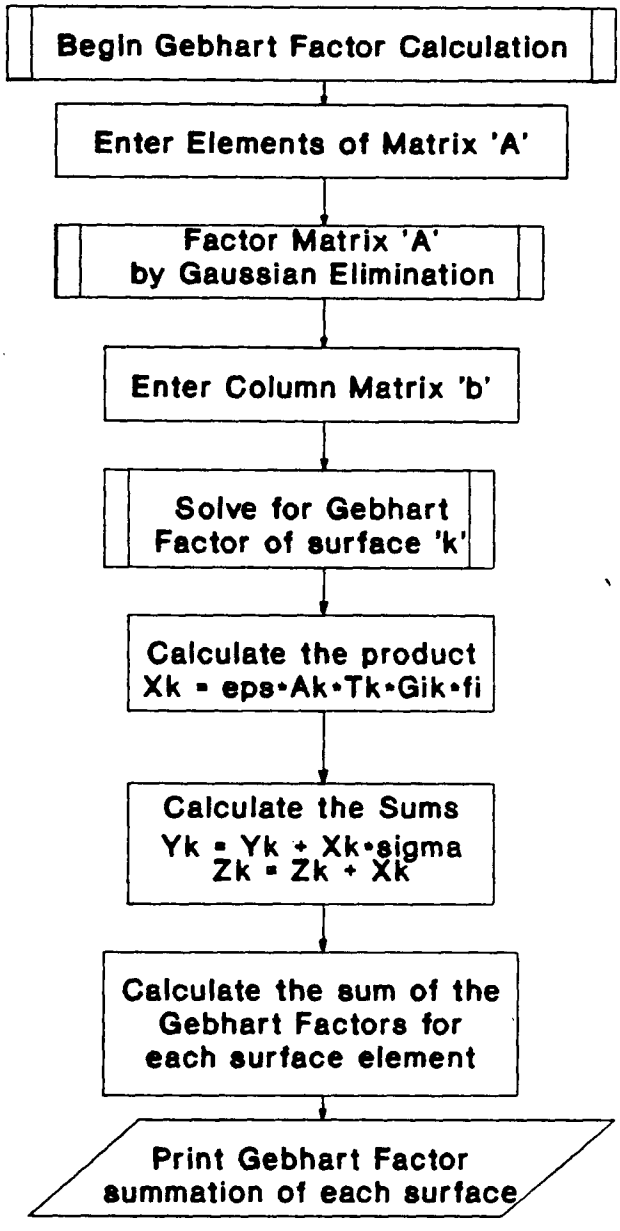

Figure C.47: Continuation of main subroutine flow chart.

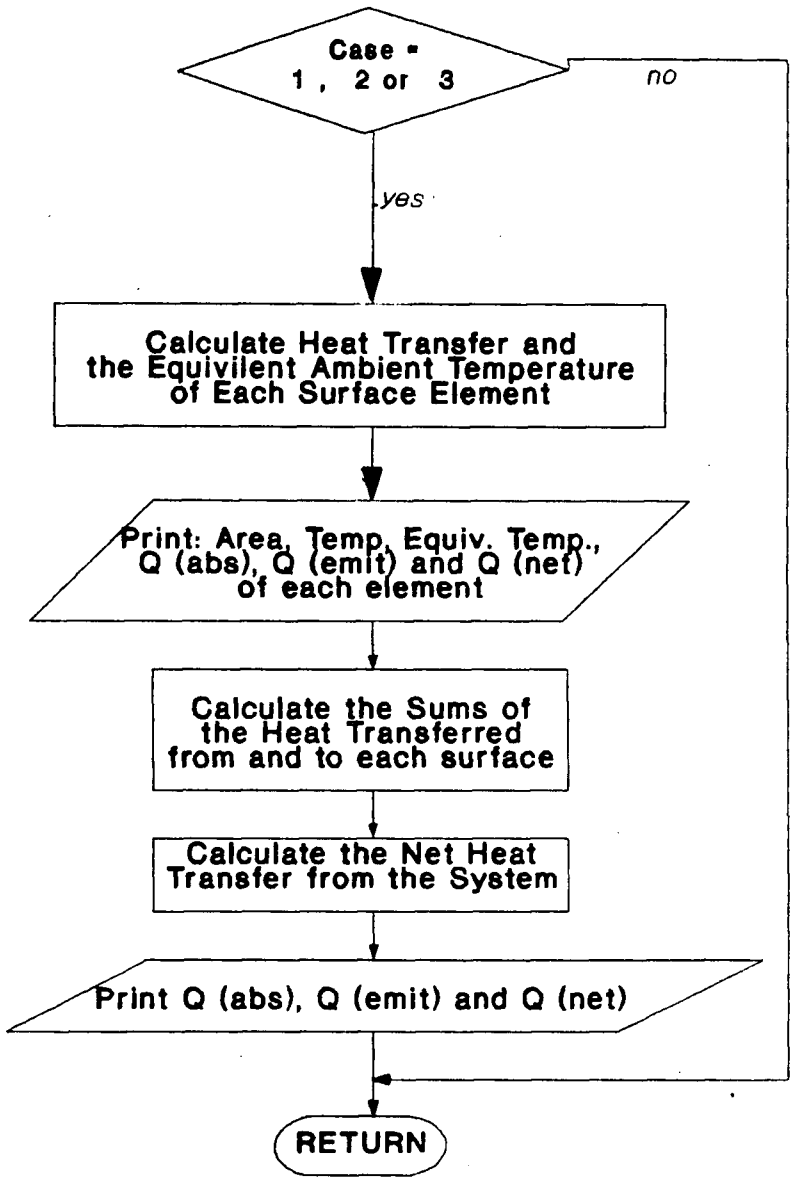

Figure C.48: Continuation of main subroutine flow chart.

Appendix D

Configuration and Gebhart Factors Calculations Results

D.1 General

This appendix gives the results of the configuration factor summation for each element calculated for cases II and III for the simplified case of one—surface enclosure. The results for case–I are given in appendix A. The Gebhart factor summation is one for all elements.

Tables D.22 and D.23 give the summation for case–II from the melt, crucible, crystal and crystal top elements, and the ambient to the melt, crucible, crystal, crystal top and ambient surfaces. Tables D.24 and D.25 gives the same information but with replacing the melt surface by the encapsulant.

Tables D.26, D.27 and D.28 give the same information stated in the previous paragraph for case–III (exchange with the melt). Tables D.29, D.30 and D.31 list the data for exchange with the encapsulant for case–III .

Table D.22: Configuration factor summation from surface j to surface i for case–II (exchange with the melt).

SURFACE j		SURFACE i				
	#	Melt	Crucible	Crystal Wall	Crystal Top	Enclosure
Melt	1	—	0.4021	0.1818	—	0.4162
	2	—	0.4668	0.2422	—	0.2910
	3	—	0.5151	0.1915	—	0.2934
	4	—	0.5586	0.1516	—	0.2898
	5	—	0.6950	0.1207	—	0.1843
Crucible	1	0.4556	0.2050	0.2543	0.0000	0.0851
	2	0.3728	0.2027	0.3251	0.0000	0.0994
	3	0.3020	0.2269	0.3540	0.0000	0.1170
	4	0.2448	0.2477	0.3685	0.0000	0.1390
	5	0.1998	0.2651	0.3685	0.0000	0.1666
	6	0.1646	0.2797	0.3540	0.0000	0.2018
	7	0.1370	0.2911	0.3251	0.0000	0.2468
	8	0.1150	0.3266	0.2543	0.0000	0.3040
	9	0.0974	0.2682	0.2050	0.0164	0.4130
	10	0.0831	0.2740	0.1307	0.0459	0.4663

Table D.23: Configuration factor summation from surface j to surface i for case–II (exchange with the melt).

SURFACE j		SURFACE i				
	#	Melt	Crucible	Crystal Wall	Crystal Top	Enclosure
Crystal	1	0.3198	0.5269	—	—	0.1534
	2	0.2643	0.6754	—	—	0.0603
	3	0.2096	0.7434	—	—	0.0470
	4	0.1601	0.7870	—	—	0.0528
	5	0.1208	0.8081	—	—	0.0711
	6	0.0913	0.8081	—	—	0.1006
	7	0.0696	0.7870	—	—	0.1434
	8	0.0537	0.7437	—	—	0.2029
Crystal Top	1	—	0.0390	—	—	0.9610
	2	—	0.0414	—	—	0.9586
	3	—	0.0469	—	—	0.9531
	4	—	0.0571	—	—	0.9429
Ambient	1	0.0706	0.1493	0.0277	0.0792	0.6732

Table D.24: Configuration factor summation from surface j to surface i for case–II (exchange with the encapsulant).

SURFACE j		SURFACE i				
	#	Encapsulant	Crucible	Crystal	Crystal Top	Enclosure
Encapsulant	1	—	0.3153	0.1772	—	0.5075
	2	—	0.3780	0.2180	—	0.4040
	3	—	0.4349	0.1589	—	0.4062
	4	—	0.4930	0.1156	—	0.3913
	5	—	0.6133	0.0850	—	0.3017
Crucible	4	0.4556	0.1834	0.2220	—	0.1390
	5	0.3728	0.1813	0.2793	—	0.1666
	6	0.3020	0.2068	0.2894	—	0.2018
	7	0.2448	0.2291	0.2793	—	0.2468
	8	0.1998	0.2742	0.2220	—	0.3040
	9	0.1646	0.2240	0.1820	0.0164	0.4130
	10	0.1370	0.2365	0.1142	0.0495	0.4663

Table D.25: Configuration factor summation from surface j to surface i for case–II (exchange with the encapsulant).

SURFACE j		SURFACE i				
	#	Melt	Crucible	Crystal Wall	Crystal Top	Enclosure
Crystal	4	0.3198	0.4940	—	—	0.1863
	5	0.2643	0.6295	—	—	0.1061
	6	0.2096	0.6788	—	—	0.1116
	7	0.1601	0.6954	—	—	0.1445
	8	0.1208	0.6788	—	—	0.2004
Crystal Top	1	—	0.0390	—	—	0.9610
	2	—	0.0414	—	—	0.9586
	3	—	0.0469	—	—	0.9531
	4	—	0.0571	—	—	0.9429
Ambient	1	0.0977	0.1292	0.0249	0.0792	0.6690

Table D.26: Configuration factor summation from surface j to surface i for case–III (exchange with the melt).

SURFACE j		SURFACE i				
	#	Melt	Crucible	Crystal Wall	Crystal Top	Enclosure
Melt	1	—	0.4937	0.1849	—	0.3213
	2	—	0.5630	0.2617	—	0.1753
	3	—	0.6047	0.2220	—	0.1733
	4	—	0.6366	0.1912	—	0.1722
	5	—	0.7446	0.1671	—	0.0883
Crystal Top	1	—	—	—	—	1.0000
Ambient	1	0.0434	0.1222	0.3274	0.0833	0.4237

Table D.27: Configuration factor summation from the crucible elements to the other surfaces for case–III (exchange with the melt).

Crucible	SURFACE i				
Element #	Melt	Crucible	Crystal Wall	Crystal Top	Enclosure
1	0.4556	0.2370	0.2763	—	0.0310
2	0.3728	0.2382	0.3543	—	0.0347
3	0.3020	0.2655	0.3935	—	0.0389
4	0.2448	0.2888	0.4225	—	0.0439
5	0.1998	0.3074	0.4432	—	0.0496
6	0.1646	0.3214	0.4576	—	0.0563
7	0.1370	0.3311	0.4677	—	0.0642
8	0.1150	0.3368	0.4748	—	0.0734
9	0.0974	0.3387	0.4798	—	0.0842
10	0.0831	0.3368	0.4833	—	0.0969
11	0.0713	0.3311	0.4858	—	0.1119
12	0.0615	0.3214	0.4874	—	0.1296
13	0.0534	0.3074	0.4886	—	0.1507
14	0.0465	0.2888	0.4892	—	0.1755
15	0.0407	0.2655	0.4894	—	0.2044
16	0.0358	0.2382	0.4890	—	0.2370
17	0.0316	0.2370	0.4806	—	0.2508

Table D.28: Configuration factor summation from the crystal wall elements to the other surfaces for case–III (exchange with the melt).

Crystal	SURFACE i				
Element #	Melt	Crucible	Crystal Wall	Crystal Top	Enclosure
1	0.3198	0.5475	—	—	0.1327
2	0.2643	0.7025	—	—	0.0332
3	0.2096	0.7795	—	—	0.0110
4	0.1601	0.8358	—	—	0.0041
5	0.1208	0.8749	—	—	0.0077
6	0.0913	0.9009	—	—	0.0131
7	0.0696	0.9173	—	—	0.0201
8	0.0537	0.9262	—	—	0.0290
9	0.0419	0.9291	—	—	0.0290
10	0.0331	0.9262	—	—	0.0407
11	0.0265	0.9173	—	—	0.0562
12	0.0215	0.9009	—	—	0.0776
13	0.0176	0.8749	—	—	0.1075
14	0.0146	0.8358	—	—	0.1496
15	0.0122	0.7795	—	—	0.2083
16	0.0103	0.7025	—	—	0.2872
17	0.0087	0.5475	—	—	0.4437
18	0.0076	0.4439	—	—	0.5484
19	0.0070	0.3060	—	—	0.6873
20	0.0059	0.2319	—	—	0.7622
21	0.0052	0.1740	—	—	0.8208
22	0.0047	0.1304	—	—	0.8649
23	0.0042	0.0982	—	—	0.8976
24	0.0037	0.0747	—	—	0.9216
25	0.0034	0.0575	—	—	0.9392
26	0.0030	0.0447	—	—	0.9522
27	0.0027	0.0352	—	—	0.9620
28	0.0025	0.0281	—	—	0.9694

Table D.29: Configuration factor summation from surface j to surface i for case–III (exchange with the encapsulant).

SURFACE j		SURFACE i				
	#	Encapsulant	Crucible	Crystal	Crystal Top	Enclosure
Encap	1	—	0.4661	0.1849	—	0.3490
	2	—	0.5334	0.2611	—	0.2055
	3	—	0.5766	0.2210	—	0.2024
	4	—	0.6114	0.1898	—	0.1988
	5	—	0.6856	0.1653	—	0.1491
Crystal Top	1	—	—	—	—	1.0000
Ambient	1	0.0525	0.1152	0.3266	0.0834	0.4223

Table D.30: Configuration factor summation from the crucible elements to the other surfaces for case–III (exchange with the encapsulant).

SURFACE j	SURFACE i				
Element #	Encapsulant	Crucible	Crystal	Crystal Top	Enclosure
4	0.4556	0.2245	0.2760	0.0000	0.0439
5	0.3728	0.2237	0.3539	0.0000	0.0496
6	0.3020	0.2486	0.3930	0.0000	0.0563
7	0.2448	0.2691	0.4219	0.0000	0.0642
8	0.1998	0.2844	0.4425	0.0000	0.0734
9	0.1646	0.2944	0.4569	0.0000	0.0842
10	0.1370	0.2993	0.4668	0.0000	0.0969
11	0.1150	0.2993	0.4738	0.0000	0.1119
12	0.0974	0.2944	0.4786	0.0000	0.1296
13	0.0831	0.2844	0.4819	0.0000	0.1507
14	0.0713	0.2691	0.4841	0.0000	0.1755
15	0.0615	0.2486	0.4855	0.0000	0.2044
16	0.0534	0.2237	0.4859	0.0000	0.2370
17	0.0465	0.2245	0.4781	0.0000	0.2508

Table D.31: Configuration factor summation from the crystal elements to the other surfaces for case–III (exchange with the encapsulant).

SURFACE j	SURFACE i				
Element #	Encapsulant	Crucible	Crystal	Crystal Top	Enclosure
4	0.3198	0.5427	—	—	0.1375
5	0.2643	0.6964	—	—	0.0393
6	0.2096	0.7717	—	—	0.0188
7	0.1601	0.8257	—	—	0.0142
8	0.1208	0.8616	—	—	0.0176
9	0.0913	0.8832	—	—	0.0254
10	0.0696	0.8933	—	—	0.0371
11	0.0537	0.8933	—	—	0.0530
12	0.0419	0.8832	—	—	0.0749
13	0.0331	0.8616	—	—	0.1053
14	0.0265	0.8257	—	—	0.1478
15	0.0215	0.7717	—	—	0.2068
16	0.0176	0.6964	—	—	0.2860
17	0.0146	0.5427	—	—	0.4427
18	0.0125	0.4399	—	—	0.5476
19	0.0107	0.3027	—	—	0.6866
20	0.0093	0.2292	—	—	0.7615
21	0.0081	0.1717	—	—	0.8203
22	0.0071	0.1284	—	—	0.8645
23	0.0062	0.0966	—	—	0.8972
24	0.0055	0.0733	—	—	0.9212
25	0.0049	0.0562	—	—	0.9389
26	0.0044	0.0437	—	—	0.9520
27	0.0039	0.0343	—	—	0.9618
28	0.0035	0.0273	—	—	0.9692

Appendix E

Stainless Steel Emittance

E.1 General

This appendix presents the emittance of various stainless steels — oxidized, polished and cleaned as obtained from [33]. Figures E.48 to E.50 show the analysed grouping of the data which give a quick reference range for the emittance of a certain type of steel for a temperature or temperature range. Figure E.51 gives the exact curves obtained from experimental data. The specification and data tables which are not included here for the sake of brevity, describe the specimen condition and exact experimental values of the emittance.

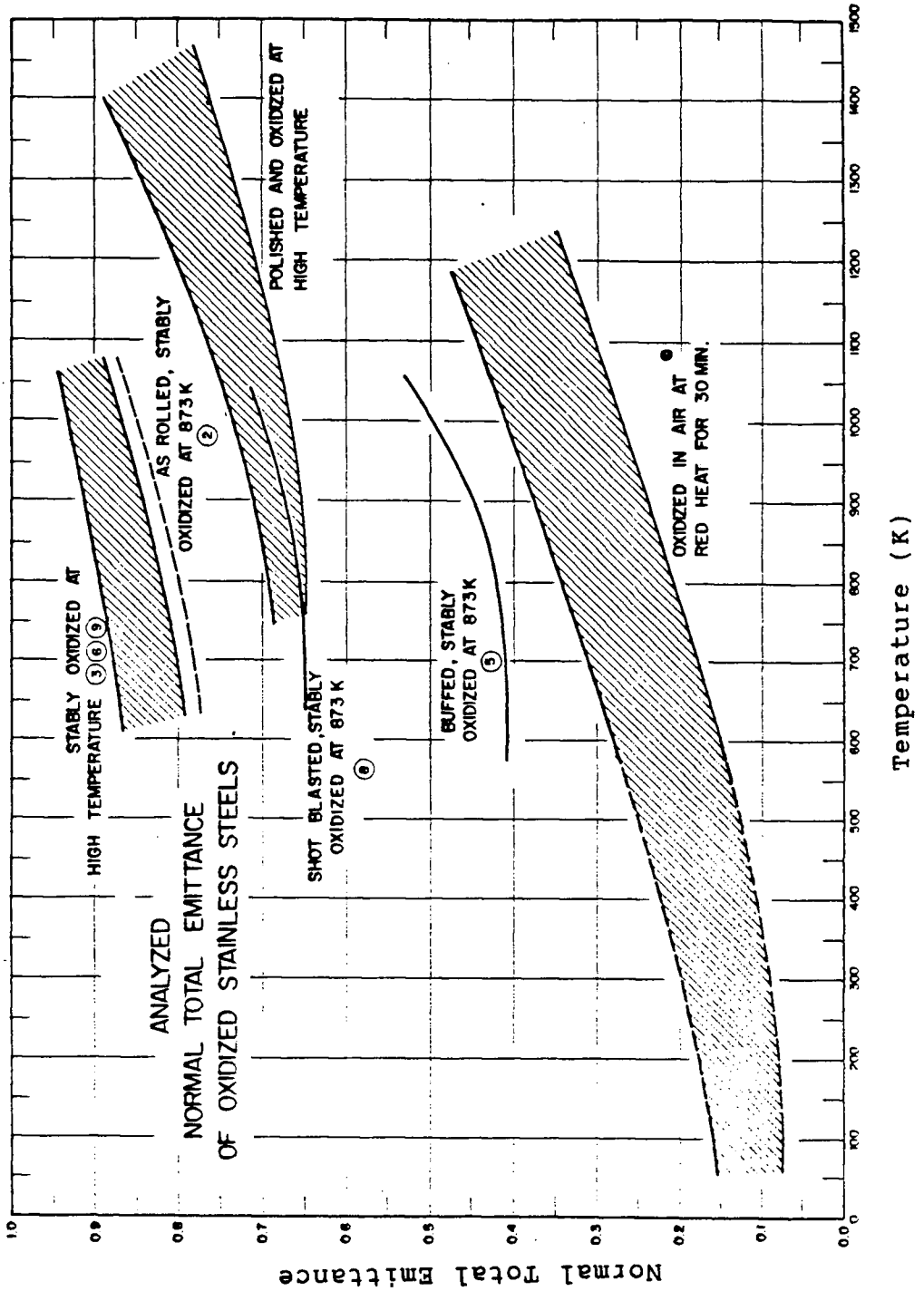

Figure E.49: Analysed normal total emittance of oxidized stainless steel.

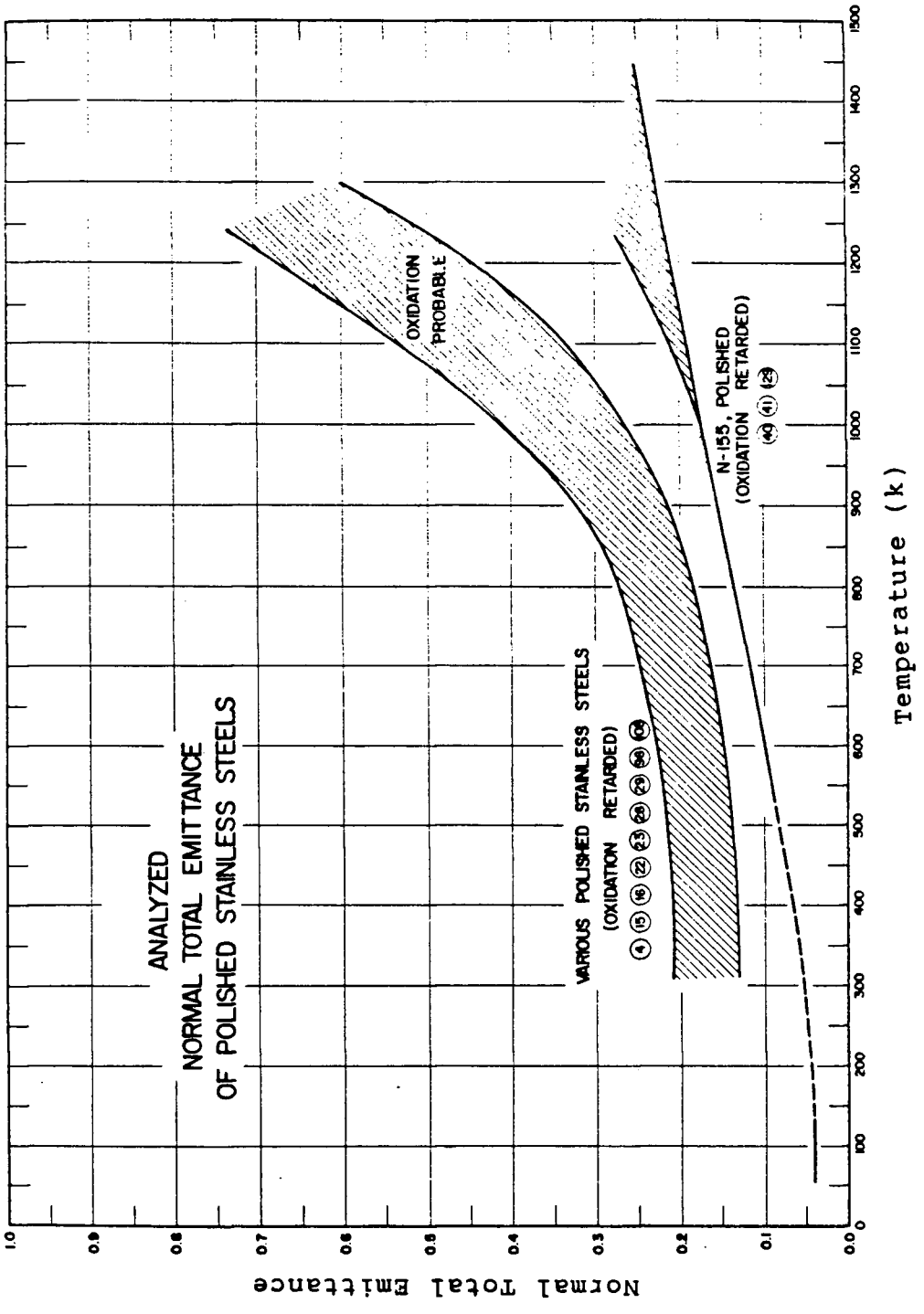

Figure E.50: Analysed normal total emittance of polished stainless steel.

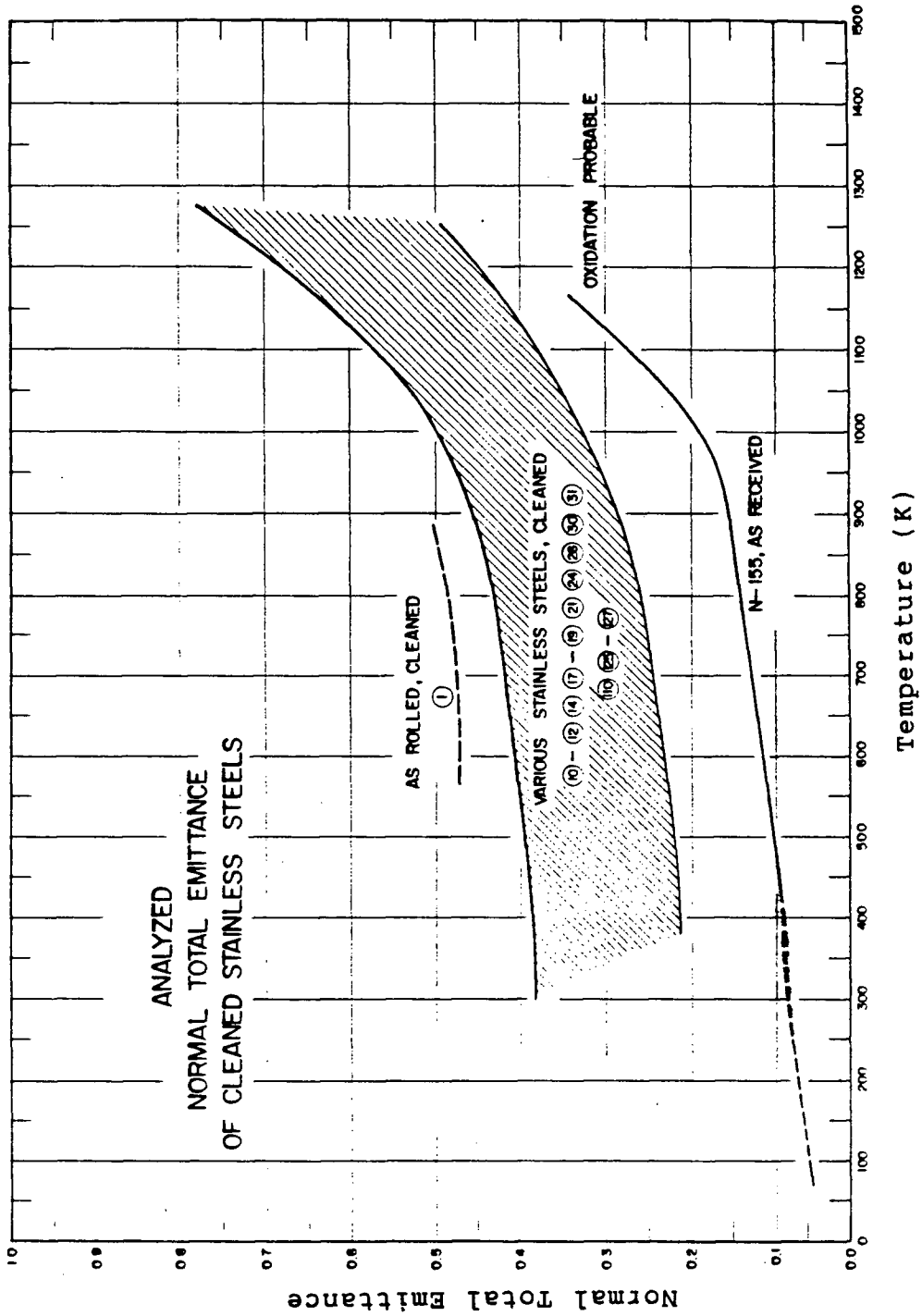

Figure E.51: Analysed normal total emittance of cleaned stainless steel.

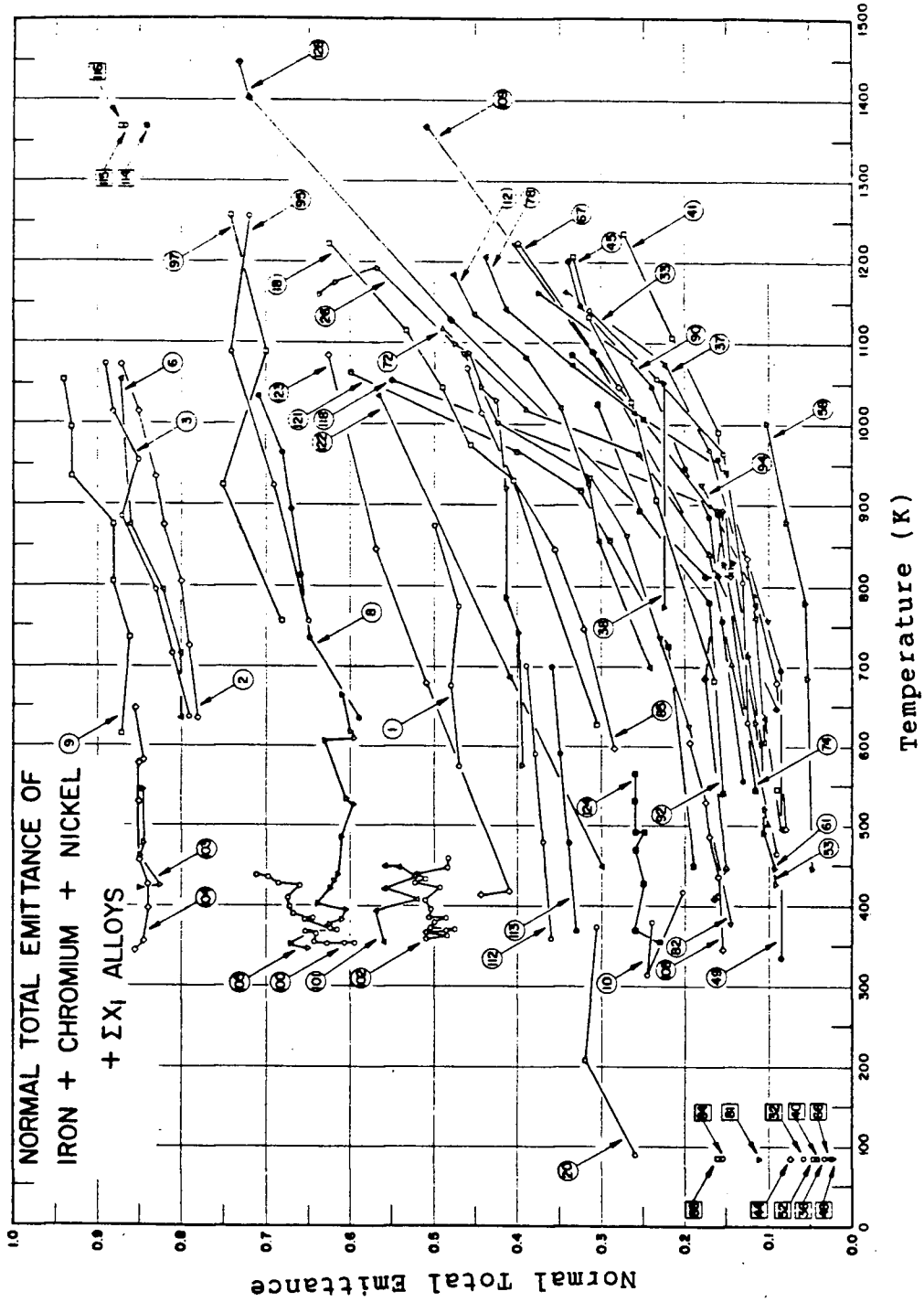

Figure E.52: Normal total emittance of various stainless steels.

Bibliography

[1] A.K. Willardson, *Advances in GaAs Crystal Growth,* Advanced Materials and Processes, 1986.

[2] E.P.A. Metz, R.C. Miller and R.Mazelsky, *A Technique for Pulling Single Crystals of Volatile Matter,* J. of Applied Physics, 33-1962-6.

[3] J.B. Mullin et al, *Liquid Encapsulation Crystal Pulling at High Pressures,* J. of Crystal Growth, 3,4(1968)281-285.

[4] R. Lamprecht et al, *Experiments on Bouyant, Thermocapillary and Forced Convection in Czochralski Configuration,* J. of Crystal Growth, 65(1983)143-152.

[5] W.E. Langlois, *Conservative Differencing Procedures for Rotationally Symmetric Flow with Swirl,* Computer Methods Appl. Mech. Eng., 25(1981)315.

[6] W.E. Langlois, *Digital Simulation of Czochralski Bulk Flow in Microgravity,* J. of Crystal Growth, 48(1980)25.

[7] W.E. Langlois, *A Parametric Sensitivity Study for Czochralsi Bulk Flow in Silicon,* J. of Crystal Growth, 56(1982)15.

[8] K.terashima and T.Fukuda, *A New Magnetic-Field Applied Pulling Apparatus for LEC GaAs Single Crystal Growth,* J. of Crystal Growth, 63(1983)423-425.

[9] J. Osaka et al, *Growth of Semi-Insulating GaAs Single Crystal by LEC Method,* Review of the Electrical Communications Laboratories, Vol 33 #1,

1985.

[10] H. Kohda et al, *Crystal Growth of Completely Dislocation- Free and Striation-Free GaAs*, J. of Crystal Growth, 71(1985)813-816.

[11] Ozawa and Fukuda, *In-Situ Observation of LEC GaAs Solid-Liquid Interface with Newly Developed X-Ray Image Processing system,* J. of Crystal Growth, 76-1986-323.

[12] K. Kakimoto et al, *Direct Observations by X-Ray Radiography of Convection of Boric Oxide in the GaAs Liquid Encapsulated Czochralski Growth*, J. of Crystal Growth, 94(1989)405-411.

[13] P.A. Ramachandran and M.P. Dudkovic, *Simulation of Temperature Distribution in Crystals Grown by Czochralski Method*, J. of Crystal Growth, 71(1985)399-408.

[14] L.J. Atherton et al, *Radiative Heat Exchange in Czochralski Crystal Growth*, J. of Crystal Growth, 84(1987)57-78.

[15] R.K. Srivastava et al, *Interface Shape in Czochralski Grown Crystals - Effect of Conduction and Radiation,* J. of Crystal Growth, 73-1985-487.

[16] S. Motakef and A.W. Witt, *Thermoelastic analysis of GaAs in LEC growth cofiguration,* J. of Crystal Growth, 80-1987-37.

[17] J.J. Derby and R.A. Brown, *Thermal Capillary Analysis of Czochralski and Liquid Encapsulant Czochralski crystal Growth,* J. of Crystal Growth, 75-1986-227.

[18] T.W. Hicks, *Fluid Motion in the encapsulant region of the LEC Growth System,* J. of Crystal Growth, 84-1987-598.

[19] A.S. Jordan, *An Evaluation of the thermal and elastic Constants Affecting GaAs Crystal Growth,* J. of Crystal Growth, 49-1980-631.

[20] P.D. Thomas et al, *Dynamics of Liquid-Encapsulated Czochralski Growth of Gallium Arsenide: Comparing Model with Experiment,* J. of Crystal Growth, 96(1989)135-152.

[21] A.G. Ostrogorsky et al, *Infrared Absorbance of B_2O_3 at Temperatures to $1250°C$,* J. of Crystal Growth, 84-1987-460.

[22] C. Schvezov et al, *Mathematical Modelling of the Liquid Encapsulated Czochralski Growth of Gallium Arsenide,* J. of Crystal Growth, 84(1987)2-218.

[23] A.S. Jordan et al, Bell System Tech. J., 59(1980)593.

[24] I. Grant, B. Smith and D. Rumsby and R.W. Ware, Cambridge Instrument Co., Rustat Road, Cambridge, UK. private communication of author, 1985.

[25] P. Sabhapathy and M. E. Salcudean, *Natural Convection in Liquid Encapsulated Czochralski Growth of Gallium Arsenide*, Canadian Journal of Chemical Engineering, Volume 68, 243-249, April, 1990.

[26] M.E. Salcudean et al, *Numerical Study of Free and Forced Convection in the LEC Growth of GaAs*, J. of Crystal Growth, 94(1989)522-526.

[27] P. Sabhapathy and M.E. Salcudean, *Numerical Analysis of Heat Transfer in LEC Growth of GaAs*, J. of Crystal Growth, 97(1989)125-135.

[28] J.J. Derby, R.A. Brown, F.T. Geyling, A.S. Jordan, and G.A. Nikolakopoulou, *Finite-Element Analysis of a Thermal Cappilary Model for LEC Czochralski Model,* J. Electrochem. Soc. 132(1986)470.

[29] J.J. Derby and R.A. Brown, *Thermal Capillary Analysis of Czochralski Crystal Growth,* J. of Crystal Growth, 74(1986)605.

[30] Napolitano et al, *Viscosity and Density of Boron Trioxide*, J. of American Ceramics Society Vol48 no.12 ,1965, pp.613-616.

[31] G.K. Greffield and A.J. Wickens, J. of Chemical Engineering Data, 20-1975-223.

[32] A.S. Jordan, *Determination of the Total Emittance of n-type GaAs with Application to Czochralski Growth,* Journal of Applied Physics, 51(4)2218-2227, April,1980.

[33] Y.S. Touloukian et al, *Thermophysical Properties of Matter,* Volumes # 2, 3, 6, 7, 8, 9 & 11 (IFI/Plenum, New York, 1970).

[34] A. Goldsmith, T.E. Waterman & H.J. Hirschhorn, *Handbook of Thermophysical Properties of Solid Materials*, Vol. 1–5, the Macmillan Company, New York, 1961.

[35] *Thermophysical Properties Research Literature Guide*, Y.S. Touloukian, J.K. Gerritsen & N.Y. Moore, Vol. 1–3, Plenum 1967; Y.S. Touloukian, J.K. Gerritsen & W.H. Shafer, Supplement–I Vol. 1–6, IFI/Plenum 1973; J.K. Gerritsen, V. Ramdas & T.M. Putnam, Supplement–II Vol 1–6, IFI/Plenum 1977.

[36] G.O.Meduoye et al, *The Minimization of Thermal Stresses During the Growth of GaAs Crystals,* J. of Crystal Growth, 88(1988)397-410.

[37] M.J. Crochet at al, *Finite Element Simulation of Czochralski Bulk Flow*, J. of Crystal Growth, 65(1983)153-165.

[38] R.A. Lemons and M.A. Bösch, *Microscopy of Si Films During Laser Melting*, Applied Physics Letters, vol.40, No.8, 1982.

[39] R. Braunstein and E.O. Kane, *The Valence Band Structure of the III-V Compounds*, J. Phys. Chem. Solids, vol.23, pp1423-1431, 1962.

[40] H.C. Hottel, Radiant-heat Transmission, in William H. McAdams (ed.), *Heat Transmission*, 3rd ed., chap. 4, McGraw-Hill Book Company, 1954.

[41] G. Poljak, *Analysis of Heat Interchange by Radiation between Diffuse Surfaces,* Tech. Phys. USSR, vol1, nos 5, 6, pp555-590, 1935.

[42] M. Jakob, *Heat Transfer,* vol. II, John Wiley & Sons, Inc., New York, 1957.

[43] R. Siegel and J.R. Howel, *Thermal Radiation Heat Transfer*, second edition, Hemisphere Publishing Corporation, 1981.

[44] J.R. Howel, *A Catalog of Radiation Configuration Factors*, McGraw Hill, Inc, 1982.

[45] S.V. Patankar, *Numerical Heat Transfer and Fluid Flow*, McGraw–Hill (Hemisphere), New York, 1980.

[46] G.D. Raithby, *A Critical Evaluation of Upstream Differencing Applied to Problem Involving Fluid Flow*, Computer Methods in Applied Mechanics and Engineering, 9(1976)75–103.